CATALYTIC ACTIVITY AND DEACTIVATION MECHANISMS OF SUPPORTED NiO IN CH_4 OXIDATION

Thesis by

Charunya Phichitkul

In Partial Fulfillment of the Requirements

for the Degree of

Doctor of Philosophy

California Institute of Technology

Pasadena, California 91125

1981

(Submitted April 22, 1981)

ACKNOWLEDGEMENTS

I would like to thank my advisor, Professor George R. Gavalas, and Dr. Gerald E. Voecks for providing help and counsel through the course of this investigation and creating a climate in which my own efforts could prosper.

I am grateful to the Union Oil Corporation, the Jet Propulsion Laboratory and the Chemical Engineering Department for providing financial support during my tenure as a graduate student.

Over the years, I have enjoyed interaction with my colleagues Mr. Mark Siddoway, Mr. Nicholas Kaffes, Dr. Basil Iatrides and Dr. Miretta Stephanopoulos. I am also thankful to my family for believing in me.

Finally, I must thank Nora Quezada together with her sister Nelia Quezada for putting up with me during the frantic period of typing this thesis into its final form.

ABSTRACT

The partial oxidation of CH_4 was studied using a commercial $Ni/\alpha\text{-}Al_2O_3$ catalyst. The results show that two operating regimes can be maintained: a low-conversion regime where CO_2 and H_2O are formed and a high-conversion regime where CO, CO_2 , H_2 and H_2O are formed. The latter regime is established by "catalytic light-off" which among other conditions depends on temperature, feed composition and catalyst activity. Prior to light-off, the catalyst is in the NiO form. Following light-off, the catalyst is in NiO form near the inlet and metallic form further downstream. A series of $NiO/\alpha\text{-}Al_2O_3$ and NiO/ZrO_2 catalysts were prepared by impregnation and calcination in air between 750 and 1050^{o}C. These catalysts were characterized by the BET method, O_2 chemisorption, X-ray diffraction, electron microscopy and ESCA. Test analyses indicate that the supported NiO particles are made up of a large number of small crystallites which become more dispersed after reduction and reunite after oxidation. The activity of these catalysts for CH_4 oxidation under pre-light-off conditions was found to decrease dramatically with increasing calcination temperature. However, the calcined catalysts can be reactivated by reduction in H_2 prior to reaction. The

change in activity is attributed mainly to the change in specific activity of NiO which is explained in terms of the change in excess oxygen content.

TABLE OF CONTENTS

CHAPTER 1

INTRODUCTION

Industrial production and use of hydrogen has increased by more than three orders of magnitude since the 1930's. Approximately 3 X 10^{12} cubic feet of hydrogen was used in the United States during 1973. Petroleum refining is the primary consumer of hydrogen in which hydrocarbon upgrading in the production of fuels and petro-chemicals is of prime importance. Ammonia production for the large fertilizer industry constitutes the second largest consumer. Methanol synthesis, treatment of foodstuffs, reduction of metals and other minor uses comprise the remaining industrial application of hydrogen.

In the past the hydrogen sources in the U.S. have been petroleum and natural gas contributing in a ratio of ∿1:3. European countries in contrast have had to rely on petroleum and coal as the primary sources of hydrogen because of the lack of natural gas availability. The process predominately used for hydrogen production from petroleum and natural gas is steam reforming because of the high hydrogen content in the effluent. However, for the heavier components in the petroleum refineries a process called thermal partial oxidation is employed. Steam reforming of hydrocarbons which are heavier than a No. 2 fuel oil, for example, is not commonly practiced because the temperatures are too high for standard tube materials, the steam requirement becomes too high to maintain

an efficient operation and the rate of catalyst degradation becomes unacceptable for continuous operation.

Thermal partial oxidation (TPO), sometimes known as the Shell or Texaco process (1,2), involves fuel-rich oxidation of hydrocarbons with air or oxygen. The result is a conversion of the hydrocarbon to hydrogen and carbon monoxide. This synthesis gas can be used for petroleum refining, ammonia production and even methane generation. However, some soot is also formed and in industrial applications of TPO an extensive part of the operation is dedicated to soot removal.

Use of a nickel catalyst was found (3) to allow operation near the soot limit region where TPO still produced soot. Other properties of catalytic partial oxidation (CPO) such as controllability, start up, and stability, in addition to improved hydrogen yield, with no soot make CPO a more efficient process than TPO. More recently the incorporation of CPO with fuel cells has gained prominence. The feasibility of using the CPO process for the production of H_2 has been studied at JPL for the past seven years. It has been found in various experiments that the activity of these alumina supported catalysts decreased slowly with time and reduce the performance in extent of conversion and maximum throughput.

The present study is addressed to basic problems in CPO which would help in the optimization of reaction conditions and the design of better catalysts. While the CPO of hydrocarbons poses many fundamental problems, the present study focused mainly on the relationship between activity and physicochemical properties of catalysts differing by the pretreatment procedure. Having established such relationship, the mechanism of catalyst deactivation were identified.

LITERATURE CITED

1. Noyes, R., Ammonia and Synthesis Gas, Chemical Process Monograph, #26 1967

2. Kuhre, C.J. and Reed, C.L., Oil and Gas Journal Jan. 12, 1976, p 110

3. Houseman, J. and Cerini, D.J., "Onboard Hydrogen Generation for Automobiles" Jet Propulsion Laboratory, NASA Contract NAS 7-100

CHAPTER 2

Catalytic Partial Oxidation of CH_4

ABSTRACT

The partial oxidation of CH_4 was studied using a coprecipitated $Ni/\alpha\text{-}Al_2O_3$ catalyst. Two distinct operating regimes were observed in the experiments. At low conversions oxidation resulted in a product of CO_2 and H_2O and at high conversions a mixture of CO, H_2, CO_2 and H_2O was produced. The latter regime is established after "catalytic light-off" which among other conditions depends on temperature, feed composition and catalyst activity. Prior to light-off, the catalyst is in the NiO form. Following light-off, the catalyst is in the NiO form near the inlet and the metallic nickel form further downstream.

INTRODUCTION

Hydrogen can be produced by the thermal or catalytic partial oxidation of hydrocarbons with oxygen or air. Most of the work in partial oxidation involved the thermal partial oxidation (TPO) processes that have been developed by Shell and Texaco (1,2) and have been applied industrially. However, a fair amount of soot is produced in the process and a considerable amount of processing equipment is required to remove the soot. The presence of a nickel catalyst has been found to permit operation at lower temperatures and without soot formation at the soot limit region (3). In light of this, hydrogen generation for fuel-cell and other small scale portable uses is being studied at JPL using the catalytic partial oxidation (CPO) of hydrocarbons.

The selective oxidation of various hydrocarbons to petrochemicals such as ethylene oxide, maleic or pthalic anhydride, butene, and formaldehyde have been studied extensively and are well covered in literature (4,5). The catalytic oxidation of hydrocarbons in low concentrations by noble metals such as Pt and Pd which is the basis for automobile emission control devices has been the subject of several fundamental studies (6-10). The catalytic partial oxidation of hydrocarbons for the production of hydrogen or synthesis gas has received only limited attention (11-15).

It differs from other oxidation processes in the catalyst (Ni) and the temperature range used (>700°C). However, these limited studies have not elucidated the fundamental aspects of the CPO of hydrocarbons.

In the present study, the CPO of methane is investigated by utilizing the high-activity catalysts which have been employed in the CPO process at JPL. The effect of process variables such as temperature and O_2/CH_4 ratio on the catalyst activity and product distribution are examined.

EXPERIMENTAL

A coprecipitated Ni/α-Al_2O_3 G-56B catalyst, containing 25% Ni, was supplied by the Girdler Catalyst Company (now United Catalyst Inc.). The catalyst total (BET) surface area was 58 m^2/g About 0.1g of crushes catalyst (60-80 mesh) was used for each loading.

The reactor consists of an alumina tube with a 0.47 cm. i.d. The temperature is measured by a movable axial chromel-alumel thermocouple in a 0.15 cm. quartz thermowell located in the center of the catalyst bed. The system has two independently controlled heating sections of 15 and 30 cm. length rated at 500 and 1000 watts repectively. The temperature in the catalyst bed is very close to the furnace temperature at low conversions. The reaction mixture contained H_2, O_2 and N_2 as diluent. CH_4 (Linde, 99.997% purity), N_2 (Linde, 99.996% purity) and O_2 (Amweld, 99.95% purity) were purified by passing through a dehydrated molecular sieve 13X. A schematic of this set up is shown in Fig. 1.

The product gases are passed through a drierite column and the dry product gases are analyzed by an HP 5830A gas chromatograph with a 10' carbosieve (100/120 mesh) column and a thermal conductivity detector. Using temperature programming from room temperature to 150°C (30°C/min.)

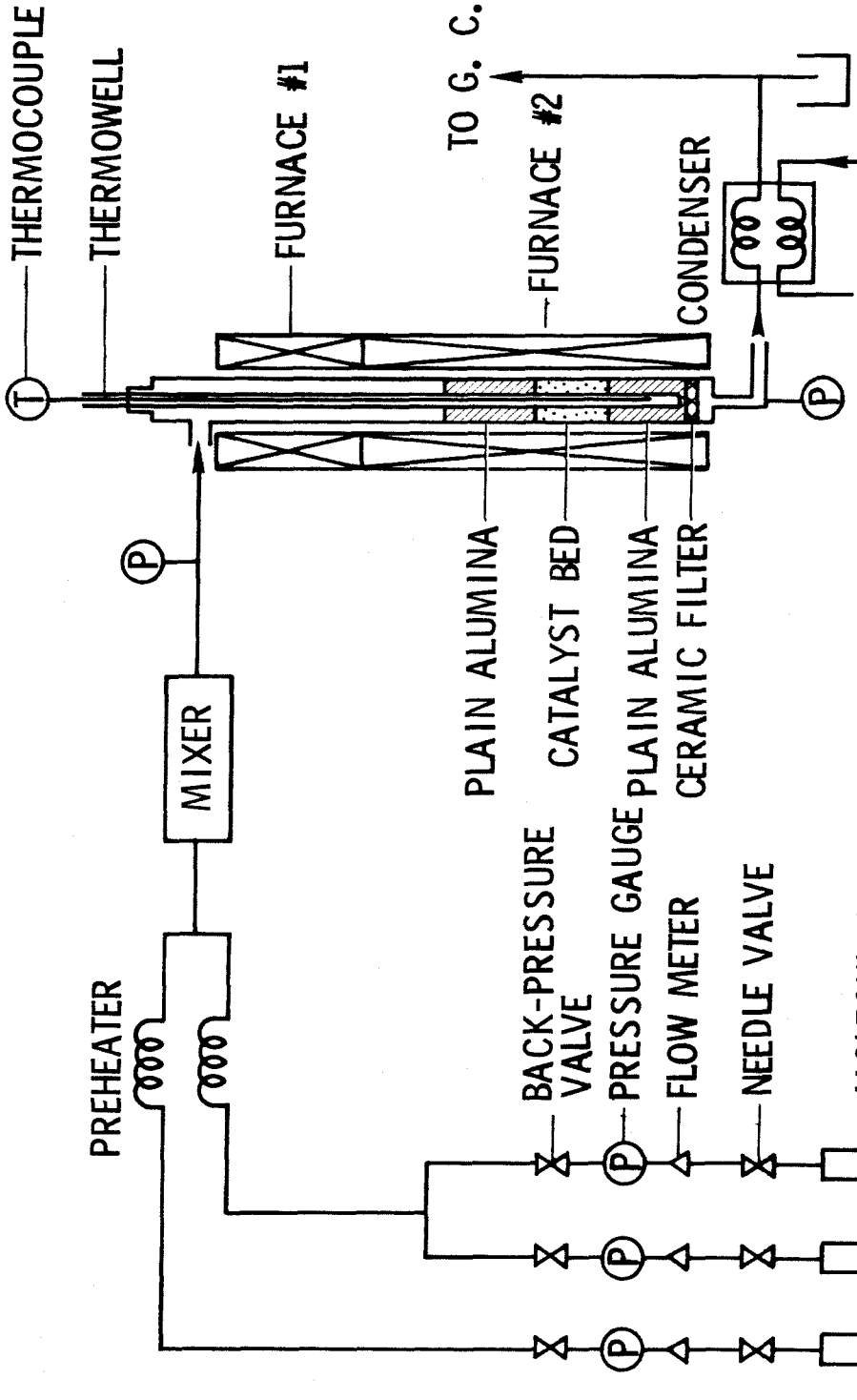

Fig. 1 Diagram of Experimental Apparatus

allows the separation of all products: O_2, N_2, CO, CO_2, H_2, CH_4. He (99.997% purity) was used as a carrier in the chromatography. Certified calibration gases (Scotty) were used for calibrating the gas chromatograph.

RESULTS

Effect of Temperature

In order to stabilize its activity, the catalyst was left under reactant flow at 700 ^{o}C for several hours prior to data collection. Since the catalyst bed is not isothermal under the experimental conditions employed, the percent of CH_4 consumed is shown with respect to furnace temperature (Fig. 2). The CH_4 consumption increases slightly with increasing temperature up to a critical temperature at which it increases abruptly to a higher level. As the temperature is decreased after reaching the high level of activity, a hysteresis is observed. The dry products composition is shown in Table 1 for a series of progressive reaction temperatures. At the "pre-light-off" conditions, only complete oxidation to CO_2 and H_2O takes place. Following light off, O_2 is completely consumed and CO and H_2 are the predominant products with some CO_2 and H_2O also formed. Prior to light-off, the temperature profile in the catalyst bed is broad, but following light-off, the temperature rises across a thin region (Fig. 3). This region is probably where most of the reaction takes place.

TABLE 1

Dry Products Composition
(mol %)

$T_{furnace}$ (°C)	T_{exit} (°C)	O_2	N_2	CH_4	CO_2	CO	H_2
696	716	5.92	68.15	19.39	6.54	—	—
718	730	4.82	68.94	18.98	7.27	—	—
740	755	—	53.49	0.58	3.89	16.55	25.49
700	725	—	54.24	1.06	4.47	15.81	24.43
675	699	—	55.70	1.72	5.00	15.29	22.29
640	670	—	58.12	2.85	5.95	14.08	19.00
612	654	—	60.76	4.07	7.04	12.68	15.45

Feed Composition: $(O_2) = 0.16$, $(CH_4) = 0.23$, (N_2) = balance;
SV = 100,000 hr^{-1}

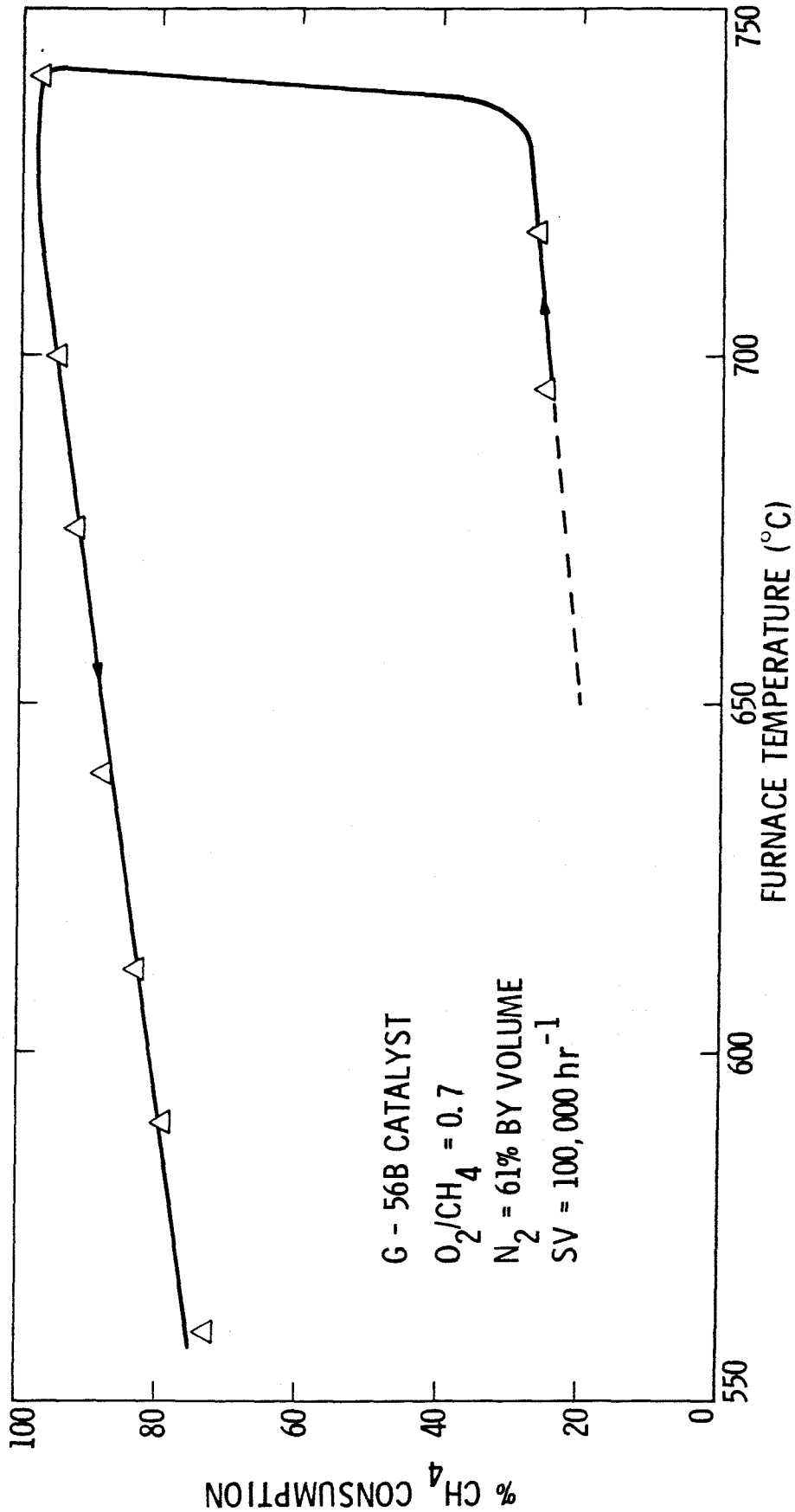

Fig. 2 Effect of Temperature on % CH_4 Consumption

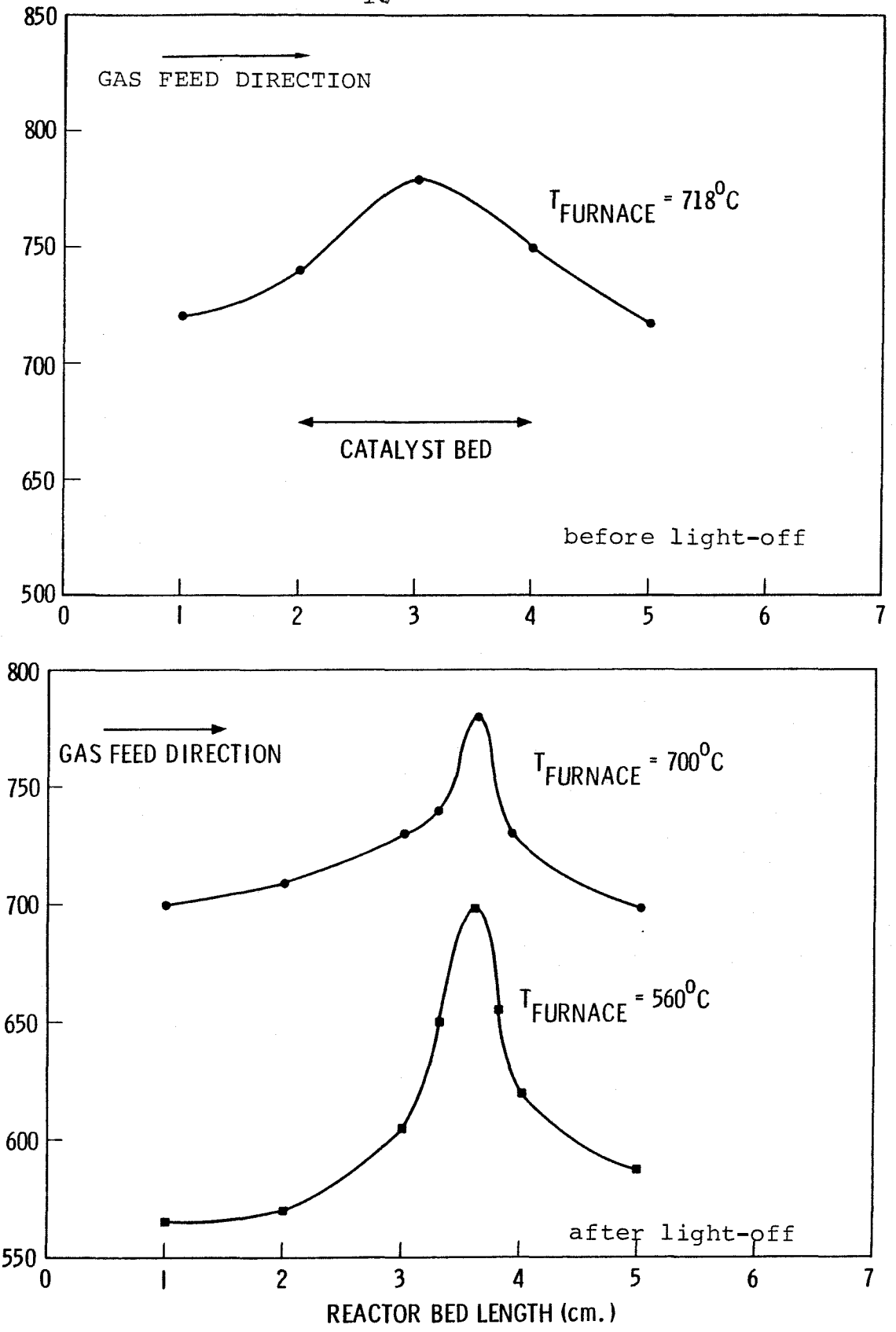

Fig. 3 Temperature Profile in the Catalyst Bed

Effect of O_2/CH_4 Ratio

In this experiment, the furnace temperature was fixed at 675°C. The mole fraction of O_2 at the inlet was varied while keeping the mole fraction of CH_4 fixed at 0.24. The N_2 flow was adjusted so that the space velocity stayed the same at all conditions. The percent of CH_4 consumed and the product yield are shown as a function of O_2 concentration in Figs. 4 and 5. Al low O_2/CH_4 ratios, the catalyst activity and the product distribution are similar to those following light-off. Upon increasing the O_2/CH_4 ratio, the CO/CO_2 in the product decreases (Fig. 5) and the position of the steep temperature gradient region is moved further down the bed (Fig. 6). At the O_2/CH_4 ratio of 1.43, this region is driven out of the catalyst bed and the CH_4 consumption drops suddenly from almost 100% to about 7%. At this point, only complete oxidation to CO_2 is observed similar to the pre-light-off condition.

bed (Fig. 6) increased with increasing O_2/CH_4 ratio. This indicates that the sudden drop in conversion was not due to thermal extinction in which the reaction rate drops suddenly when the catalyst temperature is decreased below the extinction temperature.

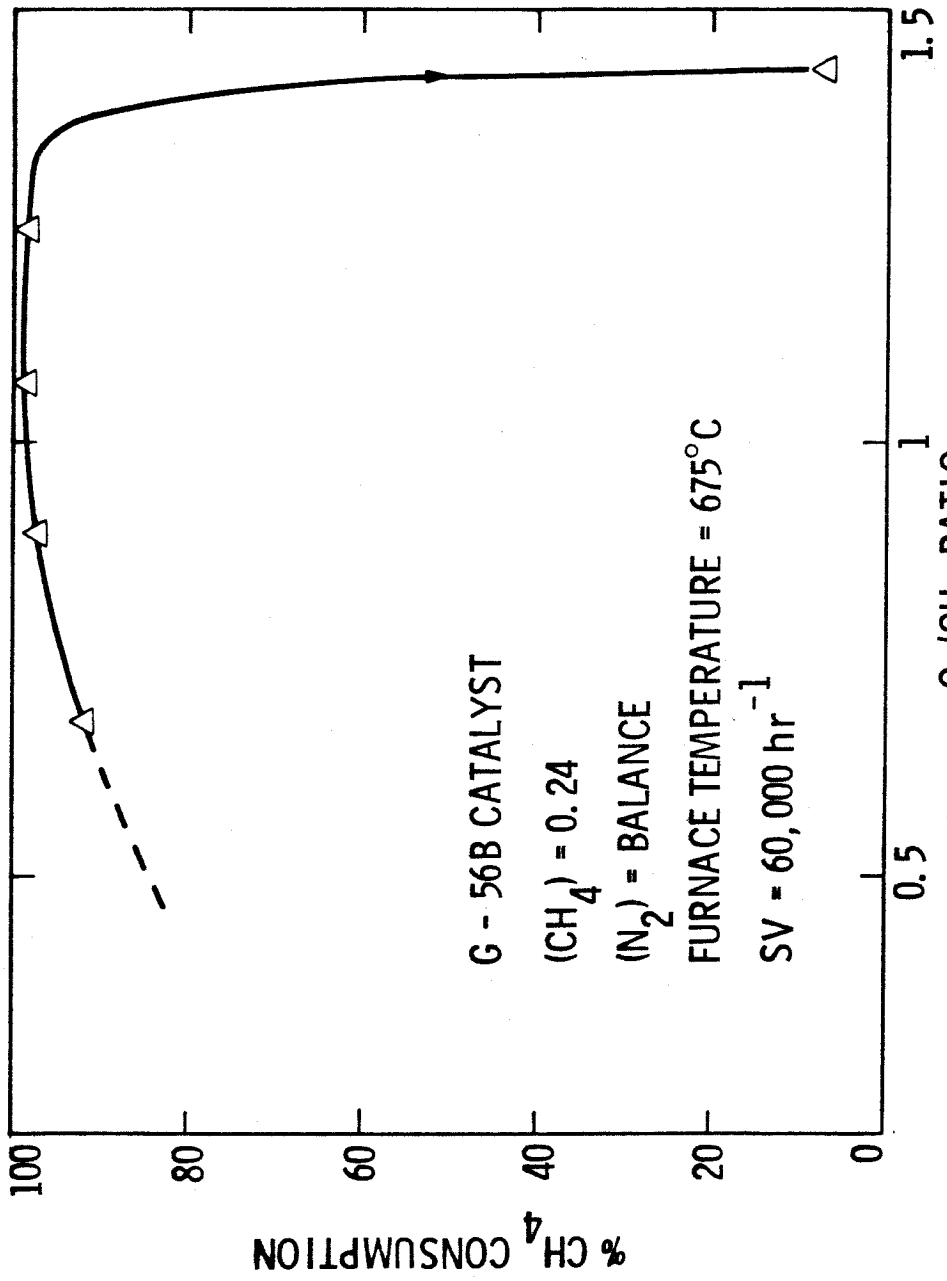

Fig. 4 Effect of O_2/CH_4 Ratio on % CH_4 Consumption

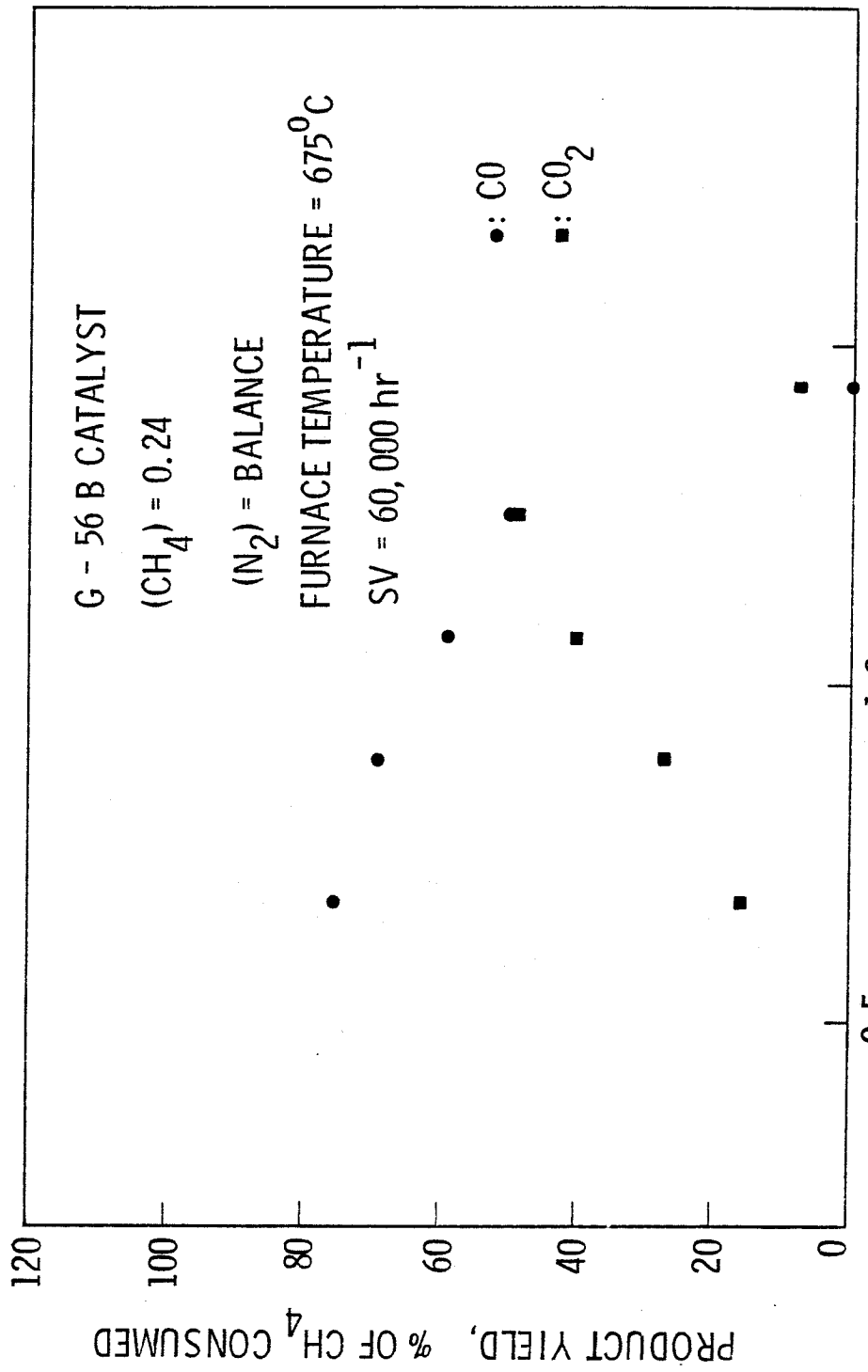

Fig. 5 Effect of O_2/CH_4 Ratio on the Product Yield

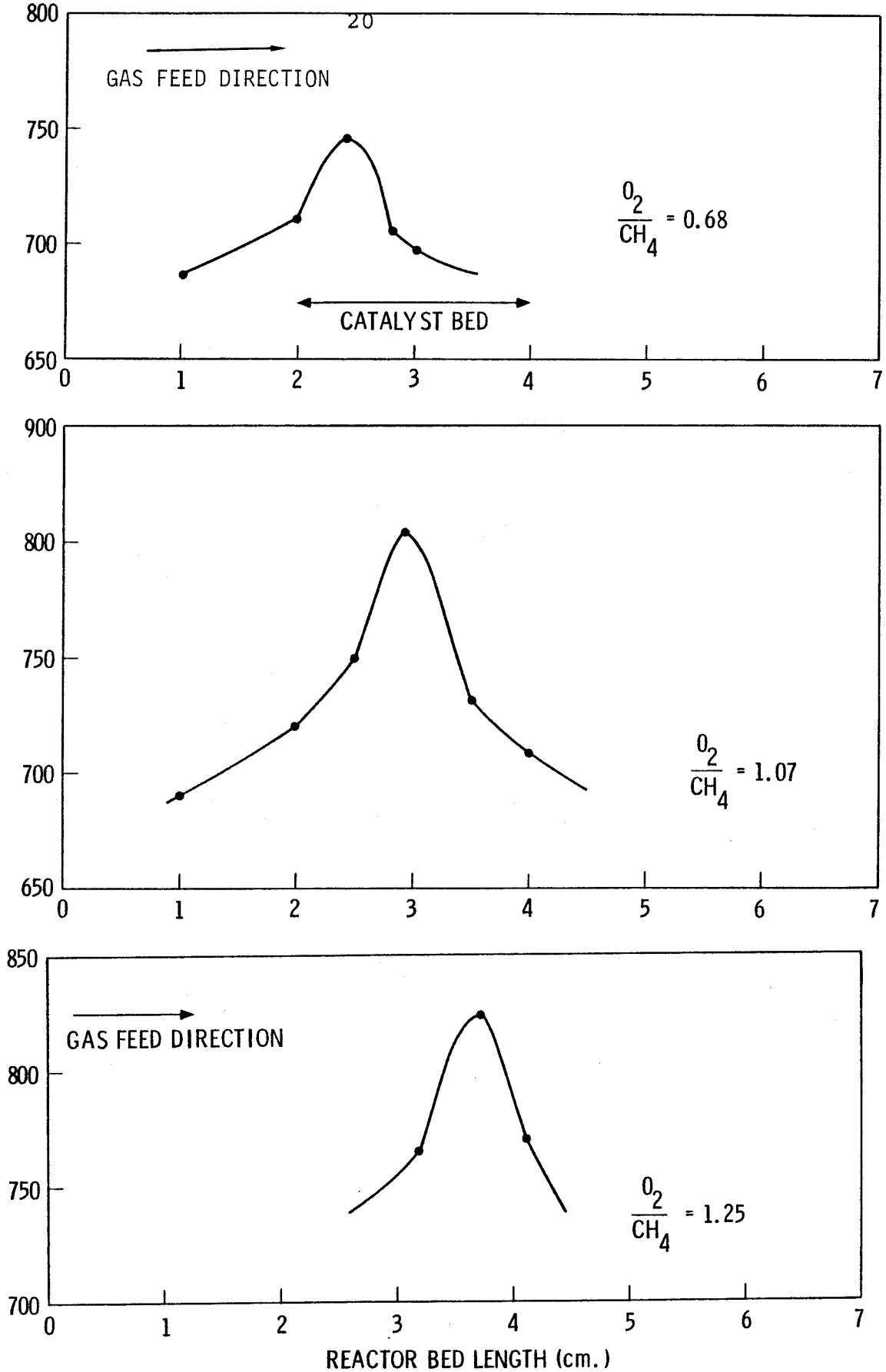

Fig. 6 Temperature Profiles at Different O_2/CH_4 Ratios

DISCUSSION

The role of a supported nickel catalyst on the reaction of methane-rich/oxygen mixtures has been investigated. The sudden change in the carbon oxide product distribution upon reaching a critical condition was observed. It is anticipated that this behavior is due to an in situ modification of the catalyst properties.

For the nickel oxidation reaction:

$$2\ Ni + O_2 \rightarrow 2\ NiO \qquad (1)$$

the dissociation pressures of NiO at various temperatures are shown in Table 2. Prior to light-off, O_2 partial pressure at the catalyst bed exit is much higher than the dissociation pressure (see Table 1). The O_2 partial pressure next to the catalyst can be calculated from:

$$rate_{O_2} = k_{O_2}(O_2^{b} - O_2^{*}) \qquad (A)$$

where $rate_{O_2}$ = rate of oxygen consumption

k_{O_2} = oxygen mass transfer coefficient

O_2^{b} = oxygen concentration in the bulk gas

O_2^{*} = oxygen concentration next to the catalyst surface

Preliminary calculation showed that O_2^{*} was about the same order of magnitude as O_2^{b} for the reaction under the pre-light-off condition. Therefore, the catalyst under the pre-light-off condition was in the NiO form throughout the bed.

TABLE 2

Dissociation Pressure of NiO as a Function of Temperature

T(^{o}C)	Dissociation Pressure (atm.)
600	1.46×10^{-19}
700	2.52×10^{-16}
800	2.86×10^{-14}
900	2.66×10^{-12}
1000	1.22×10^{-10}
1100	3.19×10^{-9}
1200	5.37×10^{-8}

From equation (A), the O_2^* is lower at higher rate of reaction. Since the rate of reaction is, among others, a function of the CH_4 partial pressure, the O_2^* will be a function of O_2/CH_4 ratio.

Following light-off, the equilibrium composition of CH_4, CO_2, CO and H_2 were calculated from the equilibrium constants of the following reactions:

$$CH_4 + H_2O \rightarrow CO + 3\ H_2 \qquad (2)$$

$$CO + H_2O \rightarrow CO_2 + H_2 \qquad (3)$$

In Table 3, the CO/CO_2 ratios (from Table 1) are compared with the thermodynamic equilibrium ratios at the catalyst bed exit temperature. Although the space velocity in the present study was extremely high (100,000 $hour^{-1}$), the CO/CO_2 ratios in the product following light-off was close to the equilibrium values. Under commercial operation in which the space velocity is much lower, the product composition should always be at equilibrium.

The reaction between hydrogen and oxygen:

$$H_2 + \tfrac{1}{2}\ O_2 \rightarrow H_2O \qquad (4)$$

is known to be much faster than reactions (2) and (3) and is most likely at equilibrium. The equilibrium partial pressures of O_2 have been calculated from the equlibrium concentrations of H_2 and H_2O and the equilibrium constants of the reaction (4). The equilibrium partial pressures of O_2 were several orders of magnitude lower than the NiO dissociation

TABLE 3

Comparison with Theoretical Thermodynamic Equilibrium

$T_{furnace}$ (°C)	T_{exit} (°C)	$(CO/CO_2)_{observed}$	$(CO/CO_2)_{equilibrium}$
740	755	4.25	5.25
700	725	3.54	4.53
675	699	3.06	3.88
640	670	2.37	3.15
612	654	1.80	2.75

Feed Composition: (O_2) = 0.16, (CH_4) = 0.23, (N_2) = balance;

SV = 100,000 hr^{-1}

pressure (Table 4). Therefore, following light-off, the catalysts downstream of the maximum temperature was in the metallic nickel form (Fig. 7).

The light-off phenomenon can be explained in terms of changes in the catalyst-oxygen interaction. Under the pre-light-off conditions, it can be seen from the stoichiometry of complete CH_4 oxidation:

$$CH_2 + 2O_2 \rightarrow CO_2 + 2H_2O$$

that the O_2/CH_4 ratio decreases with increasing extent of reaction. Thus the O_2^* decreases along the catalyst bed. Under the pre-light-off conditions, the O_2^* was higher than the dissociation pressure throughout the bed. Upon increasing the furnace temperature, the rate of reaction was increased. Consequently, the O_2^* was decreased. When the temperature was raised above the critical temperature, the O_2^* near the catalyst bed exit (where the O_2/CH_4 ratio is the smallest) became less than the dissociation pressure and NiO was reduced to metallic nickel. The activity of the metallic nickel is higher than that of the NiO and the consumption of CH_4 increased suddenly. This resulted in the temperature profile at the beginning of the metallic nickel zone becoming very steep.

A similar explanation can be given for the effect of O_2/CH_4 ratio at the inlet as Shown in Figs. 4 and 5. The light-off occured at low O_2/CH_4 ratios. When the O_2/CH_4 ratio at the inlet was increased, the extent of reaction had

TABLE 4

Equilibrium Partial Pressure of O_2 as a Function of Temperature

T_{exit} (^{o}C)	O_{2} equilibrium (atm.)
755	1.31×10^{-21}
725	2.24×10^{-22}
699	5.32×10^{-23}
670	9.15×10^{-24}
654	3.11×10^{-24}

Feed Composition: (O_2) = 0.16, (CH_4) = 0.23, (N_2) = balance

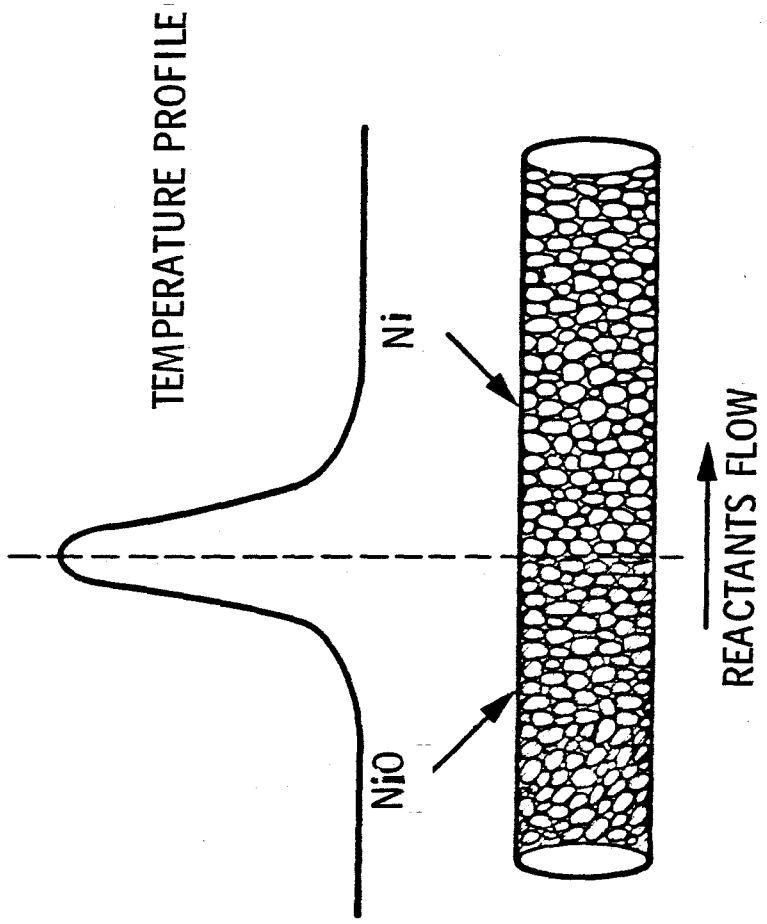

Fig. 7 The Nature of Catalyst After Light-Off

to increase before the O_2^* equaled the dissociation pressure. Consequently, the position of the steep temperature profile zone was moved further down the catalyst bed. When the O_2/CH_4 ratio at the inlet was too high, the O_2^* near the exit of the bed was still higher than the dissociation pressure. As a result, the metallic nickel zone could not exist in the bed and the reaction rate drops dramatically.

The observation that the CO/CO_2 ratio was less than the equilibrium value (Table 3) was consistent with the fact that CO_2 was the primary product formed in the NiO zone. In order to better understand the reaction mechanism in the metallic nickel zone, the % CO_2 conversion $[(CO_2)/(CH_4)_{inlet} \times 100]$ was calculated. In Table 5, it can be seen that the amount of CO_2 formed prior to light-off was higher than that after light-off. Thus, some CO_2 that had been formed in the NiO zone was consumed in the zone of metallic nickel.

Finally, it can be seen that the critical conditions for light-off are strongly dependent on the activity of NiO (upstream of the maximum temperature). When the activity of NiO is increased, the O_2/CH_4 ratio decreases more rapidly along the bed and the O_2^* is lower for a fixed O_2/CH_4 ratio. Accordingly, the light-off occurs at lower temperature and/or higher O_2/CH_4 ratio. After light-off, it can be seen

TABLE 5

Comparison of % CO_2 conversion before and after Light-off

	$T_{Furnace}$ (°C)	$\frac{(CO_2)}{(CH_4)_{inlet}} \times 100$
before light-off	696	25.2
	718	26.8
after light-off	740	18.51
	700	20.6
	675	22.7
	640	26.0
	612	29.6

that the maximum temperature also depends on the activity of NiO.

LITERATURE CITED

1. Noyes, R. Ammonia and Synthesis Gas, Chemical Process Mongraph, #26,]967
2. Kuhre, C.J. and Reed, C.L. Oil and Gas Journal, Jan. 12, 1976 p. 110
3. Houseman, J. and Cerini, D.J. "Onboard Hydrogen Generation for Automobiles", Jet Propulsion Laboratory NASA Contract NAS 7-100
4. Emmett, P.H., Catalysis Vol. VII, Rheinhold Publishing Corp. (1960)
5. Dadyburjor, D.B., Jewur, S.S. and Ruckenstein, E., Catal. Rev. Sci. Eng. 19 (2), 293 (1979)
6. Patterson, W.R. and Kemball, C., J. Catal. 2,465 (1965)
7. Mezaki, R. and Watson, Ind. Eng. Chem. Process Design Develop. 5,62 (1966)
8. Accomazzo, M.A. and Nobe, K., Ibid. 4,425 (1965)
9. Cullis, C.F. and Keene, D.E., J. Catal. 19,378 (1970)
10. Wei, J. Advan. Catal. 24, 57 (1975) and references therein
11. Yoshitomi, S., Morita, Y. and Yamamoto, K., Bull. Japan Petro. Inst. 4,15,(1962)
12. Schmulder, Brennstaff-Chemie, 46,23 (1965)
13. Prettre, M. et al. Trans. Faraday Soc. 42,335 (1946)
14. Peter, K. et al. Brennstoff-Chemie, 36,257 (1955)

15. Huszar, K., Racz, Gy, and Szekely, Gy, Acta. Chim. (Budapest) 70,4,287 (1971)

CHAPTER 3

Examination of Supported NiO Catalysts

ABSTRACT

A series of $NiO/\alpha\text{-}Al_2O_3$ and NiO/ZrO_2 catalysts were prepared by impregnation and calcination in air between 750 and 1050°C. Examination of the catalysts by means of the BET method, O_2 chemisorption, X-ray diffraction, electron microscopy and ESCA showed marked variations in physical properties as a function of calcination temperature. The results indicate that NiO does not interact with ZrO_2 whereas $NiO\text{-}Al_2O_3$ interaction is extensive above about 850°C. The results also indicate that the supported NiO particles are made up of a large number of small crystallites which disperse after reduction and agglomerate after reoxidation.

INTRODUCTION

The partial oxidation of hydrocarbons for the production of hydrogen has been demonstrated at the Jet Propulsion Laboratory (1) with a process development reactor utilizing Ni/Al_2O_3 catalysts. However, the activity of these catalysts was found to decrease slowly with time with an attendant decrease in reactor performance. To better understand how to maintain catalyst activity and reduce the severity of catalyst degradation, we have begun to study the relationship between the physicochemical properties of the catalyst and the activity for CH_4 oxidation of supported NiO catalysts.

An initial study of partial oxidation of CH_4 utilizing the Girdler nickel steam reforming catalyst G-56 B was reported in the previous chapter. This catalyst, however, was too active and the reaction temperature could not be controlled to maintain isothermal conditions. In the present study, several catalysts were prepared by impregnation of low surface area supports. These catalysts were then calcined in air at high temperatures commensurate with those typical of hydrocarbon partial oxidation. The study reported in this chapter deals with the physicochemical properties of these catalysts. The next chapter will report the activity of the same catalysts for CH_4 oxidation.

EXPERIMENTAL

Catalyst Preparation and Pretreatment

Three commercially available supports were crushed and screened to 60-80 U.S. mesh. Table 1 lists the supports and their properties.

The supports were impregnated with 2M $Ni(NO_3)_2$ solution at room temperature. After 15 minutes of impregnation, the solution was drained off and the sample was dried at 80-100^{o}C for 24 hours. The sample was then heated in air at 400^{o}C for 1 hour to decompose the $Ni(NO_3)_2$. This procedure was repeated several times to obtain the desired nickel weight percent. These catalysts which had not been heated above 400^{o}C were labeled as "non-calcined". Subsequent heating in air at 750 to 1050^{o}C of the non-calcined catalysts prepared from the T-61 α-Al_2O_3 and ZrO_2 supports provided the calcined catalyst samples.

Chemical Analyses

The amount of nickel as NiO was determined by acidic extraction of nickel from the support followed by dimethylglyoxime precipitation (2). The first step in the chemical analysis was to dissolve the NiO in 5N HCl. Since it is known (3-8) that NiO can react with the Al_2O_3 support to form $NiAl_2O_4$ (nickel aluminate spinel) at high temperatures, the nickel

TABLE 1

Properties of Supports

Support	Crystalline Compound	Total Surface Area (m^2/g)	Pore Volume (cc/g)
Alcoa T-61 α-Al_2O_3	α-Al_2O_3	0.11	0.015
Girdler T-375 α-Al_2O_3	α-Al_2O_3	3.88	0.27
Norton SZ5464 ZrO_2	ZrO_2	0.39	*

* Data not available

content which was available as nickel oxide was analyzed after the high temperature calcination. It has been shown in our laboratory that the nickel in the $NiAl_2O_4$ matrix is not extracted by this method. Hence, the difference in the nickel weight percent before and after the high temperature calcinations is the amount of nickel in the $NiAl_2O_4$ form. For comparison purposes, similar analyses were carried out for the zirconia-supported catalysts.

Total Surface Area Measurements

A Quantachrome Corp. Sorption System was used to measure the total (BET) surface area by N_2 adsorption by a continuous flow method (9). The application of the Brunauer-Emmet-Teller (BET) (10) equation to calculate the amount of monolayer adsorption is discussed in all modern texts on surface chemistry. In the present work, the effective cross sectional area of N_2 was taken as 16.2 A^2.

Nickel Surface Area Measurements

A pulse flow method based on chemisorption of oxygen at room temperature (11) was used to measure the nickel surface area. Ultra-pure helium (Linde, O_2<0.5 PPM) was used as the carrier gas. all the catalysts were reduced in flowing H_2 (20 cc/min) at 450^{o}C for 15 hours and then the

H_2 was flushed out with the He carrier gas at the same temperature for 1 hour. After the catalyst was cooled to room temperature, pulses of 0.5 to 2 cc of 1% O_2 in He were injected. The nickel surface area was calculated by assuming 1.3×10^{19} molecules of oxygen adsorbed on 1 m^2 of nickel surface (11) which is equivalent to two layers of epitaxial NiO (See Appendix I).

X-ray Diffraction Analyses

The crystalline compound and the average crystallite size of NiO were determined by X-ray diffraction analysis (XRD) using a G.E. XRD spectrometer with Ni filter and CuK_α radiation.

The mean dimension (D) of the crystallites is related to the pure X-ray broadening (β) by the Scherrer formula (12):

$$D = K\lambda/\beta \cos\theta$$

In the present work, D was defined as $(\text{volume})^{1/3}$ and this leads to the value of $K \simeq 0.95$ (13-15) when β is defined as the half-maximum line width. The half-maximum line width from NiO (220) and NiO (111) reflecting planes were employed for the alumina-supported and zirconia-supported catalysts respectively to eliminate overlap with support-derived peaks. The instrumental line broadening is determined from the half-maximum line width of a single silicon crystal.

SEM Studies

The catlysts were studied using an AMR 900 scanning electron microscope which has a resolution of about 500-1000 A^{O}. The samples were coated with gold to about 100-200 A^{O} thickness prior to observation.

ESCA Studies

ESCA spectra were obtained using a HP 5950 B ESCA spectrometer. The sample chamber was pumped to a pressure of 5×10^{-9} torr and a monochromatized AlK_{α} exciting radiation was used.

All samples were dusted onto a double-sided adhesive taped onto a gold-plated copper sample holder. The electron binding energies for the $Ni(2P_{3/2})$, O(1S) and Al(2P) were recorded and compared with those for the NiO and $NiAl_2O_4$ standards. Since the standards and the catalysts built up a charge from 1-3 e.v. due to their insulating nature, the displacement of the binding energy of the contaminant C(1S) peak from a standard value of 284.6 e.v. was used for correction. of 284.6 e.v. was used for correction.

The NiO standard used was a commercially available, high purity NiO powder (Ventron Corp., 99.99% purity). The $NiAl_2O_4$ standard was prepared by calcination of the non-calcined NiO/T-375 α-Al_2O_3 catalyst in air at 1370^{O}C

for 50 hours. After calcination, the XRD spectrum (Fig.1) and the chemical analysis showed that $NiAl_2O_4$ was the only compound of nickel. The properties of the $NiAl_2O_4$ standard are shown in Table 2.

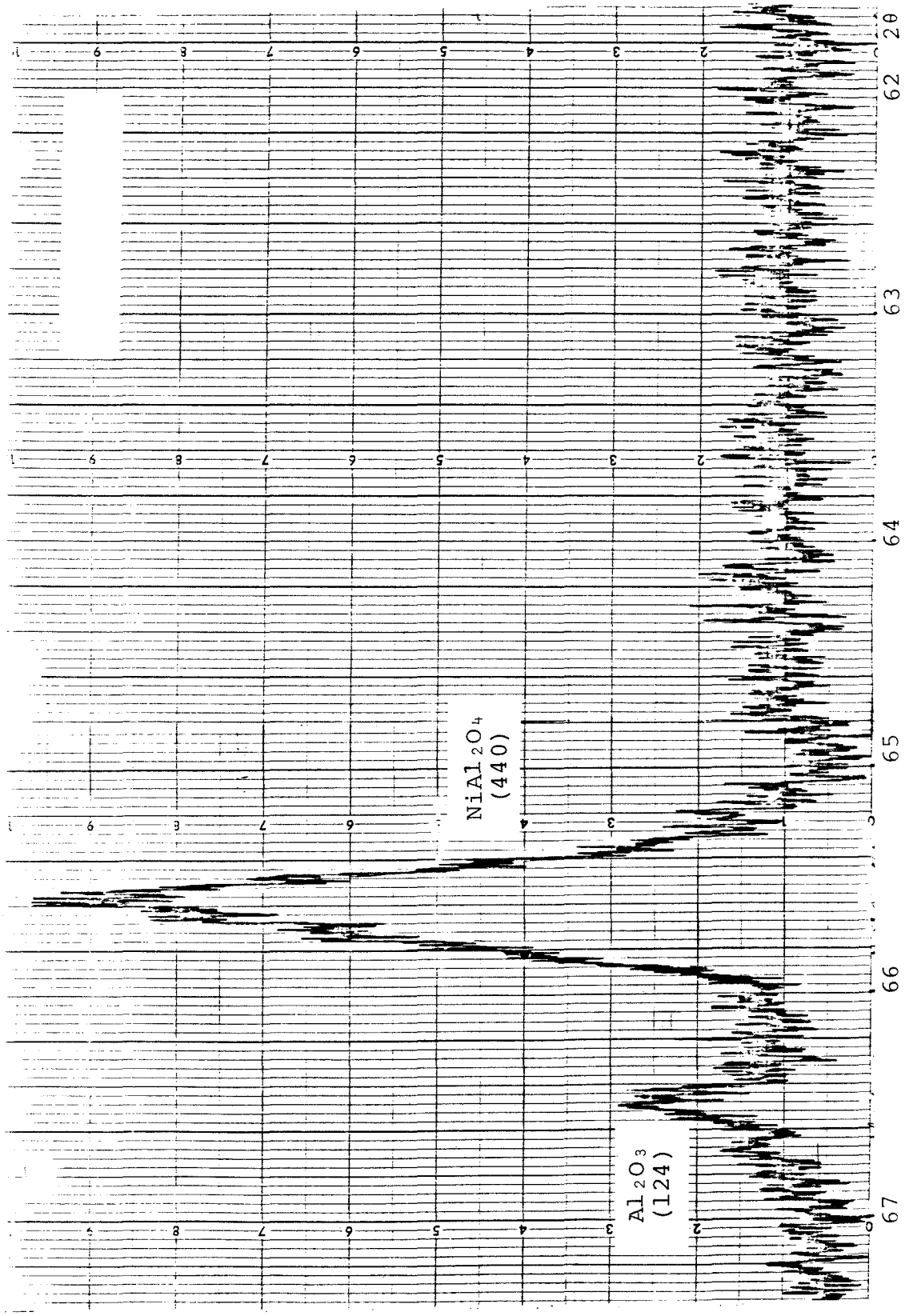

Fig. 1 XRD Spectrum of the $NiAl_2O_4$ Standard

TABLE 2

Properties of $NiAl_2O_4$ Standard

Support	T-375 α-Al_2O_3
Ni Wt. % [a]	17.3
Total Surface Area	2.37 m^2/g
Average Crystallite Size of $NiAl_2O_4$	630 A^O
XRD Crystalline Compound	$NiAl_2O_4$, α-Al_2O_3
Color	Blue

a Chemical analysis prior to calcination

RESULTS

The calcination procedures and properties of various catalysts are shown in Table 3 to 6. Chemical analyses have shown that the nickel weight percent of the NiO/ZrO_2 catalysts before and after calcination are the same in all cases. Further evidence of any chemical reaction between NiO and ZrO_2 to form $Zr_{0.67}Ni_{0.22}O_{0.11}$ (Zirconium Nickel Oxide) was sought with XRD but no characteristic lines were observed in the spectra. On the contrary, chemical analyses of the $NiO/\alpha\text{-}Al_2O_3$-950 and $NiO/\alpha\text{-}Al_2O_3$-1050 catalysts show that a significant amount of NiO reacts with the Al_2O_3 support to form $NiAl_2O_4$ and the interation is more extensive at higher temperature. Since the XRD spectra of these catalysts do not show the lines that are attributed to the $NiAl_2O_4$, it is assumed that the $NiAl_2O_4$ must be in an amorphous state (crystallite size <50-100 A^{O}). The XRD spectrum of the $NiO/\alpha\text{-}Al_2O_3$-1050 is shown as an example in Fig. 2.

The average crystallite size of NiO on both the $NiO/\alpha\text{-}Al_2O_3$ and NiO/ZrO_2 catalysts, estimated from X-ray line broadening, is not affected by the calcinations. A slight decline in the average crystallite size of NiO is observed in the $NiO/\alpha\text{-}Al_2O_3$-950 and $NiO/\alpha\text{-}Al_2O_3$-1050 catalysts for which the $NiAl_2O_4$ formation is extensive.

TABLE 3

Properties of Zirconia-Supported Catalysts

Catalyst	Support	Ni Wt. % (Prior to Calcination)	Calcination in air	Ni Wt. % (After Calcination)	D^{a}_{NiO}	XRD (Crystalline Compound)	Color
NiO/ZrO_2 (Non-calcined)	SZ5464 Zirconia	6.6	None	6.6	440	NiO, ZrO_2	Black
NiO/ZrO_2-750	SZ5464 Zirconia	6.6	750°C, 15 hours	6.6	440	NiO, ZrO_2	Gray
NiO/ZrO_2-850	SZ5464 Zirconia	6.6	850°C, 15 hours	6.6	440	NiO, ZrO_2	Gray
NiO/ZrO_2-950	SZ5464 Zirconia	6.6	950°C, 15 hours	6.6	440	NiO, ZrO_2	Gray
NiO/ZrO_2-1050	SZ5464 Zirconia	6.6	1050°C, 15 hours	6.6	440	NiO, ZrO_2	Grayish-yellow

a Average NiO crystallite size estimated form X-Ray line broadening

TABLE 4

Physical Properties of Alumina-Supported Catalysts

Catalyst	Support	Ni Wt. % (prior to calcination)	Calcination in air	Ni Wt. % (after calcination)	D^{a}_{NiO} (A°)	XRD (crystalline compound)	Color
$NiO/\alpha\text{-}Al_2O_3$ (non-calcined)	T-61 $\alpha\text{-}Al_2O_3$	2.20	None	2.20	300	NiO, $\alpha\text{-}Al_2O_3$	Black
$NiO/\alpha\text{-}Al_2O_3$-750	T-61 $\alpha\text{-}Al_2O_3$	2.20	750 C, 2 hours	2.20	300	NiO, $\alpha\text{-}Al_2O_3$	Gray
$NiO/\alpha\text{-}Al_2O_3$-850	T-61 $\alpha\text{-}Al_2O_3$	2.20	850 C, 3hours	2.20	300	NiO, $\alpha\text{-}Al_2O_3$	Gray
$NiO/\alpha\text{-}Al_2O_3$-950	T-61 $\alpha\text{-}Al_2O_3$	2.20	950 C, 15 hours	1.54	290	NiO, $\alpha\text{-}Al_2O_3$	Green
$NiO/\alpha\text{-}Al_2O_3$-1050	T-61 $\alpha\text{-}Al_2O_3$	2.20	1050 C, 15 hours	1.29	290	NiO, $\alpha\text{-}Al_2O_3$	Greenish-blue

a Average NiO crystallite size estimated from X-Ray line broadening

TABLE 5

Ni and Total Surface Area of Zirconia-Supported Catalysts

Catalyst	Ni Surface Area (m^2/g)	Total Surface Area (m^2/g)		
		Before Reduction	After Reduction	After Reoxidation [a]
NiO/ZrO_2-750	0.45	0.53	0.78	*
NiO/ZrO_2-850	0.49	0.47	0.81	0.49
NiO/ZrO_2-950	0.61	0.42	0.93	0.53
NiO/ZrO_2-1050	0.85	0.34	1.13	0.59

* Data not available

a In air at 500°C, 3 hours

TABLE 6

Ni and Total Surface Area of Alumina-Supported Catalysts

Catalyst	Ni Surface Area (m^2/g)	Total Surface Area (m^2/g)		
		Before Reduction	After Reduction	After Reoxidation [a]
$NiO/\alpha\text{-}Al_2O_3\text{-}750$	0.24	0.38	0.44	*
$NiO/\alpha\text{-}Al_2O_3\text{-}850$	0.30	0.24	0.45	0.25
$NiO/\alpha\text{-}Al_2O_3\text{-}950$	0.15	0.15	0.24	*
$NiO/\alpha\text{-}Al_2O_3\text{-}1050$	0.12	0.10	0.20	0.10

* Data not available

a In air at 500°C, 3 hours

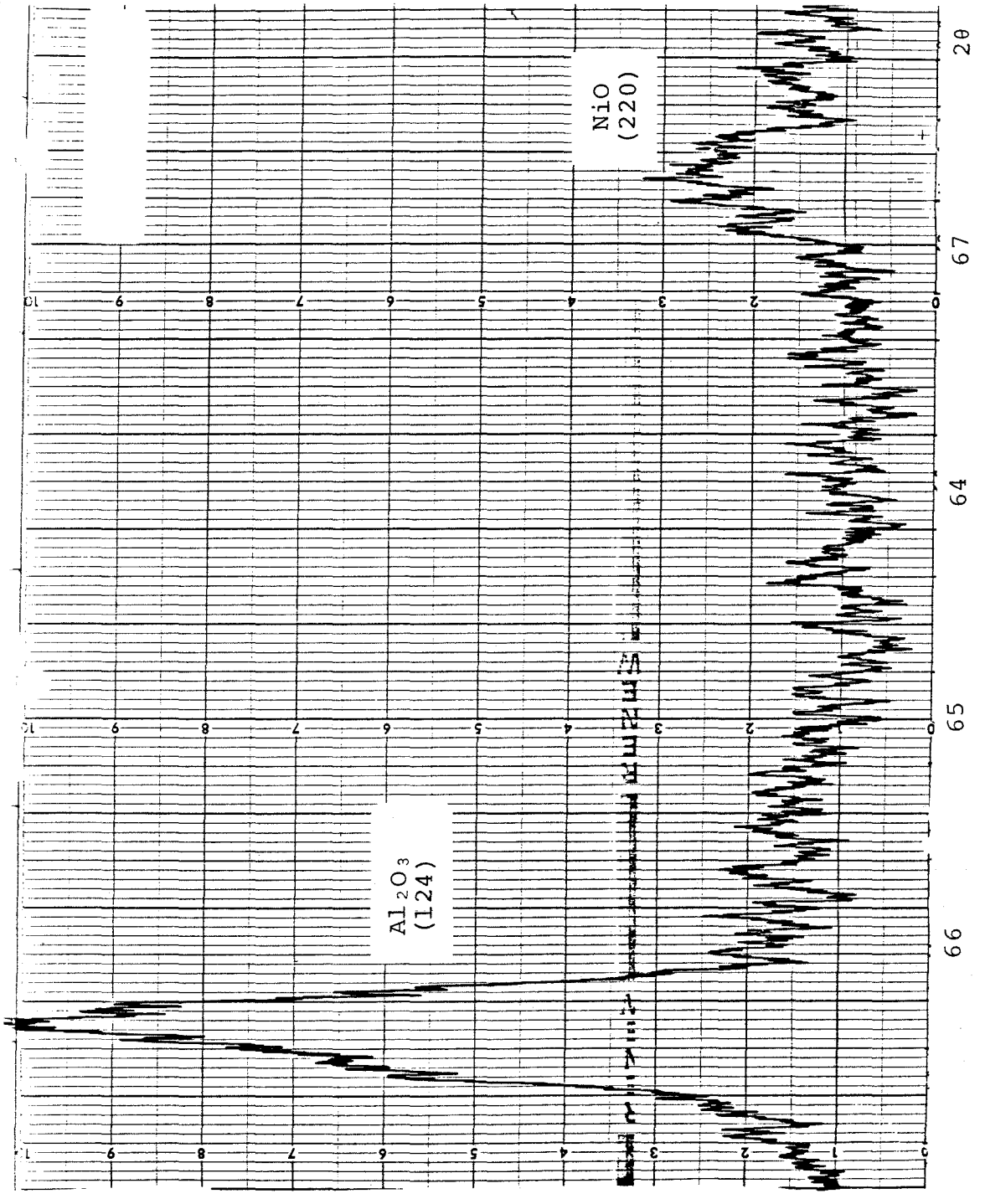

Fig. 2 XRD Spectrum of the NiO/α-Al_2O_3-1050 Catalyst

The nickel surface area of NiO/ZrO_2 catalysts increases with increasing calcination temperature. The nickel surface area of $NiO/\alpha\text{-}Al_2O_3$ catalysts increases with increasing calcination temperature up to about $850^{\circ}C$. Above about $850^{\circ}C$ at which temperature the $NiAl_2O_4$ formation becomes significant, the nickel surface area decreases with increasing calcination temperature.

As expected, the total surface areas of $NiO/\alpha\text{-}Al_2O_3$ and NiO/ZrO_2 catalysts decrease with increase in calcination temperature. In order to better understand the properties of catalysts after reduction, the total surface area of the reduced catalysts was also measured. It has been found that a monolayer chemisorption of O_2 does not affect the total surface area of the reduced catalysts. Thus, the total surface areas of the reduced catalysts were measured in situ after the O_2 chemisorption experiments. The total surface areas after reduction are also much higher than those prior to reduction. An increase in the total surface area after reduction, however, is not observed with the ZrO_2 and the Al_2O_3 supports that have been previously calcined at $1050^{\circ}C$ for 15 hours. Similar to the nickel surface area, the total surface area of reduced NiO/ZrO_2 catalysts increases with increasing calcination temperature. The total surface area of reduced $NiO/\alpha\text{-}Al_2O_3$ catalysts

increases with increasing calcination temperature up to about 850°C and then decreases. The reduced catalysts were reoxidized in air at 500°C for 3 hours. From the reported nickel oxidation rates (16), these catalysts were completely reoxidized by this procedure. The total surface areas were again measured and it was found that after reoxidation they are much lower than after reduction but slightly higher than prior to reduction.

The non-calcined NiO/ZrO_2 catalyst is black. After calcination between 750 and 950°C, the catalyst becomes gray and a grayish-yellow catalyst is obtained at 1050°C. Similarly, the non-calcined $NiO/\alpha\text{-}Al_2O_3$ catalyst is black. After calcination at 750 and 850°C, the catalyst becomes gray. However, after calcination at 950 and 1050°C green and greenish-blue catalysts, respectively, are obtained. Although these catalysts have been kept in an air atmosphere at room temperature for several months, their color remained unchanged. However, after the reduction and reoxidation as indicated earlier, all catalysts became black. The significance of catalyst color will be discussed in some detail later on.

SEM

The surface of the T-61α-Al_2O_3 support has been examined by SEM and found to be quite smooth as shown in Fig. 3a and 3b. The catalysts on this support were also examined by SEM. For each catalyst, several catalyst particles were examined and appeared to be quite uniform in terms of NiO coverage and particle size. Thus, the following electron micrographs are representative of the respective catalyst.

In the micrographs of the NiO/α-Al_2O_3 750, 850 and 1050 catalysts (Fig. 4 to 6), irregular NiO particles of about 1000-2000 A° sizes can be identified. These NiO particle sizes are much larger than the average crystallite size of 300 A° estimated from X-ray line broadening. The surface coverage of the support by NiO is very extensive and a large number of NiO particles are contacting each other. For the sample that has been calcined at higher temperature, the NiO particles are more rounded, and contacts of the NiO particles with each other and with the Al_2O_3 support are more intimate. As a result, the surface appears smoother. The NiO particle size appears unaffected by the calcinations.

a)

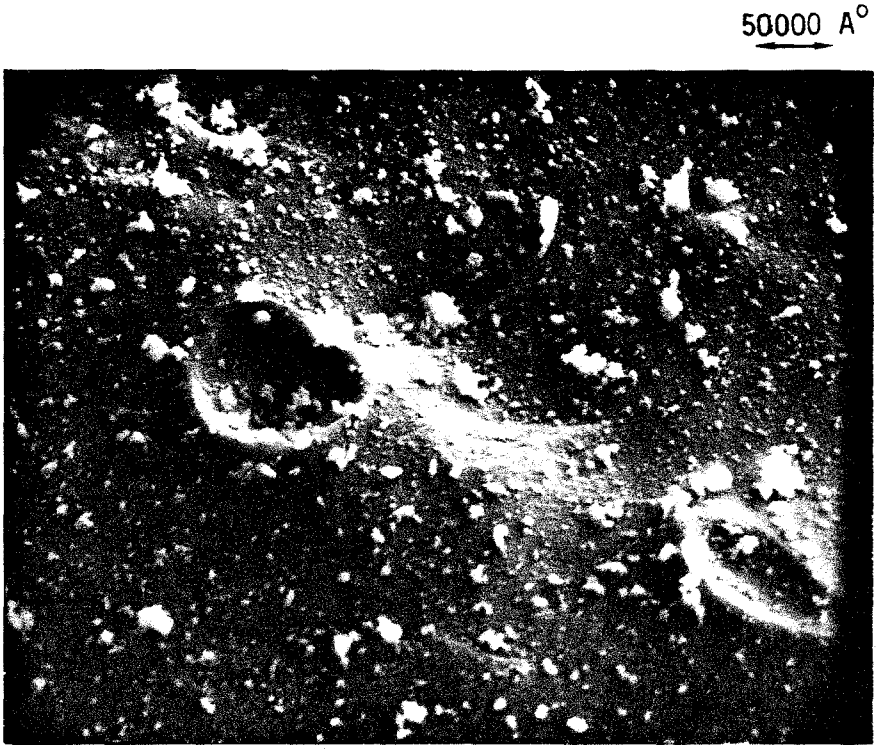

b)

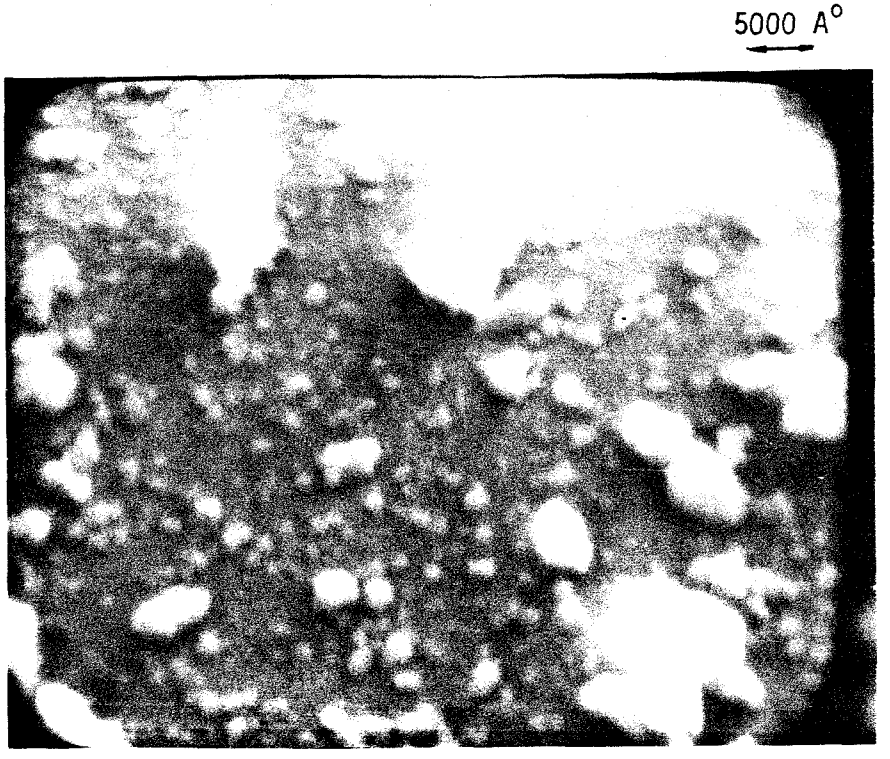

Fig. 3 Micrographs of T-61 α-Al_2O_3 at 2000X (a) and 20000X (b)

a)

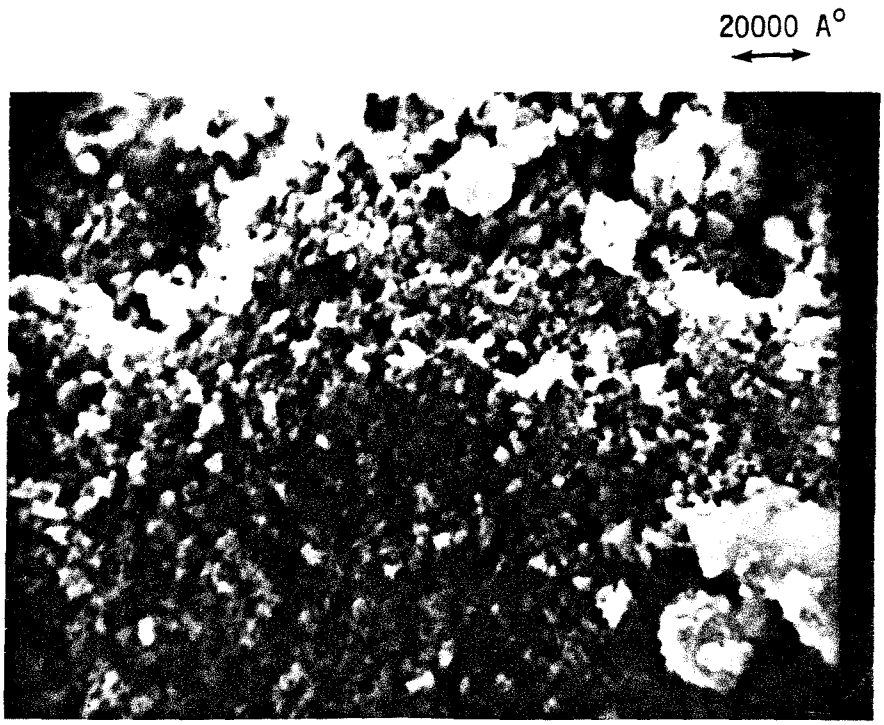

b)

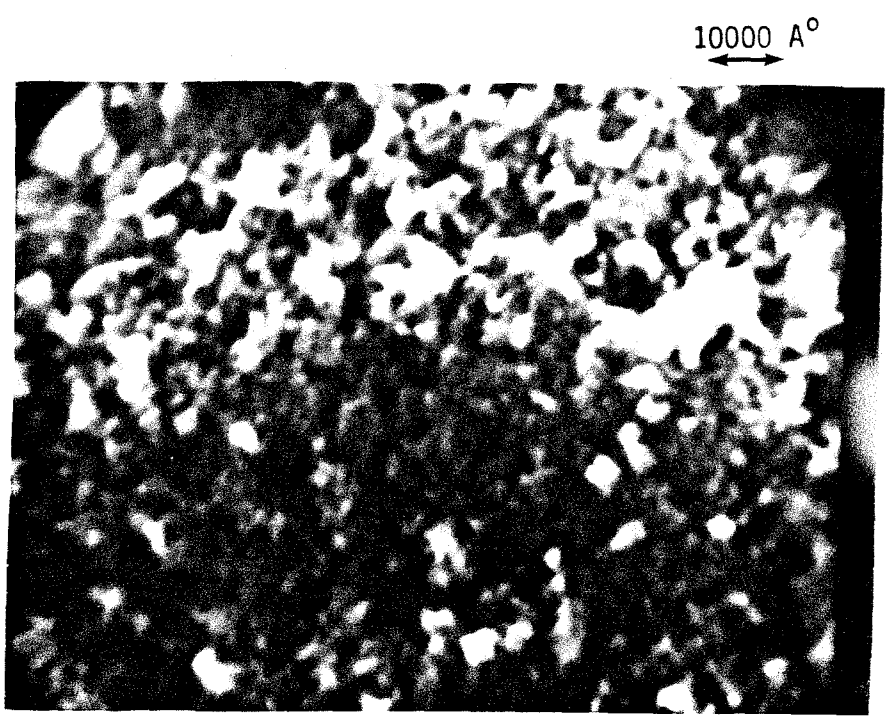

Fig. 4 Micrographs of $NiO/\alpha\text{-}Al_2O_3$-750 catalyst at 5000X (a) and 10000X (b)

a)

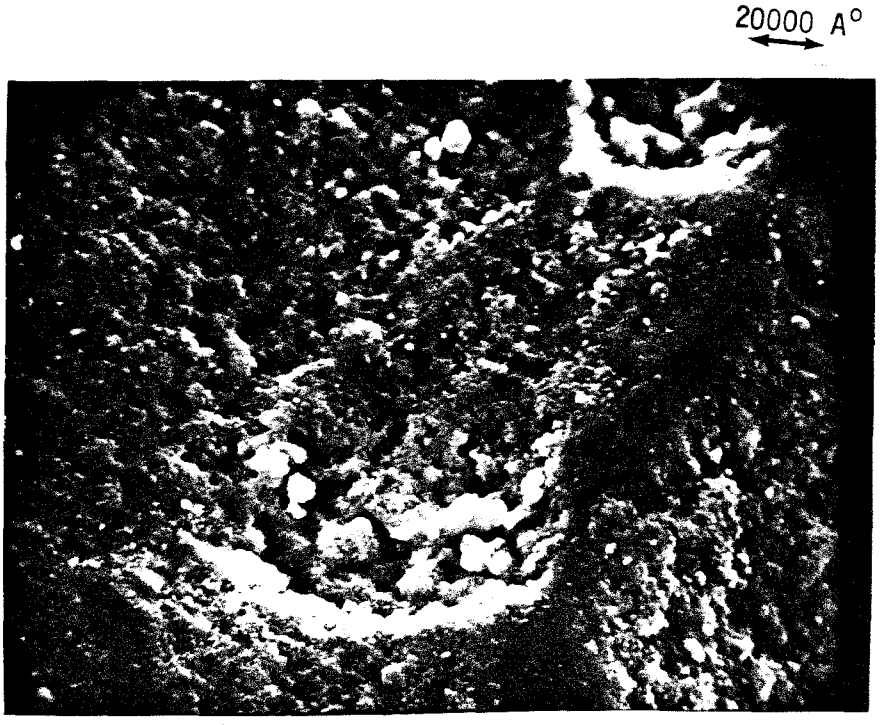

b)

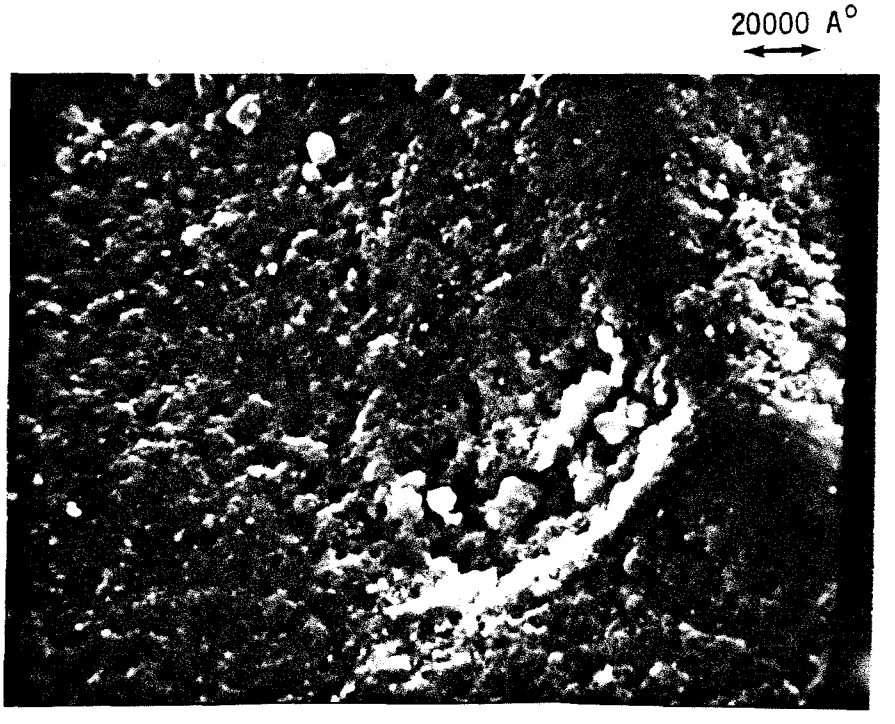

Fig. 5 Micrographs of $NiO/\alpha\text{-}Al_2O_3$-850 catalyst at 5000X

a)

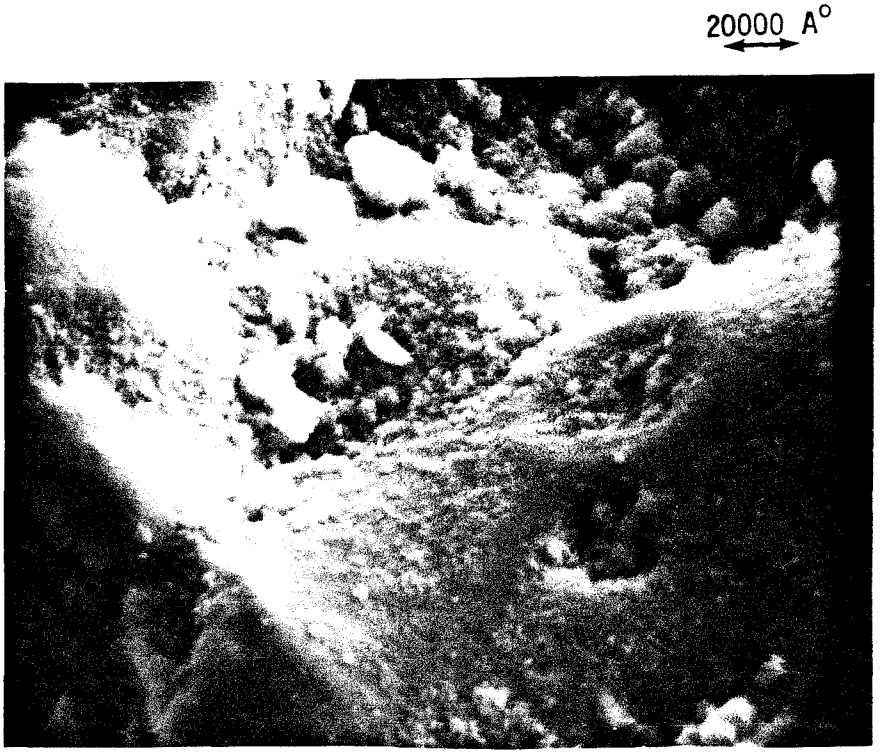

b)

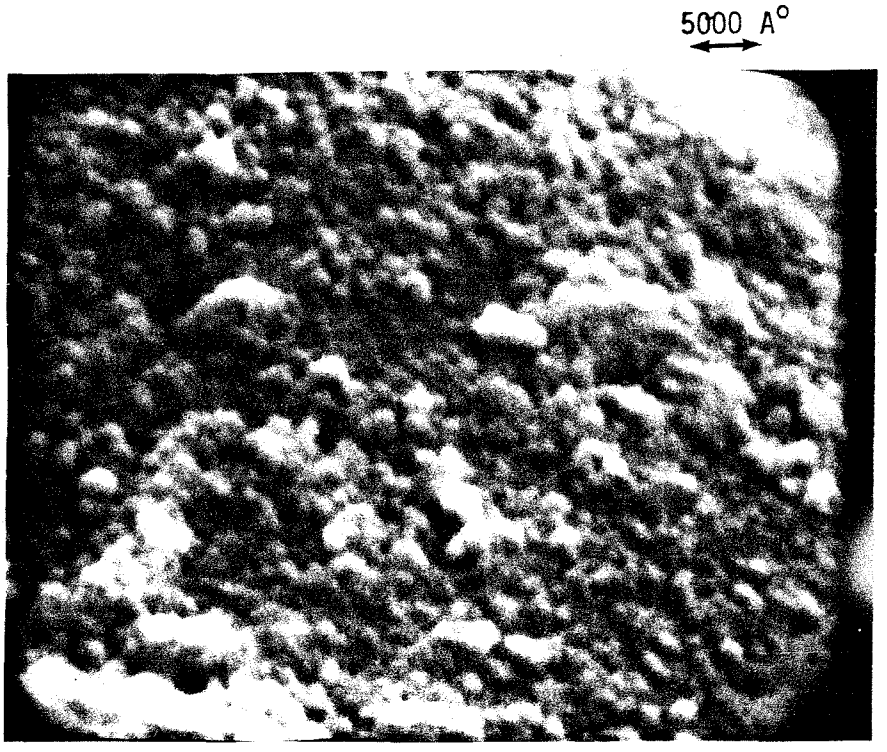

Fig. 6 Micrographs of $NiO/\alpha\text{-}Al_2O_3$-1050 catalyst at 5000X (a) and 20000X (B)

ESCA

The $NiO/\alpha\text{-}Al_2O_3$-850 and $NiO/\alpha\text{-}Al_2O_3$-1050 catalysts were studied by ESCA. In order to search for amorphous $NiAl_2O_4$ by ESCA, the $NiO/\alpha\text{-}Al_2O_3$-1050 catalyst from which the NiO has been dissolved in a dilute acid was also studied.

The surface elemental compositions are shown in Table 7. They reveal only Ni, O and Al for the $NiO/\alpha\text{-}Al_2O_3$-850 catalyst and additional traces of Ca and Na for the $NiO/\alpha\text{-}Al_2O_3$-1050 catalyst. Thus, the catalysts prepared and calcined in our laboratory are free from any foreign metals that can affect the overall catalytic activity.

The electron binding energies for the standard samples and the catalysts are shown in Tables 8 and 9. Figs. 7 to 9 show the spectra of interest in all samples. The results, corrected according to the C(1S) peak position, are described below:

a) NiO Standard

The $Ni(2P_{3/2})$ spectrum has a principal peak at 854.4 e.v. and is accompanied by a satellite shoulder at 855.9 e.v. The origin of the shoulder is still a matter of debate (17). Wertheim and Hufner (18) have suggested that the shoulder is due to the shake-up transition $d^8 \rightarrow d^{8*}$. Kim and Davis (19) have suggested that the shoulder is due to the exchange interaction of 2P and 3d electrons. A broad satellite peak at 861.4 e.v. is also observed.

TABLE 7

Surface Elemental Compositions
(At. %)

Sample	Ni	Al	O	C	Na	Ca	Ti	Cl	Ni/Al
NiO	33.	-	43.	23.	-	-	-	1.2	-
$NiAl_2O_4$	4.0	24.	52.	19.	-	-	0.2	-	0.17
NiO/α-Al_2O_3-850	24.	∿14.	42.	20.	-	-	-	-	∿1.71
NiO/α-Al_2O_3-1050	15.	15.	48.	21.	0.9	0.5	-	-	1.00
NiO/α-Al_2O_3-1050 (NiO extracted)	8.9	21.	51.	18.	1.1	-	-	-	0.42

Note: Values followed by (-) indicates no observation of signal; (∿) indicates an approximate value.

TABLE 8

Electron Binding Energies for Standard Samples
(e.v.)

Sample	$Ni(2P_{3/2})$	O(1S)	Al(2P)	S
NiO	854.4(P)	529.4(P)	-	325
	855.7	531.4		
	861.4			
$NiAl_2O_4$	856.7(P)	531.3	74.5	325.4

S $Ni(2P_{3/2})$-O(1S) binding energy separation (principal peaks)

P principal peaks

TABLE 9

Electron Binding Energies of the Catalysts
(e.v.)

Catalyst	Ni($2P_{3/2}$)	O(1S)	Al(2P)	S
NiO/α-Al_2O_3-850	854.9(P)	530.0(P)	73.5	324.9
	856.5	b		
	861.8			
NiO/α-Al_2O_3-1050	855.2(P)	530.4(P)	73.8	324.8
	856.6	b		
	861.8			
NiO/α-Al_2O_3-1050 (NiO extracted)	856.1(P)	530.7	73.8	325.4
	862.1			

S Ni($2P_{3/2}$)-O(1S) binding energy separation (principal peaks)

P principal peak

b A broad satellite shoulder

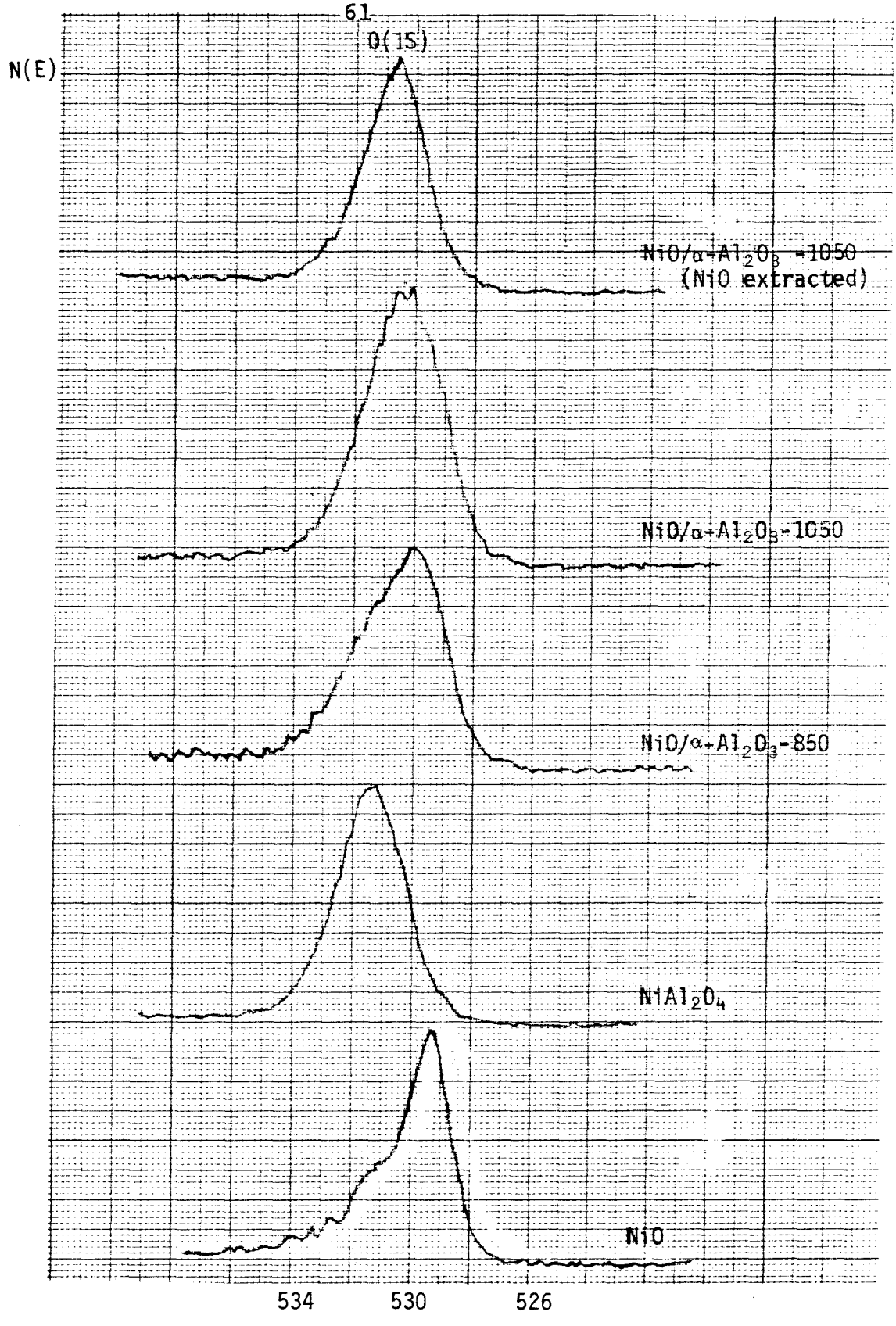

Fig. 7 The O(1S) core level peak for the catalysts and the standard samples. All binding energies are corrected for charging (C(1S) = 284.6 e.v.).

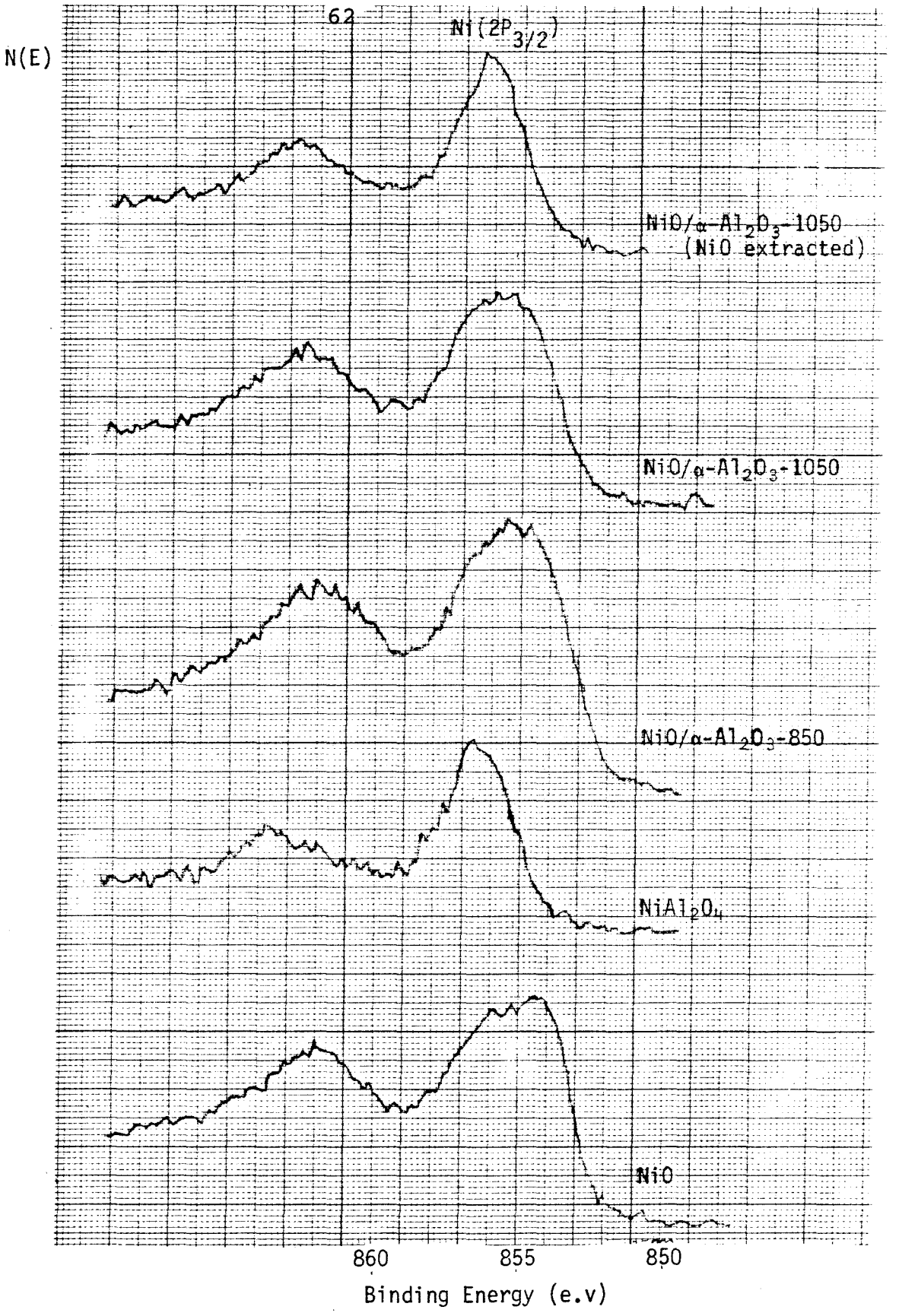

Fig. 8 The $Ni(2P_{3/2})$ core level peak for the catalysts and the standard samples. All binding energies are corrected for charging (C(1S) = 284.6 e.v.).

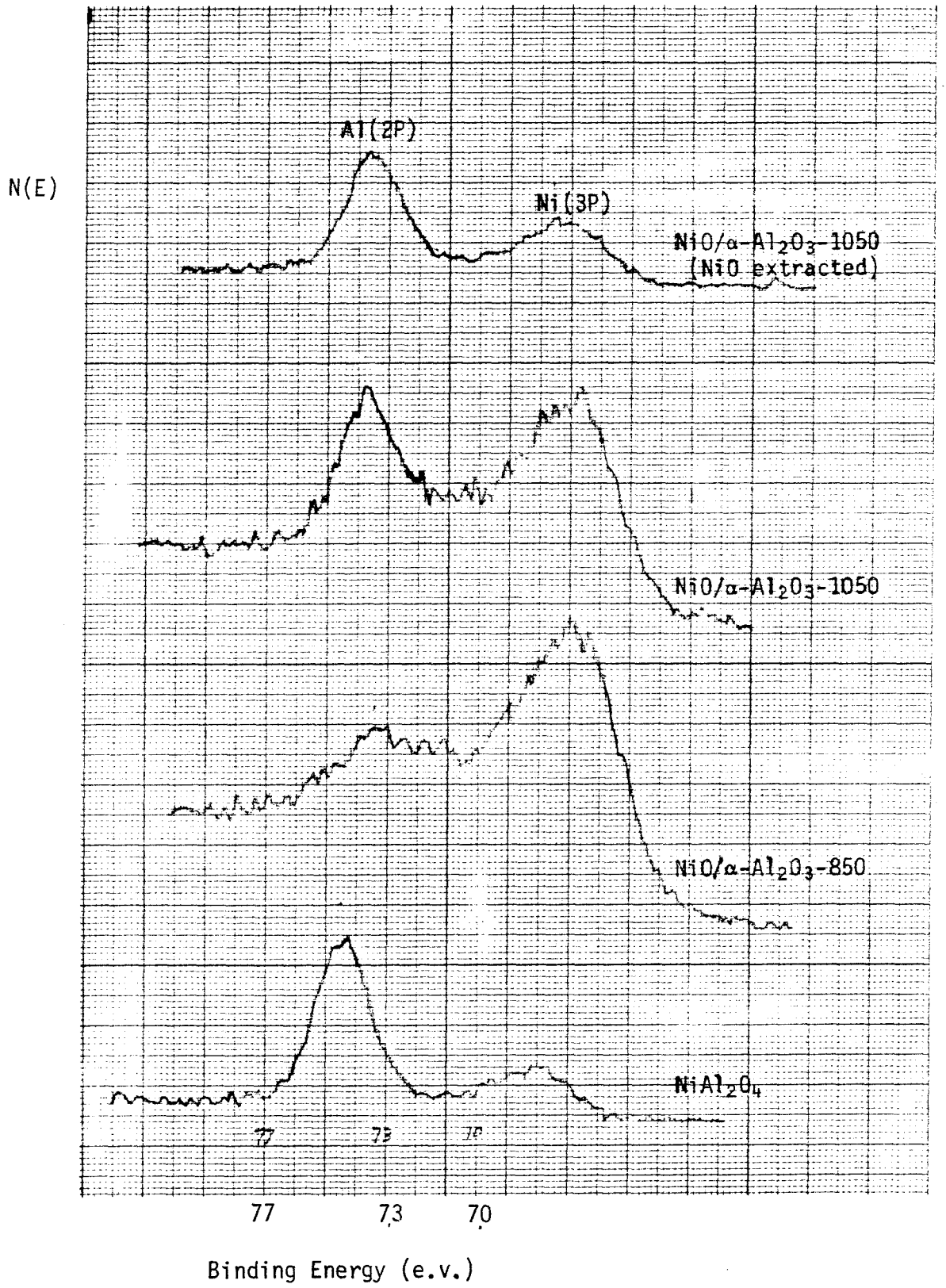

Fig. 9 The Al(2P) core level peak for the catalyst and the standard samples. All binding energies are corrected for charging (C(1S) = 284.6 e.v.).

The O(1S) spectrum has a principal peak at 529.4 e.v. and is accompanied by a satellite shoulder at 531.3 e.v. The spectra are similar to those reported from other laboratories (17-21).

b) $NiAl_2O_4$ Standard

The Ni($2P_{3/2}$) spectrum has a principal peak at 856.7 e.v. without an accompanying satellite and a broad peak at 863.3 e.v. The spectrum of O(1S) is also a singlet with a binding energy of 531.3 e.v. Hence, the Ni($2P_{3/2}$) and O(1S) binding energy separation is 0.4 e.v. higher than that observed for NiO. The Al(2P) binding energy is observed at 74.5 e.v.

c) $NiO/\alpha\text{-}Al_2O_3$-1050 (NiO extracted)

The XRD spectrum has confirmed a complete extraction of surface NiO from this sample but portrays no evidence of NiAl O . Th Ni($2P_{3/2}$) and O(1S) spectra are similar to those observed for the $NiAl_2O_4$ both in overall line shape and line width. The Ni($2P_{3/2}$) and O(1S) binding energies are 0.6 e.v. lower than those observed for the $NiAl_2O_4$. Consequently, the Ni($2P_{3/2}$) and O(1S) peak separation for this sample is identical to that of the $NiAl_2O_4$. Since the separation of peaks is independent of charging, the spectrum of this sample is consistent with the presence of nickel in the $NiAl_2O_4$ form. The result clearly verifies the existence of an X-ray amorphous

$NiAl_2O_4$ layer on the $NiO/\alpha-Al_2O_3$-1050 catalyst in agreement with the result from chemical analysis.

d) $NiO/\alpha-Al_2O_3$-850 and $NiO/\alpha-Al_2O_3$-1050

The $Ni(2P_{3/2})$ spectra for both catalysts exhibit a structural characteristic similar to that observed for the NiO. These spectra have broader line widths than that observed for the $NiAl_2O_4$ due to an accompanying satellite shoulder. The O(1S) spectra also appear quite similar to those observed for NiO, with a broad weak shoulder on the higher binding energy side. Although the observed $Ni(2P_{3/2})$ and O(1S) peaks for these two catalysts are shifted to about 1 e.v. higher than those for NiO, their $Ni(2P_{3/2})$ and O(1S) binding energy separations agree quite well with those of NiO. The peak separation, which is a more realiable parameter, indicates that the surface nickel on both catalysts is present primarily as NiO. In addition, there is no detectable difference in the overall line shape between the two catalysts and the NiO. Thus, the contribution to the $Ni(2P_{3/2})$ spectra by the $NiAl_2O_4$ is negligible. Evidently, the $NiAl_2O_4$ on the $NiO/\alpha-Al_2O_3$-1050 is shielded from the ESCA analyzer by the surface NiO. In some earlier studies (20,21), it was suggested that the supported NiO particles might be covered by an amorphous spinel overlayer. The present data show that only a very small fraction of the surface could be covered by the

$NiAl_2O_4$ overlayer.

The above differences in charging shift observed earlier are probably caused by an uncertainty in the binding energy calibration technique due to the following reasons: differences in the forms of adsorbed carbon species (22), possible carbon reactions with the surface to form a new carbon species, and uneven charging on different parts of the sample (22).

DISCUSSION

For a typical catalyst, the surface coverage by active metal (or oxide) is usually a small fraction of the support surface. The active metal (or oxide) particles are single crystals (crystallites) and the average particle size can be estimated from X-ray line broadening. In the present study, however, the SEM studies of calcined $NiO/\alpha\text{-}Al_2O_3$ catalysts have shown that most of the NiO particles are about 1000-2000 A° in size, much larger than the average crystallite size of NiO (300A°) estimated from X-ray line broadening. Although the particle size distribution of supported NiO prepared by impregnation is usually broad and some NiO particles of <1000 A° size which were not observed by SEM probably exist, it is unlikely that the X-ray line broadening analysis would grossly underestimate the average size of mostly 1000-2000 A° single crystal particles as 300 A°. We believe that the NiO particles that are observed by the SEM are aggregates of several NiO crystallites which are crystallographically misoriented, termed as "mosaic single crystals" (23). An idealized sketch of NiO particles is shown in Fig. 10. It is reasonable to assume that these mosaic single crystals are also formed in the calcined NiO/ZrO_2 catalysts inasmuch as they have been

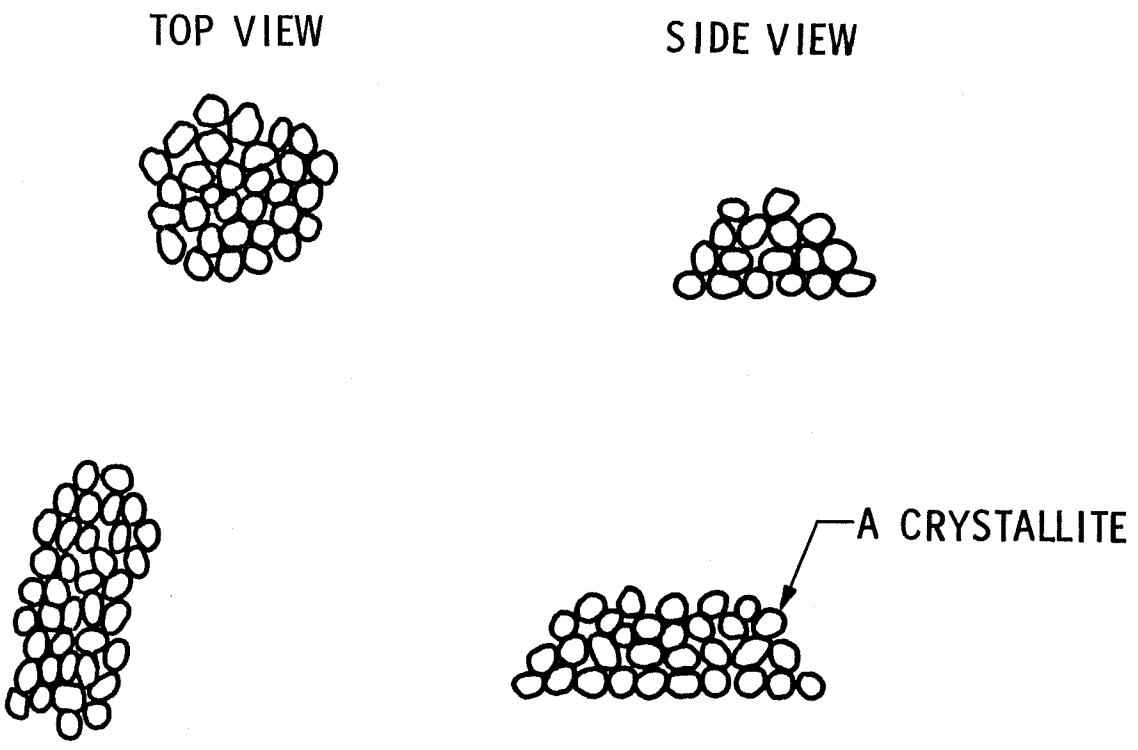

Fig. 10 Idealized Sketch of NiO Particles

prepared by the same procedure and have about the same nickel loading per unit surface area of support as that of the $NiO/\alpha\text{-}Al_2O_3$ catalysts.

The X-ray line broadening established that the contacting NiO crystallites on both $NiO/\alpha\text{-}Al_2O_3$ and NiO/ZrO_2 catalysts did not coalesce completely during the calcination. Under this treatment, however, the necks between contacting NiO crystallites (both within and between NiO particles) grow (Fig. 11) resulting in lower NiO surface area and smoother surface.

NiO Surface Area

Although the NiO surface area has not been measured directly, it can be estimated from:

$$\text{NiO surface area} = (\text{total surface area}) - (\Lambda) + (\text{correction}) \qquad (1)$$

where Λ is the exposed surface area of the support after reduction.

The exposed surface areas of the support after reduction are simply the differences between the total surface areas after reduction and the corresponding nickel surface areas. They are shown in Tables 10 and 11. The correction in (1) is needed because the exposed surface area of the support in an oxidized state is different from that in a reduced state. The volume ratio (Pilling-Bedworth Ratio) of oxide to metal

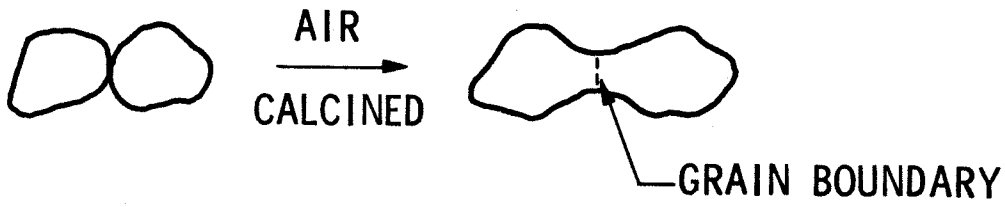

Fig. 11 Idealized Sketch of Neck Growth Between NiO Crystallites

for nickel on a molar basis at room temperature is 1.6 (24). If the particle strain at the particle-support interface is assumed to be zero at all times, the relationship between the NiO/support and the Ni/support (after reduction) contact areas is:

$$\frac{A_{NiO}}{A_{Ni}} = (V_{NiO}/V_{Ni})^{2/3} = (1.6)^{2/3} = 1.4$$

However, the friction at the interface hinders interfacial movement between particles and support and causes a finite strain. Hence:

$$1.4\ A_{Ni} \geq A_{NiO} \geq A_{Ni}$$

For convenience, we assume that $A_{NiO} = 1.2\ A_{Ni}$ so that correction = $0.2\ A_{Ni}$. The detailed calculation of A_{Ni} is shown in the Appendix. Although the above assumption is probably invalid, it can be seen that the accuracies of the NiO surface areas are estimated to $\leq 0.2\ A_{Ni}$ which are adequate for our purpose (Tables 10 and 11).

As expected, the NiO surface area decreases with increasing calcination temperature (Table 10 and 11). The NiO surface area of the NiO/ZrO_2-750 catalyst is a factor of three higher than that of the NiO/ZrO_2-1050 catalyst where as the NiO surface area of the NiO/α-Al_2O_3-750 catalyst is a factor of nine higher than that of the NiO/α-Al_2O_3-1050 catalyst. The NiO surface area is much lower than the

TABLE 10

Estimated NiO Surface Area of Zirconia-Supported Catalysts

Catalyst	Exposed Surface Area of the Support After Reduction (m^2/g)	Correction (m^2/g)	NiO Surface Area [a] (m^2/g)	
			Before Reduction	After Reduction and Reoxidation
NiO/ZrO_2-750	0.33	0.012	0.21	*
NiO/ZrO_2-850	0.32	0.012	0.16	0.18
NiO/ZrO_2-950	0.32	0.012	0.11	0.22
NiO/ZrO_2-1050	0.28	0.012	0.07	0.32

a The accuracy of the NiO surface areas is estimated to ≤ 0.012 m^2/g

* Data not available

TABLE 11

Estimated NiO Surface Area of Alumina-Supported Catalysts

Catalyst	Exposed Surface Area of the Support After Reduction (m^2/g)	Correction (m^2/g)	NiO Surface Area [a] (m^2/g)	
			Before Reduction	After Reduction and Reoxidation
$NiO/\alpha\text{-}Al_2O_3$-750	0.20	0.006	0.18	*
$NiO/\alpha\text{-}Al_2O_3$-850	0.15	0.006	0.09	0.10
$NiO/\alpha\text{-}Al_2O_3$-950	0.09	0.006	0.06	*
$NiO/\alpha\text{-}Al_2O_3$-1050	0.08	0.006	0.02	0.02

a The accuracy of the NiO surface areas is estimated to ≤ 0.006 m^2/g

* Data not available

corresponding Ni surface area (Table 5 and 6). The NiO surface area after reduction and reoxidation is slightly higher that that prior to reduction.

Nickel Redispersion

The increase in the total catalyst surface area following reduction is very interesting. If one Ni particle is formed from one NiO particle, the change in the total surface area can be computed (assuming hemispherical crystallites) from:

$$\begin{aligned}\Delta\text{Area} &= \Delta\text{Area}_{\text{crystallite}} + \Delta\text{Area}_{\text{substrate}} \\ &= (2\pi r^2_{\text{Ni}} - 2\pi r^2_{\text{NiO}}) + (r^2_{\text{NiO}} - r^2_{\text{Ni}}) \\ &= -\pi(r^2_{\text{NiO}} - r^2_{\text{Ni}}) \\ &< 0\end{aligned}$$

Hence, the total surface area should decrease with reduction. The observed increase in the total surface areas indicates that nickel redisperses during reduction of NiO.

Similarly, if one Ni crystallite is formed from one NiO crystallite, the NiO surface area is related to the Ni surface area by the following relation:

$$\frac{A_{\text{NiO}}}{A_{\text{Ni}}} = (1.6)^{2/3} = 1.4$$

Thus, the Ni surface area should be less than the corresponding NiO surface area. However, the opposite was observed. The

results further support the hypothesis that nickel is redispersed during reduction. As indicated earlier, the nickel surface areas are higher for the catalysts that have been calcined at higher temperature. This is contrary to the numerous reports (25-27) which indicate that the nickel surface area of supported catalysts decrease with increasing pretreatment temperature due to nickel particle-growth. In order to explain this paradox, we hypothesize that the redispersion is more extensive for catalysts that have been calcined in air at higher temperature prior to reduction. A further explanation for this phenomenon is given below. In the case of the NiO/α-Al_2O_3 catalysts, NiO is consumed in the interaction with the Al_2O_3 which becomes extensive above 850^{o}C. The effect of increased redispersion is offset by the loss of nickel in the NiO - Al_2O_3 interaction and the surface area therefore decreases with increasing calcination temperature ($\geq$850^{o}C).

It is anticipated that the nickel redispersion involves actual fracture of nickel particles. When a NiO particle is completely reduced to a Ni particle, its volume decreases by about 40%. Accordingly, there is an increasing tensile stress on the particle and a balancing compressive stress on the support as the degree of reduction increases. At a critical point the particle can move along the particle/substrate interface to relax this strain energy. The

critical stress (friction force) for the movement at the particle/substrate interface is dependent on the interfacial bonding and contact area. In the present study, the NiO particles have been postulated to consist of several NiO crystallites. Since grain boundaries which separate crystallites have incomplete bonding across the interface, the particle will fracture along the grain boundaries at a lower stress than the critical tensile stress for a crystallite splitting. When the friction force is strong and the stress is not relaxed by the interface movement a particle can fracture into smaller particles along the grain boundaries of the constituting crystallites (Fig. 12).

As suggested earlier, the redispersion is more extensive for the catalysts that have been calcined at higher temperatures. Following the above interpretation, this is probably due to a stronger bonding between NiO and substrate after calcination at higher temperature. As a result, the particle/substrate interface movement is hindered and particle fracture is more probable.

When a nickel crystallite is reoxidized, its volume increases and most of the crystallites that have been segregated from each other during reduction contact each other again. Accordingly, the total surface area that has previously been increased by reduction decreases after

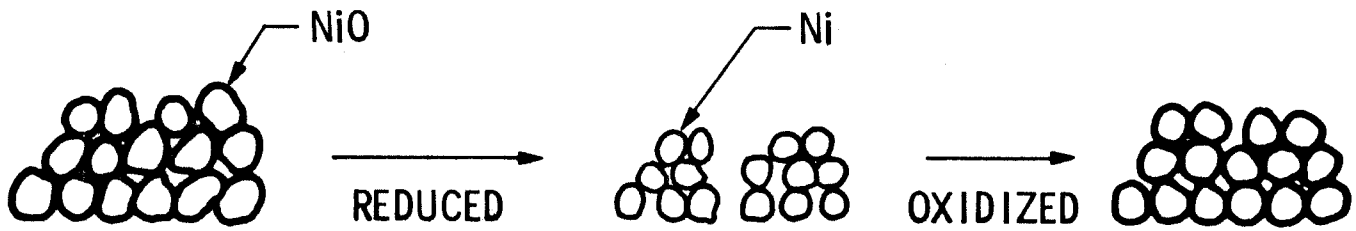

Fig. 12 Idealized Sketch of Nickel Particle Splitting

reoxidation. As indicated earlier, the NiO surface areas after reduction and reoxidation are higher than those prior to reduction. This is not totally unexpected. The neck growth between contacting crystallites which decrease NiO surface area, is more extensive after calcination at higher temperature. Since the reoxidation temperature ($500^{\circ}C$) is much lower than the calcination temperature prior to reduction ($\geq 750^{\circ}C$), the neck growth between crystallites that have been separated during reduction and reunited during reoxidation is less extensive than that prior to reduction.

The Colors of Catalyst

We would like to draw attention to the significance of the changes in catalyst colors after the calcination. These changes are similar to the results obtained by several authors (28-32) in the calcination of NiO in air. They are caused by the change in the concentration of excess oxygen in the lattice and on the surface of NiO (28-33). The concentration of lattice Ni^{3+} ions (positive hole) is related to the concentration of lattice excess oxygen by the following reaction:

$$\tfrac{1}{2}O_{2(g)} + 2Ni^{2+} = O^{2-} + 2Ni^{3+} + Ni[]$$

where Ni[] is a cation vacancy. Thus, two lattice Ni^{3+} ions are formed from one excess atomic oxygen. (This relationship,

however, is not accurate at the surface because some of the surface excess oxygen might exist in the O_2^- or O^- form (30)). Accordingly, the nonstoichiometric NiO is a p-type semicondutor in which the electrical conductivity increases with the increasing concentration of Ni^{3+} ions (or excess oxygen). Bielan'ski et al. (32) have determined, by the Bunsen-Rupp method, the concentration of the surface and the lattice Ni^{3+} ions of the NiO prepared by calcination of $Ni(NO_3)_2$ in air at various temperatures. The results, shown in Table 12, indicate that the surface and the lattice Ni^{3+} ions decrease with increasing calcination temperature. After calcination above 800°C, the surface Ni^{3+} ions is the dominant part of the total Ni^{3+} ions and the concentration of the lattice Ni^{3+} ions is below the sensitivity of the analytical method. Prasad and Tendulkar (28) measured the specific resistance of NiO prepared by calcination of $Ni(NO_3)_2$ in air and observed an increase in specific resistance with increasing calcination temperature up to above 900°C (Table 12). According to Mitoff (34) the equilibrium concentration of Ni^{3+} ions in the NiO lattice at 1000°C is in on the order of 10^{-4} ions/pair of ions and increases with increasing temperature. Hence, the concentration of Ni^{3+} ions in the NiO lattice which decreases with increasing calcination temperature up to above 900°C are not at equilibrium (30).

TABLE 12

Properties of Nonstoichiometric NiO

Calcination Temperature (°C)	Ni^{3+} ions [a] (At. %)		Specific Resistance [b] (Ohms)
	Surface	Lattice	
400	*	3.0	4880
500	0.28	1.44	*
600	0.192	0.148	7598
700	0.170	0.10	9034
800	0.144	0.00	14772
900	0.122	0.00	very high
1000	0.084	0.00	very high

a) From Ref. 32

b) From Ref. 28

* Data not available

From the results above, the concentration of Ni^{3+} ions in the catalysts that have been calcined at different temperatures cannot be observed by ESCA which is capable of detecting only about 5-10% of a new species (Ni^{3+} ions as opposed to Ni^{2+}).

The black color of all catalysts after reduction and reoxidation indicates that the Ni^{3+} concentration in the NiO is increased. Thus, it appears that the Ni^{3+} concentration in the NiO that has been calcined at high temperature can be restored to that prior to the calcination by a reduction and reoxidation at low temperature.

Appendix: Estimations of Ni/Support Contact Area

The value of A_{Ni} can simply be obtained from the following relationship:

$$A_{Ni} = (\text{total surface area of the support} - \Lambda) \quad (2)$$

It has also been shown that the average NiO (or Ni) crystallite size of both NiO/ZrO_2 and $NiO/\alpha\text{-}Al_2O_3$ catalysts is not affected by calcination. Since the decrease in Ni/support contact area is caused mainly by crystallite growth, it is reasonable to assume that their Ni/support contact areas are not affected by calcination. This conclusion is supported by a constant value of Λ for the Zirconia-supported catalyst that have been calcined at different temperatures (Table 10). A slight decrease in Λ

for the NiO/ZrO_2-1050 catalyst is consistent with a slight decrease in the total surface area of the ZrO_2 support after calcination at 1050°C for 15 hours.

On the other hand, the values of Λ for the NiO/α-Al_2O_3-750 and NiO/α-Al_2O_3-850 catalyst (Table 11) are higher than the total surface area of the T-61 α-Al_2O_3 support (Table 1). This led us to speculate that some fine $NiAl_2O_4$ crystallites are formed after calcination at 750 and 850°C. This speculation is based on the results from several studies (3,5,6) which show that $NiAl_2O_4$ is formed on a coprecipitated $NiAl_2O_4$ catalyst even after calcination at 500°C. Although the amount of $NiAl_2O_4$ on these two catalysts is minute and not detectable by the chemical analysis, these fine $NiAl_2O_4$ crystallites can considerably increase the total surface areas of the catalysts. Since it has been shown in our laboratory that $NiAl_2O_4$ is not reducible at 450°C (the reduction temperature prior to nickel surface area measurements) the value of Λ is therefore overestimated. After calcination at 950 and 1050°C, the values of Λ become less than the total surface area of the support. It has been found that the total surface area of the T-61 α-Al_2O_3 support is unchanged after calcination at 1050°C for 15 hours. Thus, it appears that these fine $NiAl_2O_4$ crystallites coalese with each other or with larger NiO particles after calcination at about 950°C. Since the

total surface area of the $NiO/\alpha\text{-}Al_2O_3$-1050 catalyst (0.10 m^2/g) is about the same as that of the T-61 $\alpha\text{-}Al_2O_3$ support (0.11 m^2/g), the increase in the total surface area from fine $NiAl_2O_4$ crystallites is evidently negligible.

Taking the above interpretation into account, the values of Λ from the NiO/ZrO_2-750 and $NiO/\alpha\text{-}Al_2O_3$-1050 catalysts are used in equation (2).

Hence, for the Zirconia-supported catalysts:

$$A_{Ni} = 0.39 - 0.33 = 0.06 \ m^2/g,$$

for the alumina-supported catalysts:

$$A_{Ni} = 0.11 - 0.08 = 0.03 \ m^2/g$$

LITERATURE CITED

1. Stephanopoulos, M.F., and Voecks, G.E., "Catalytic Autothermal Reforming of Hydrocarbon Liquid", Presented at AIChE National Meeting, Houston, Texas April 5-9,1981
2. Welcher, F.J., "Organic Analytical Regents" Vol.III, Van Nostrand, New York, 1947, P 157-199
3. Milligan, W.O. and Merten, L., J.Phys. Chem. 50,465(1946)
4. Richardson, J.T. and Milligan W.O., J.Phys. Chem. 60,1223 (1956)
5. Rubinstein, A.M., Slinkin, A.A. and Pribytkova, N.A., IZV. Akad. Nauk. SSSR, Otd.Khim. N. 814 (1958)
6. Rubinstein, A.M., Akimov, V.A. and Kretalova, L.D., ibid 929 (1958)
7. Lo Jacono, M., Schiavello, M. and Cimino, A., J. Phys. Chem. 75,8,1044 (1971)
8. Simonova, L.G. et al., Kinet. Katal. 14,6,1566 (1973)
9. Nelson, F.M. and Eggerton, F.T., Anal. Chem. 30,8,1387 (1958)
10. Brunauer, S., Emmett, P.H. and Teller, E., J. Amer. Chem. Soc. 60,309 (1938)
11. Buyanova, N.E. et al., Kinet. Katal. 8,868 (1967)
12. Scherrer, P., Gottinger Nachrichten 2,98 (1918)
13. Murdoch, C.C., Phys. Rev. 31,304 (1928) and 35,8 (1930)

14. Stokes, A.R. and Wilson, A.J.C., Proc. Cambridge Phil. Soc. 38, 313 (1942)

15. Klug, H.P. and Alexander, L.E., "X-ray Diffraction Procedures", Wiley, New York 1954

16. Gulbransen, E.A. and Andrew, K.F., J. Electrochem. Soc. 101,3,128 (1954)

17. Oku, Masaoki and Hirokawa,K.,J. Electron. Spectros. 10,103 (1977)

18. Werthiem, G.K. and Hufner, S., Phys. Rev. Letters 28, 16,1028 (1972)

19. Kim, K.S. and Davis, R.E., J. Electron Spectros. 1,251 (1972/73)

20. Kim, K.S. and Winograd, W., Surf. Sci. 43,625 (1974)

21. Shalvoy, R.B., Rencroft, P.J. and Davis, B.H., J. Vac. Sci. Technol. 17 (1), 209 (1980)

22. Madey, T.E. and Wagner, C.D., J. Electron. Spectrosc. 10, 359 (1977)

23. Figlarz, M., Vincent, F., Lacaille, C. and Amiel, J., J. Powder Technol. 1,121, (1967)

24. CRC Handbook of Chemistry and Physics

25. Shephard, F.E., J. Catal. 14,148 (1969)

26. Richardson, J.T. and Crump, J.G., J. Catal. 57,417 (1979)

27. Kou, H.K.,Ganesan, P. and De Angeles, R.J., J. Catal. 64,303 (1980)

28. Prasad, M. and Tendulkar, M.G., J. Chem. Soc., P 407 (1931)

29. Deren', J., Haber, J. and Stoczyn'ski, J., Bull. Acad. Pol. Sci. Ser. Sci. Chim. 9,245 (1961)

30. Deren', J. and Stoch, J., J. Catal. 18, 249 (1970)

31. Tourky, A.R., Hanafi, Z. and Salem, T.M., Z. Phys. Chem. (Leipzig) 243,145 (1970)

32. Bielan'ski, A., Deren', J. and Wolter, M., Kinet. i Katal. 5,849 (1964)

33. Krylov, O.V., "Catalysis by Nonmetal", Academic Press (1970), P 66

34. Mitoff, S.P., J. Chem. Phys. 35,882 (1961)

CHAPTER 4

Catalytic Activity for CH_4 Oxidation of Supported NiO Catalysts

ABSTRACT

The activity of supported NiO catalysts for CH_4 oxidation decreases substantially with increasing calcination temperature. However, the calcined catalysts can be reactivated by reduction in H_2 prior to reaction. The changes in activity are attributed to changes in NiO surface area and the changes in specific activity of NiO with the latter being more important. The change in specific activity of NiO is explained in terms of the change in excess oxygen content.

INTRODUCTION

In the previous chapter, the physicochemical properties of supported NiO catalyst were examined and found to vary markedly with calcination temperature. In particular, both NiO surface area and concentration of excess oxygen in NiO decrease with increasing calcination temperature. The concentration of excess oxygen in the NiO that has been calcined in air at high temperature appears to be restored by reduction, and reoxidation at lower temperature than the calcination temperature.

This chapter reports measurements of the catalytic activities of these catalysts for CH_4 oxidation. The main objective is to correlate the catalytic activity in terms of different physicochemical properties and, in particular, to determine the effect of reduction prior to reaction.

EXPERIMENTAL

The catalysts used in the present work were obtained from the same batches as those examined in Chapter 2. Table 1 and 2 list the catalysts and their NiO and total surface areas.

The catalysts' activities for CH_4 oxidation were measured with the same apparatus and procedure used previously (1). The reaction mixture contained CH_4 , O_2 and diluent N_2 . The catalyst packing consisted of 10-100 mg. of catalyst diluted with low surface area α-Al_2O_3 to reduce the heat produced per unit volume. In order to achieve isothermal operations and obtain a uniform velocity profile, packing of 5 cm. length of low surface area α-Al_2O_3 were placed before and after the catalyst bed. The reactor was operated in a differential mode with CH_4 conversion of 2% or less. The temperature gradient along the catalyst bed was always within $\pm 2^{\circ}C$. On this basis, the reactor could be considered isothermal.

The experiments were conducted at O_2/CH_4 ratios which are substoichiometric relative to complete combustion. The reaction temperature was maintained within a range wherein the CH_4 which reacted was oxidized completely to CO_2 and H_2O. Under these conditions, the nickel catalyst was present in the NiO form (1).

TABLE 1

NiO and Total Surface Area of Zirconia-Supported Catalysts

Catalyst	Total Surface Area (m^2/g)	NiO Surface Area [a] (m^2/g)	
		Before Reduction	After Reduction and Reoxidation [b]
NiO/ZrO_2 (non-calcined)	0.74	*	*
NiO/ZrO_2-750	0.53	0.21	*
NiO/ZrO_2-850	0.47	0.16	0.18
NiO/ZrO_2-950	0.42	0.11	0.22
NiO/ZrO_2-1050	0.34	0.07	0.32
ZrO_2 (Norton SZ5464)	0.39	—	—

a The accuracy of NiO surface areas was estimated to ≤ 0.012 m^2/g (2)

b Reduced in H_2 at 450°C for 15 hours and reoxidized in air at 500°C for 3 hours

TABLE 2

NiO and Total Surface Area of Alumina-Supported Catalysts

Catalyst	Total Surface Area (m^2/g)	NiO Surface Area [a] (m^2/g)	
		Before Reduction	After Reduction and Reoxidation [b]
$NiO/\alpha\text{-}Al_2O_3$(non-calcined)	0.45	*	*
$NiO/\alpha\text{-}Al_2O_3$-750	0.38	0.18	*
$NiO/\alpha\text{-}Al_2O_3$-850	0.24	0.09	0.10
$NiO/\alpha\text{-}Al_2O_3$-950	0.15	0.06	*
$NiO/\alpha\text{-}Al_2O_3$-1050	0.10	0.02	0.02
$\alpha\text{-}Al_2O_3$ (Girdler T-375)	3.88	—	—

a The accuracy of NiO surface areas was estimated to ≤ 0.006 m^2/g

b Reduced in H_2 at 450°C for 15 hours and reoxidized in air at 500°C for 3 hours

The differential rate of CH_4 consumption was calculated from:

$$r = F \cdot \frac{x}{w}$$

where F = the CH_4 flow rate, mol/sec.

x = the fraction of CH_4 consumed

w = the catalyst loading, g.

RESULTS

Catalyst Activity

The activity of the non-calcined NiO/ZrO_2 catalyst at 750°C is shown in Fig. 1. The activity declines rapidly during the first few hours and more slowly thereafter. In Fig. 2, the same behavior is seen for the non-calcined $NiO/\alpha\text{-}Al_2O_3$ catalyst. Also in Fig. 2, the activity of the $NiO/\alpha\text{-}Al_2O_3$-850 catalyst is shown to be stable at a reaction temperature of 705°C but the activity is measurably reduced in comparison. Therefore, the deactivation can be accelerated by calcination in air for a few hours above the reaction temperature.

The catalytic activities and kinetic parameters of the catalysts that have been calcined at high temperatures showed little change during reaction. To avoid possible errors due to activity changes during reaction, verification of all the reaction rate measurements was established by making measurements under standard conditions before and after data collection.

Preliminary tests showed that the extent of the gas phase reaction and reaction at the reactor wall were negligible. From the analytical criteria reviewed by Mears (3), the reaction rates were free of mass and heat transfer effects.

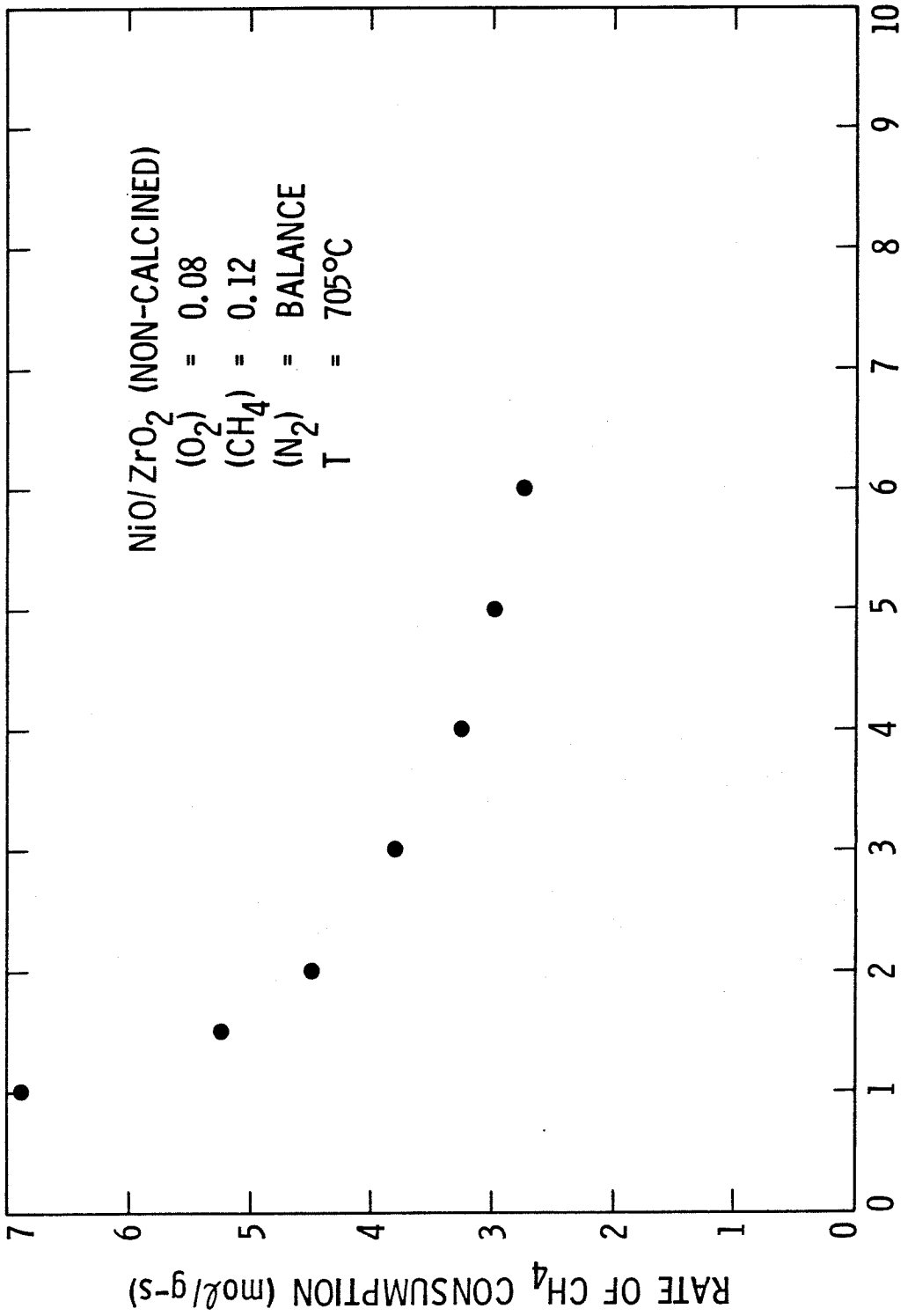

Fig. 1 Deactivation of the Non-Calcined Zirconia-Supported Catalyst

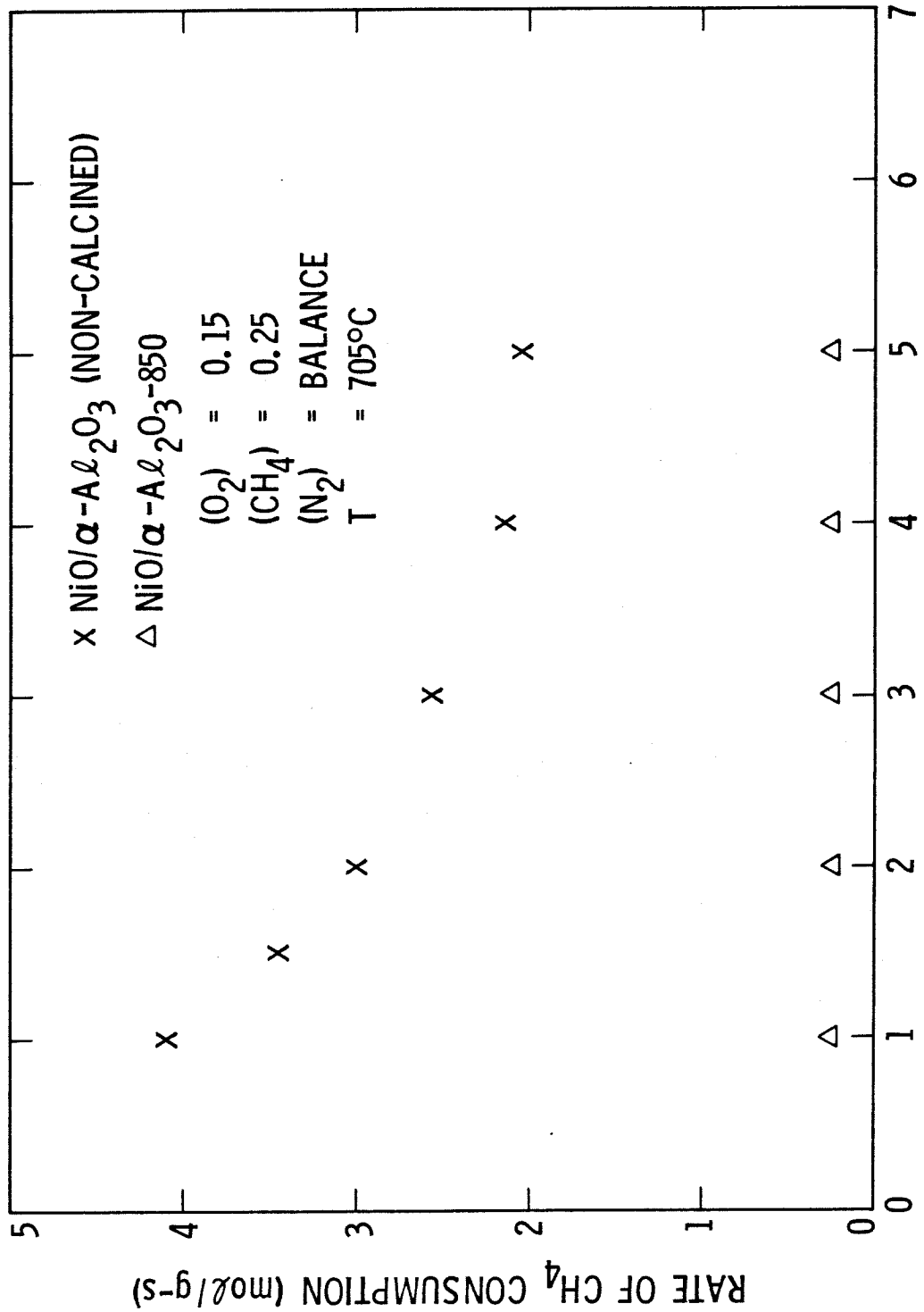

Fig. 2 Deactivation of the Non-Calcined Alumina-Supported Catalyst

In Fig. 3, the specific activities (activity per unit surface area) of the α-Al_2O_3 and ZrO_2 supports are presented in Arrhenius plots and shown to be about the same. The activation energies (Table 3) of the two supports are also comparable.

The specific activities (activity per unit NiO surface area) of various catalysts are shown in Figs. 4 and 5. The reaction rates of the catalysts that had been calcined at 950 and 1050°C were corrected for the contributions from the supports. The specific activities of both NiO/α-Al_2O_3 and NiO/ZrO_2 catalysts decrease substantially with increasing calcination temperature. The activation energies were found to be independent of gas composition. After calcination at and below 950°C, the activation energies (Table 3) change very little and without any noticeable trend. Thus, there is no compensation effect. The activation energies of the NiO/α-Al_2O_3 catalysts are slightly higher than those of the NiO/ZrO_2 catalysts. All of these activation energies are between those obtained under oxygen-rich conditions by Anderson et al. (4) [31.3] and Andrushkevich et al. (5) [20.0]. When the calcination temperature is increased to 1050°C, the activation energies increase dramatically (Table 3). These activation energies are excessively high for a catalytic reaction. The dramatic increases in activation energy might be caused by errors associated with the correction indicated earlier. At 700°C, the contributions from the supports of

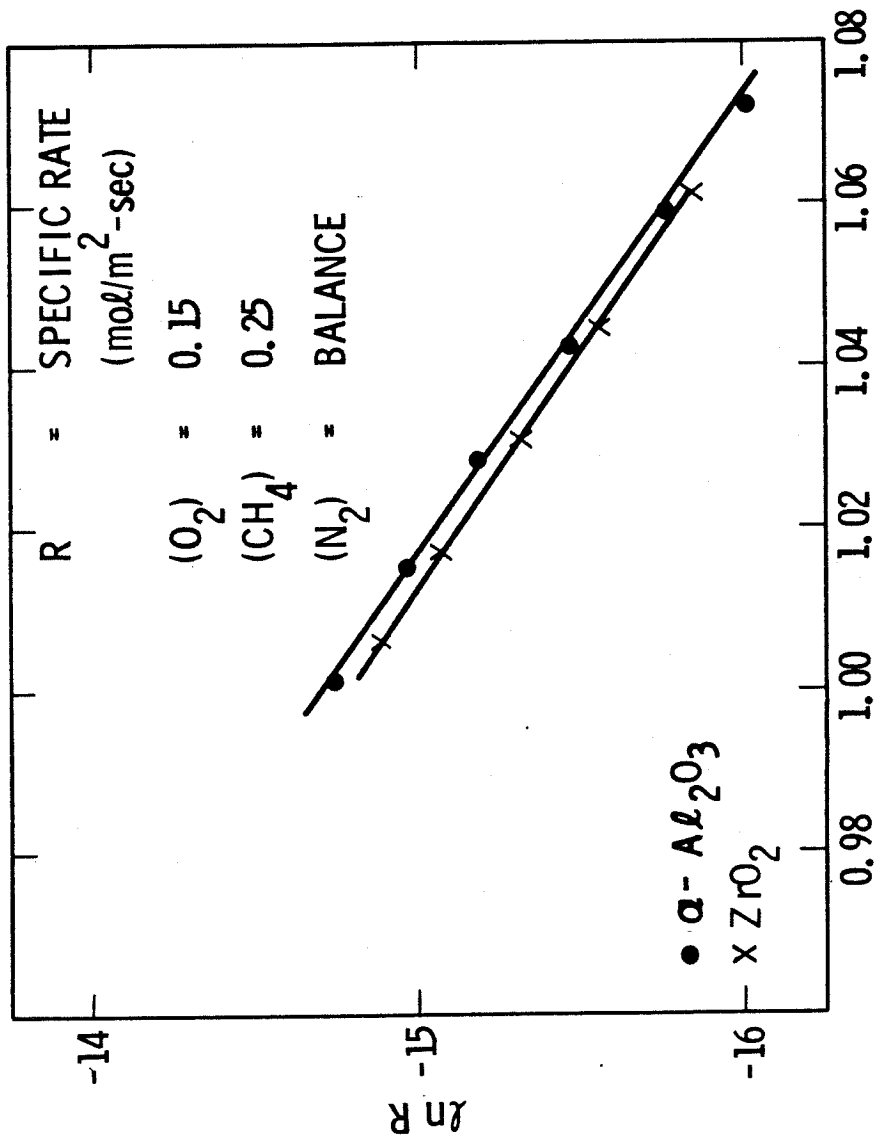

Fig. 3 Arrhenius Plots of Alumina and Zirconia Supports

TABLE 3

Kinetic Parameters

Catalyst	Ea (kcal/mol)	α	β
NiO/ZrO_2-750	23.6		
NiO/ZrO_2-850	21.0		
NiO/ZrO_2-950	21.7		
NiO/ZrO_2-1050	53.3		
NiO/α-Al_2O_3-750	28.2	0.43	0.43 [a]
NiO/α-Al_2O_3-850	29.3		
NiO/α-Al_2O_3-950	26.1		
NiO/α-Al_2O_3-1050	52.4		
ZrO_2	36.7		
α-Al_2O_3	35.9		

a At 600°C

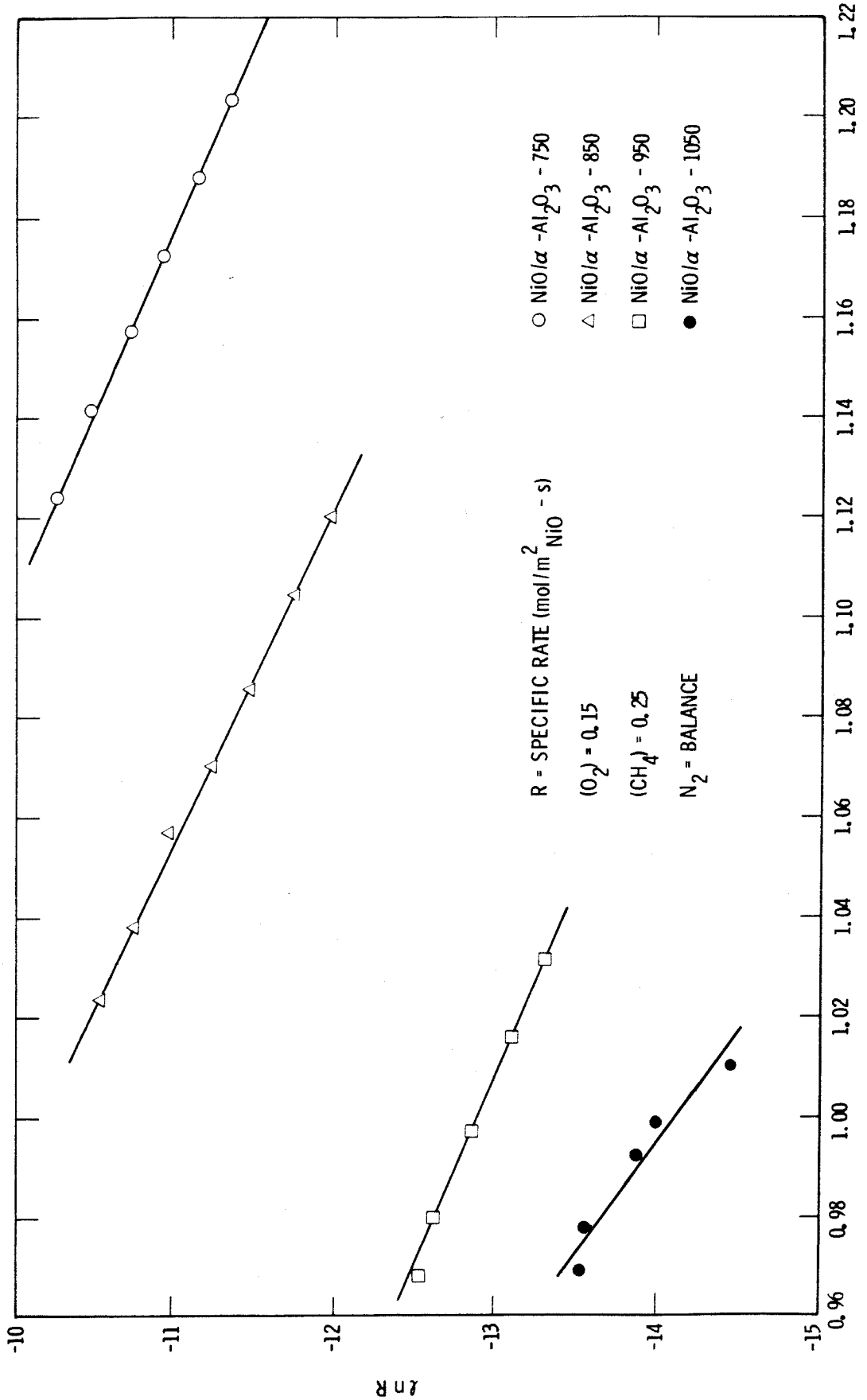

Fig. 4 Arrhenius Plots of Alumina-Supported Catalysts

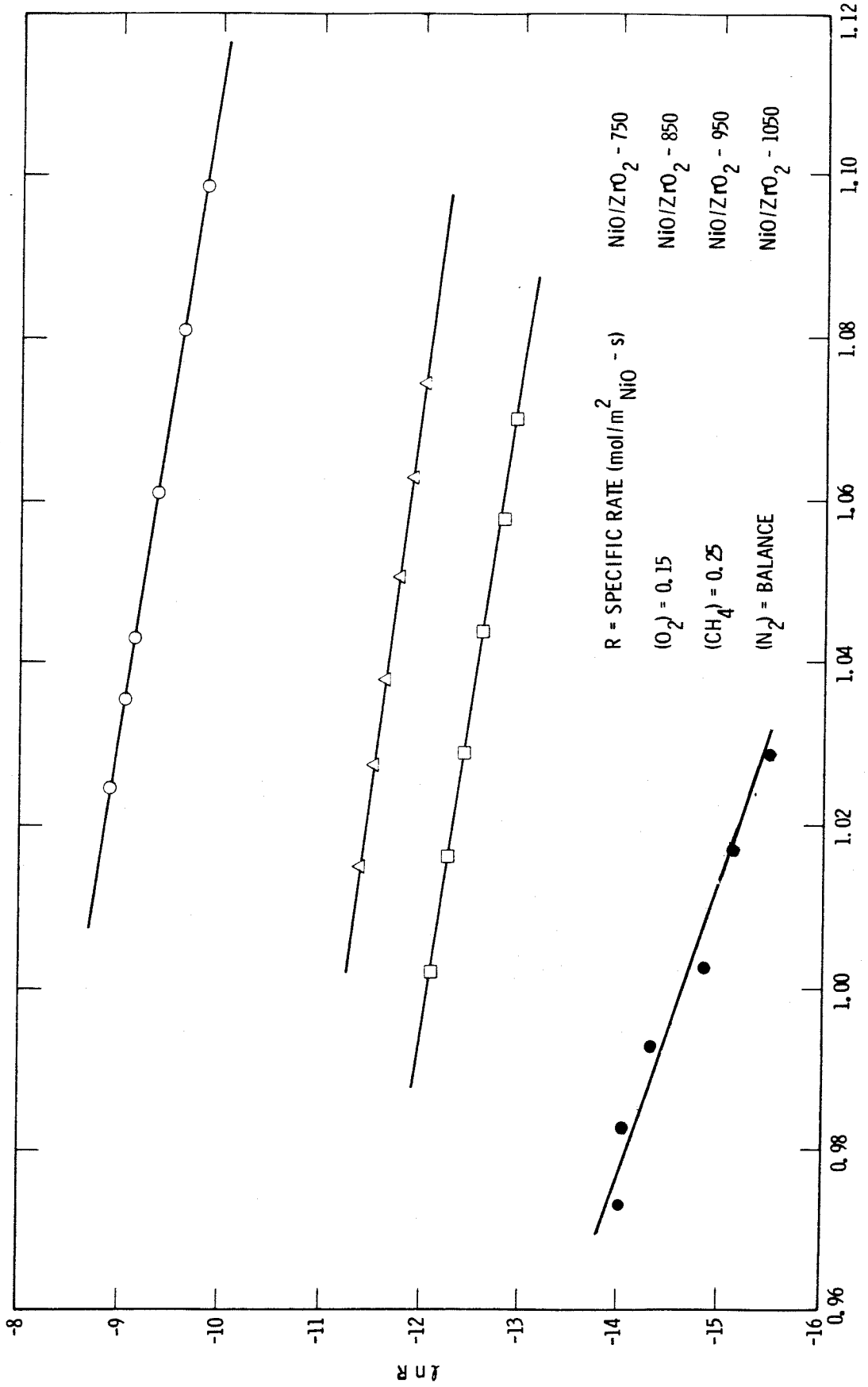

Fig. 5 Arrhenius Plots of Zirconia-Supported Catalysts

the NiO/ZrO_2-1050 and the NiO/α-Al_2O_3-1050 catalysts are about 70% of total catalyst activity. It is plausible that activation energies of the supports that have been subjected to repetitive impregnation with $Ni(NO_3)_2$ solution during catalyst preparation and then calcination in air at 1050°C for 15 hours are higher than those of the respective non-calcined supports. Since the reaction rates from non-calcined supports were used in the correction, the activation energies were overestimated.

The rate of CH_4 consumption is fitted by a power law rate expression:

$$r = k \cdot (CH_4)^{\alpha} \cdot (O_2)^{\beta}$$

The reaction orders on the NiO/α-Al_2O_3-750 catalyst are shown in Table 3. The reaction order with respect to CH_4 was obtained by maintaining the O_2 mole fraction at 0.15 and varying the CH_4 mole fraction from 0.10 to 0.40. Similarly, the reaction order with respect to O_2 was obtained by maintaining the CH_4 mole fraction at 0.25 and varying the O_2 mole fraction from 0.1. to 0.35. The reaction order with respect to CH_4 is comparable to that obtained by Andruskevich et al. (5). The fractional order with respect to both CH_4 and O_2 indicates that the rate determining step is the surface reaction between preadsorbed oxygen and methane.

The specific activities of various catalysts at 700°C are compared in Table 4. The results show that the specific activity of supported NiO decreases

TABLE 4

Comparison of the Activity of Various Catalysts

Catalyst	Specific Rate [a] (mol/m^2 NiO-S)
NiO/ZrO_2-750	1.29×10^{-4}
NiO/ZrO_2-850	1.04×10^{-5}
NiO/ZrO_2-950	4.23×10^{-6}
NiO/ZrO_2-1050	1.86×10^{-7}
ZrO_2	(2.05×10^{-7}) [b]
NiO/α-Al_2O_3-750	1.46×10^{-4}
NiO/α-Al_2O_3-850	2.64×10^{-5}
NiO/α-Al_2O_3-950	1.73×10^{-6}
NiO/α-Al_2O_3-1050	5.35×10^{-7}
α-Al_2O_3	(2.50×10^{-7}) [b]

a Measured at 700°C, $(O_2) = 0.15$ and $(CH_4) = 0.25$

b $(mol/m^2\text{-}s)$

substantially with increasing calcination temperature. For each increase of 100°C, the specific activity decreases by almost an order of magnitude. As a result, the specific activities of supported NiO after calcination at 1050°C are over two orders of magnitude lower than those after calcination at 750°C. Moreover, the specific activity of NiO that has been calcined at 1050°C becomes comparable to those of the ZrO_2 and the Al_2O_3 supports.

In comparing NiO surface areas (Tables 1 and 2) and the specific activities of NiO (Table 4) of the catalysts that have been calcined between 750 and 1050°C, it can be seen that the dominant mode of deactivation is the decrease in the specific activity of NiO due to calcining.

Inspection of used catalysts shows that the color of the non-calcined catalyst changes from black to grayish-black with time of operation, whereas that of the calcined catalysts remains the same. This seems to indicate that the concentration of excess oxygen in calcined NiO is not altered during activity measurements.

Effect of Reduction

To explain the relatively stable but less active character of the calcined catalysts which had undergone the high temperature treatment under oxidizing atmosphere, the catalysts were reduced in H_2 prior to activity measurements.

Although most of the nickel is in metallic form after reduction, it is reoxidized again when the reactant flow is resumed. As shown in the last chapter, all catalysts have an average Ni crystallite size $< 500\ A^{\circ}$ based on XRD analysis. From the reported nickel oxidation rate (6), these catalysts should be completely reoxidized in less than 10 minutes under all reaction conditions employed. Thus, the activities after reduction are measured when nickel is in the NiO form. The activities of the $NiO/\alpha\text{-}Al_2O_3$-850 and $NiO/\alpha\text{-}Al_2O_3$-1050 catalysts before and after reduction at $650^{\circ}C$ for 1 hour are shown in Fig. 6. The activity of the former is increased by more than an order of magnitude after reduction whereas that of the latter is increased by about 3 orders of magnitude. The activity of the $NiO/\alpha\text{-}Al_2O_3$-850 catalyst after reduction is higher than that of the $NiO/\alpha\text{-}Al_2O_3$-750 catalyst prior to reduction while the activity of the $NiO/\alpha\text{-}Al_2O_3$-1050 catalyst after reduction is comparable to that of the $NiO/\alpha\text{-}Al_2O_3$-750 catalyst prior to reduction.

In Fig. 7, a similar behavior is observed with the NiO/ZrO_2-850 and NiO/ZrO_2-1050 catalysts. After reduction at $600^{\circ}C$ for 1 hour, the activity of the former is increased by more than an order of magnitude while that of the latter is increased by about 3 orders of magnitude. As a result of reduction, activities of both catalysts are higher than those of the NiO/ZrO_2-750 catalyst prior to reduction.

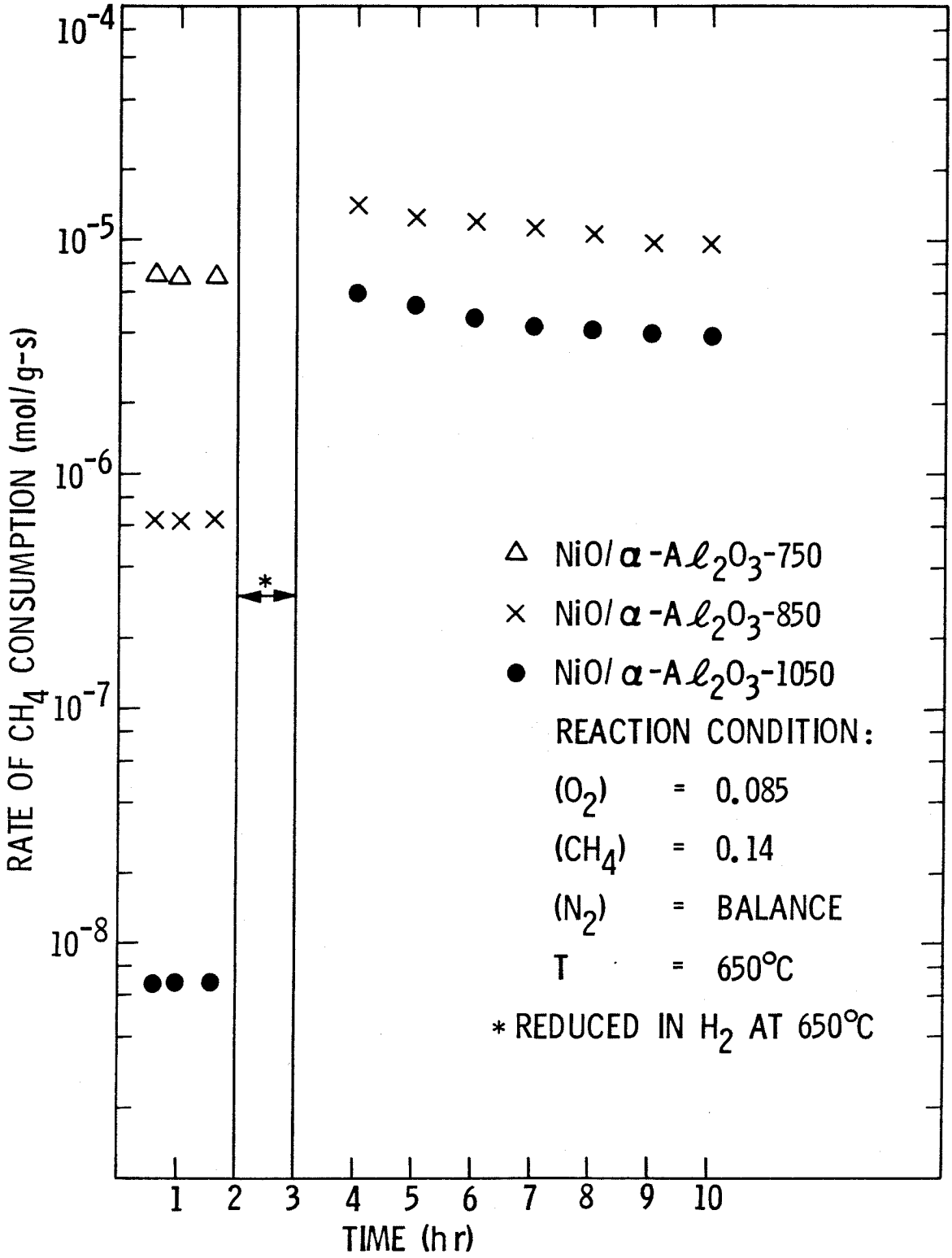

Fig. 6 Activation of Alumina-Supported Catalysts

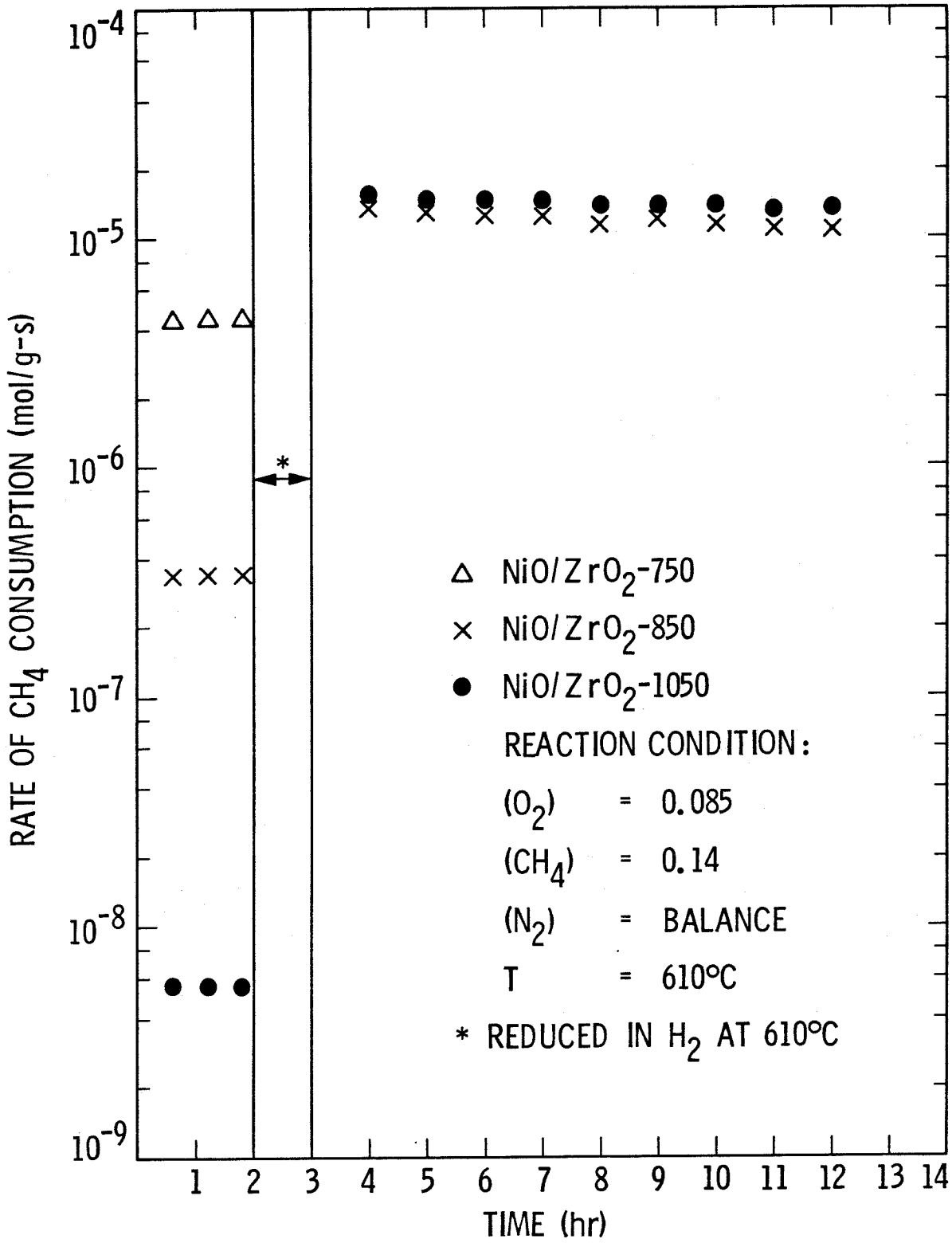

Fig. 7 Activation of Zirconia-Supported Catalysts

Although prior to reduction the activity of the NiO/ZrO_2-850 catalyst is much higher than that of the NiO/ZrO_2-1050 catalyst, after reduction the activity of the latter becomes slightly higher than that of the former consistent with their NiO surface areas after reduction and reoxidation (Table 1). In all cases the catalyst activities that have been increased by reduction decline slowly with time on stream.

It is reasonable to assume that the NiO surface areas of the catalysts that have been reduced and reoxidized under reaction (>600°C) are comparable to those after reduction and reoxidation (500°C) in Table 1. The increase in NiO surface area after reduction and reoxidation (Table 1) is relatively small compared to the increase in catalyst activity. For example, the NiO surface area after reduction and reoxidation of the NiO/α-Al_2O_3-850 catalyst is about the same as that prior to reduction whereas the activity increased by over an order of magnitude after reduction. The NiO surface area after reduction and reoxidation of the NiO/Zro_2-1050 catalyst increases by a factor of two or three whereas its activity increases by about three orders of magnitude. Thus, the increase in catalyst activity is due mainly to the increase in specific activity of the NiO.

In order to better understand the changes in the specific activity, rate measurements were made for an

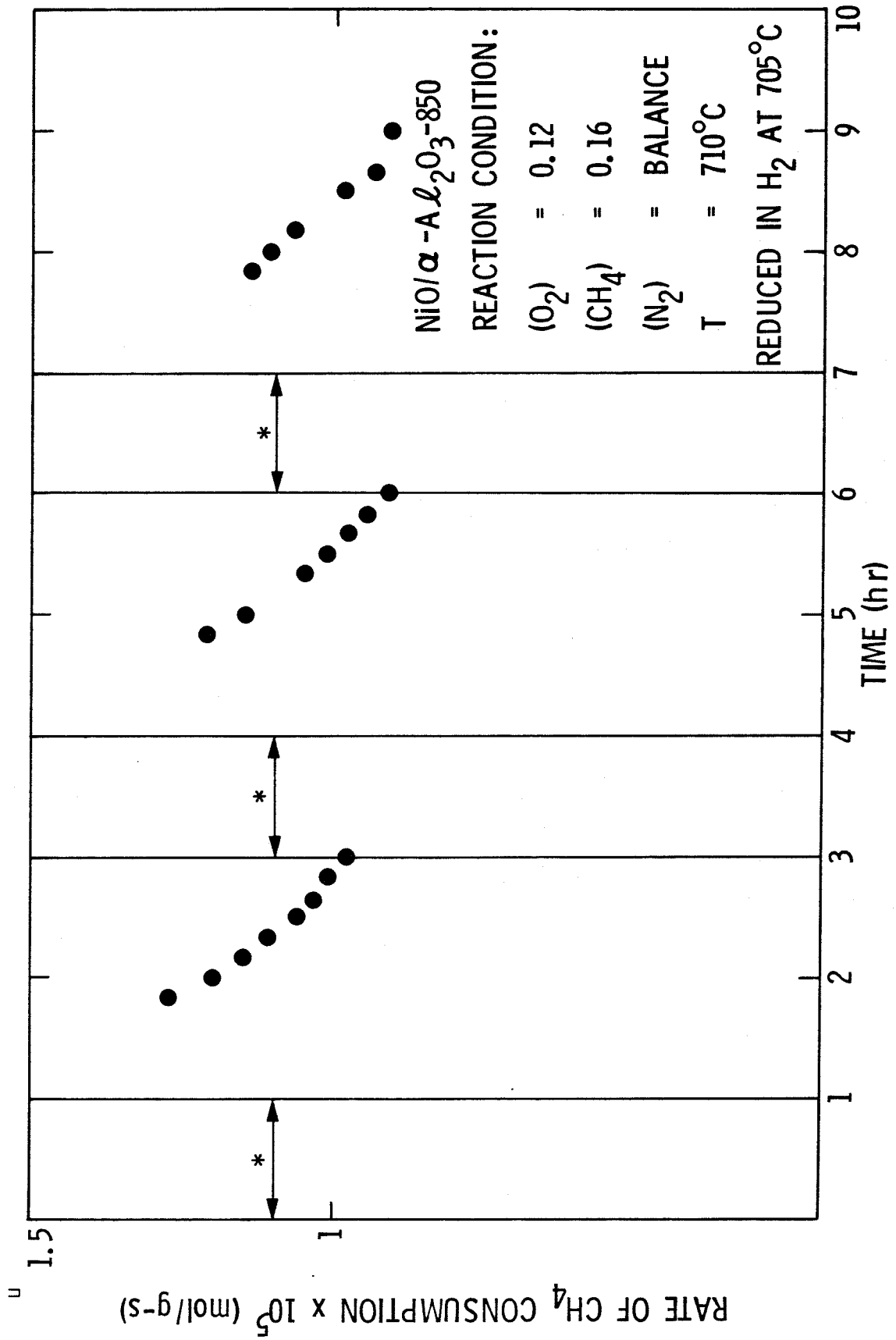

Fig. 8 Effect of Alternating Reduction and Oxidation on Catalyst Activity

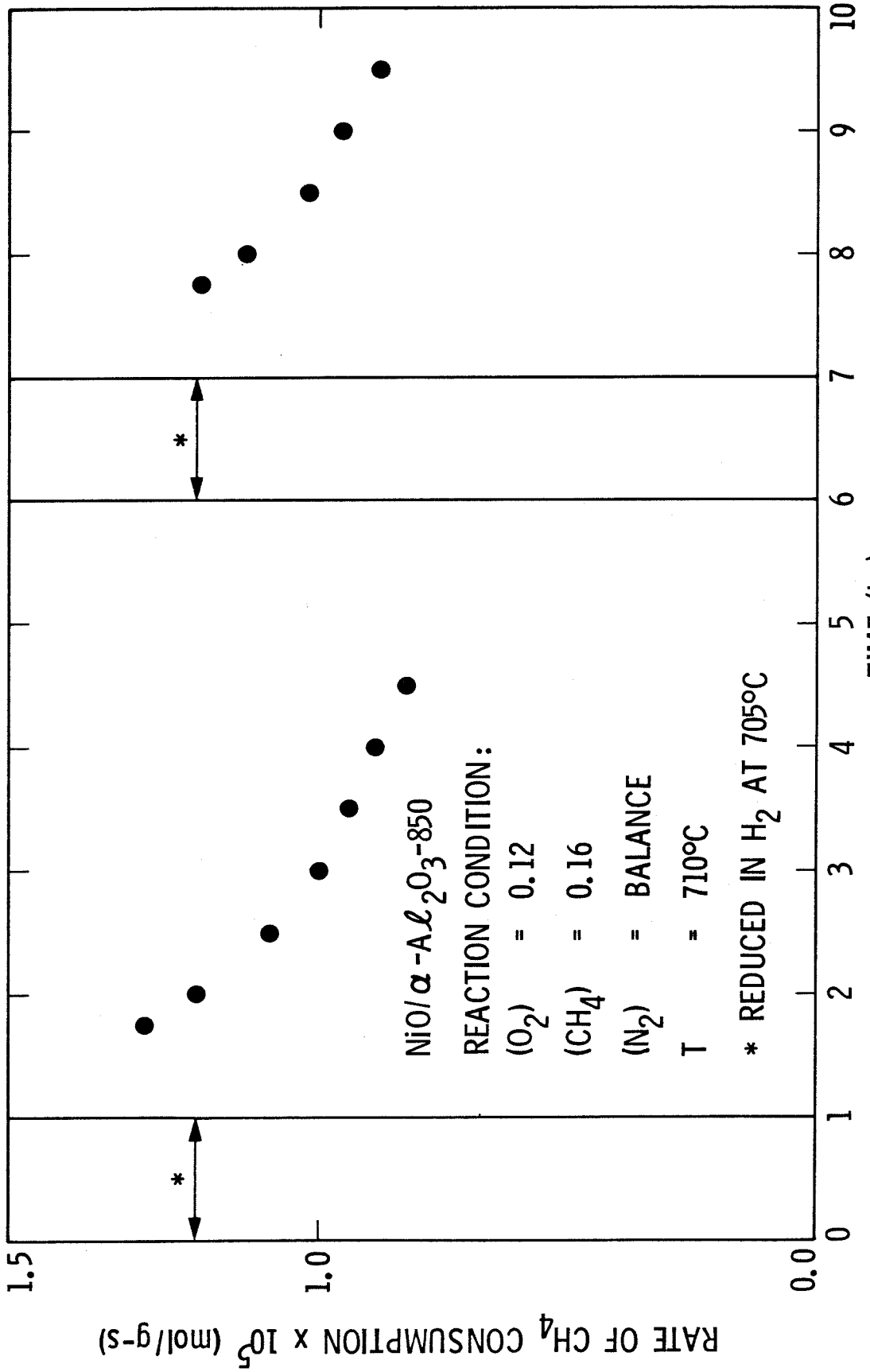

Fig. 9 Effect of Alternating reduction and Oxidation on Catalyst Activity

alternating reduction and reaction (oxidation) sequence. The results are shown in Fig. 8 and 9. The activity gain after reduction is less prominent after each additional cycle. It appears that a slow irreversible process is taking place. In an attempt to explain this phenomenon, the effect of reduction time and temperature were examined. In Fig. 10, a longer reduction time results in approximately the same loss in activity as if the catalyst was under reaction conditions. Thus, the irreversible process continues even in the presence of H_2. Reduction at higher temperature (Fig. 11) has no beneficial effect on restoring the catalyst activity. The effect of reduction temperature is also shown in Fig. 12. The rate of CH_4 consumption after reduction (measured at the reduction temperature) decreases with increasing reduction temperature from 650 to 750^{o}C. Without any correction for the differences in reaction temperature, it is evident that reduction for 1 hour at >650^{o}C decreases the activity gain after reduction

The effect of O_2/CH_4 ratio on the rate of decline is shown in Fig. 13. At 710^{o}C the rate of activity decline appears to be independent of the O_2/CH_4 ratio in the range 0.2 to 1.2. It is important to stress that, thus far, the activities were measured under reaction conditions in which CO_2 was the only oxygenated carbon product and the catalyst

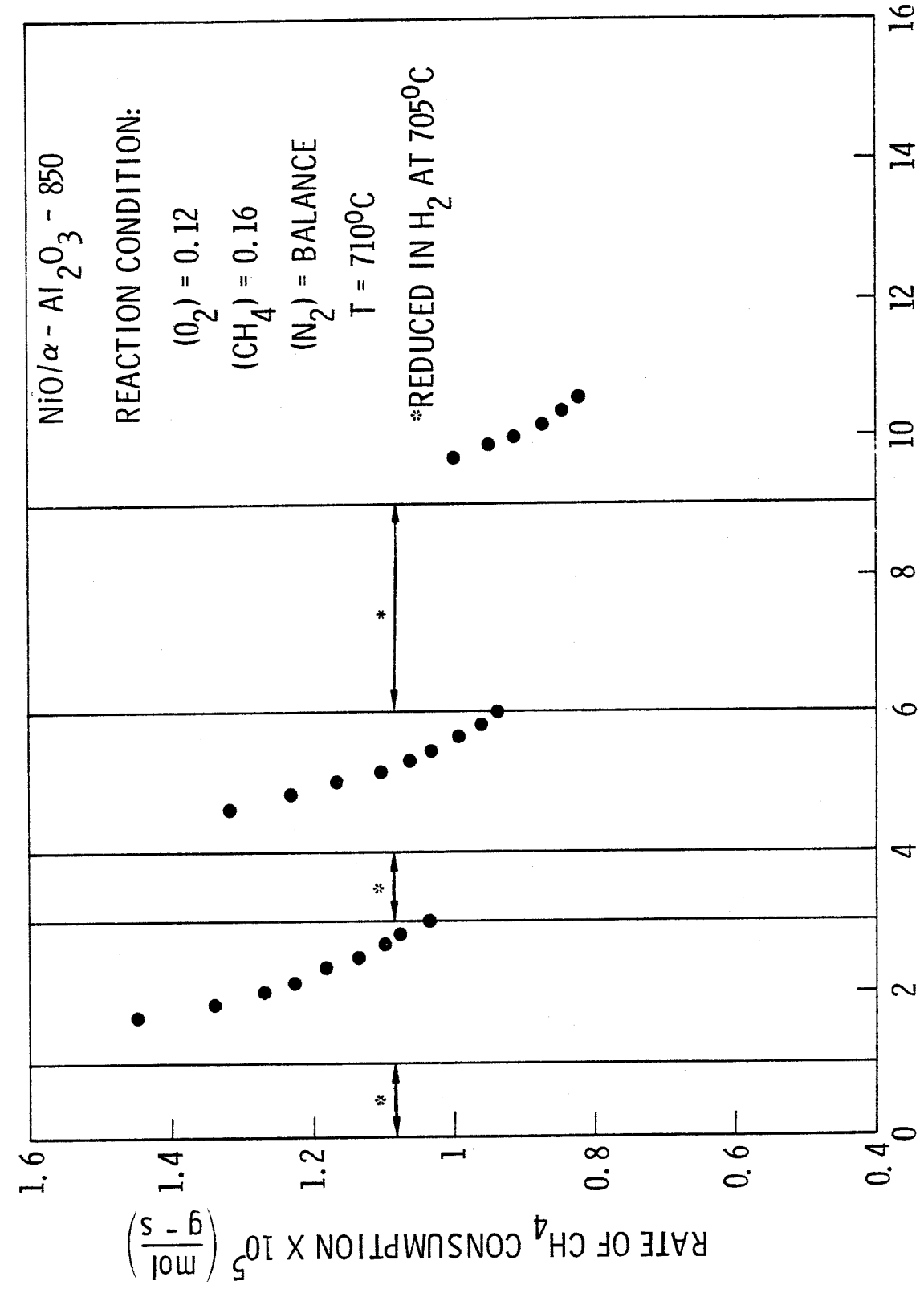
NiO/α - Al2O3 - 850
REACTION CONDITION:
(O2) = 0.12
(CH4) = 0.16
(N2) = BALANCE
T = 710°C
*REDUCED IN H2 AT 705°C
RATE OF CH4 CONSUMPTION X 10^5 (mol / g - s)
TIME (hr)
1.6
1.4
1.2
1
0.8
0.6
0.4
0
2
4
6
8
10
12
14
16
*
*
*

Fig. 10

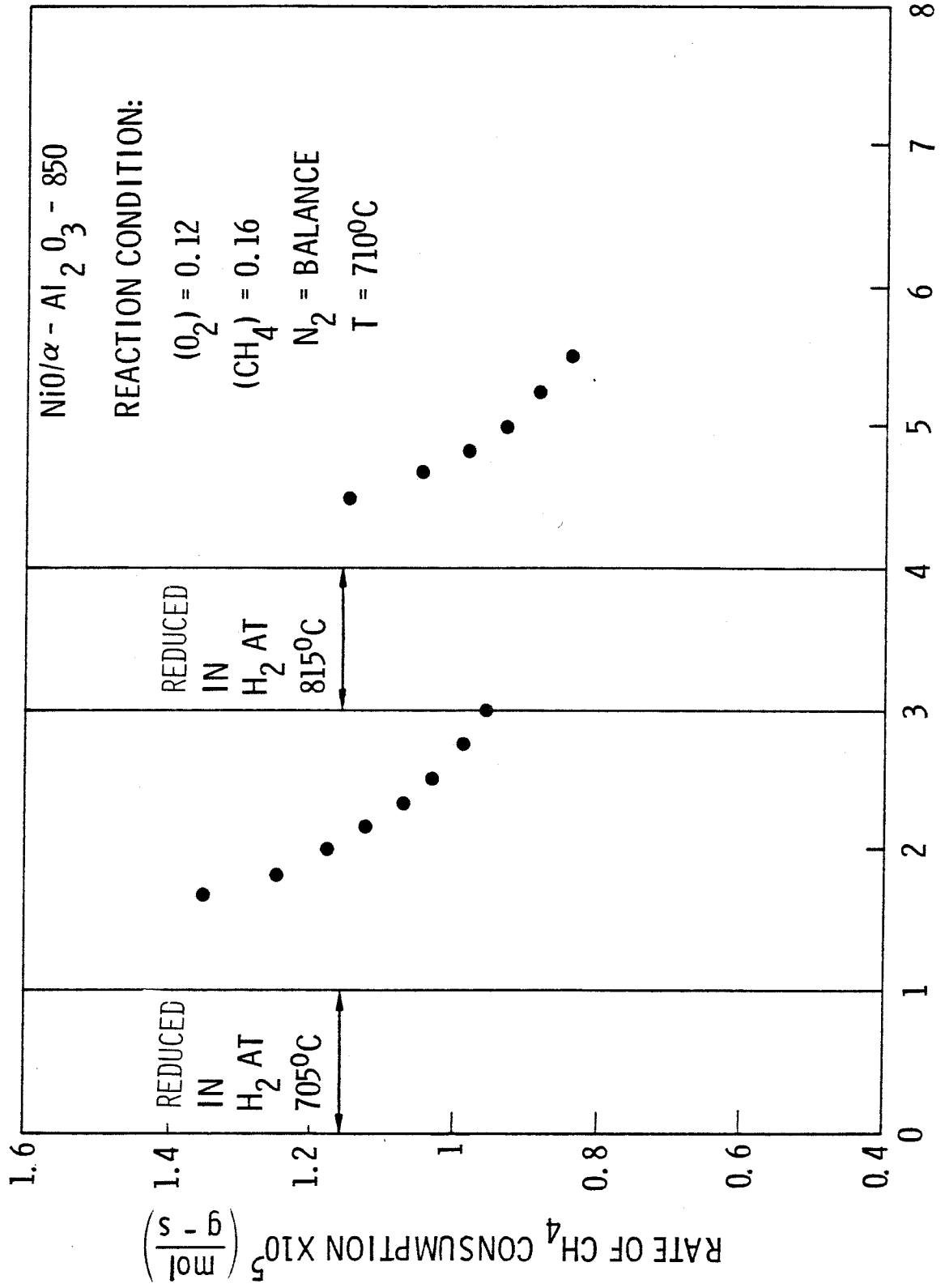

Fig. 11 The Effect of Reduction Temperature on Catalyst Activity

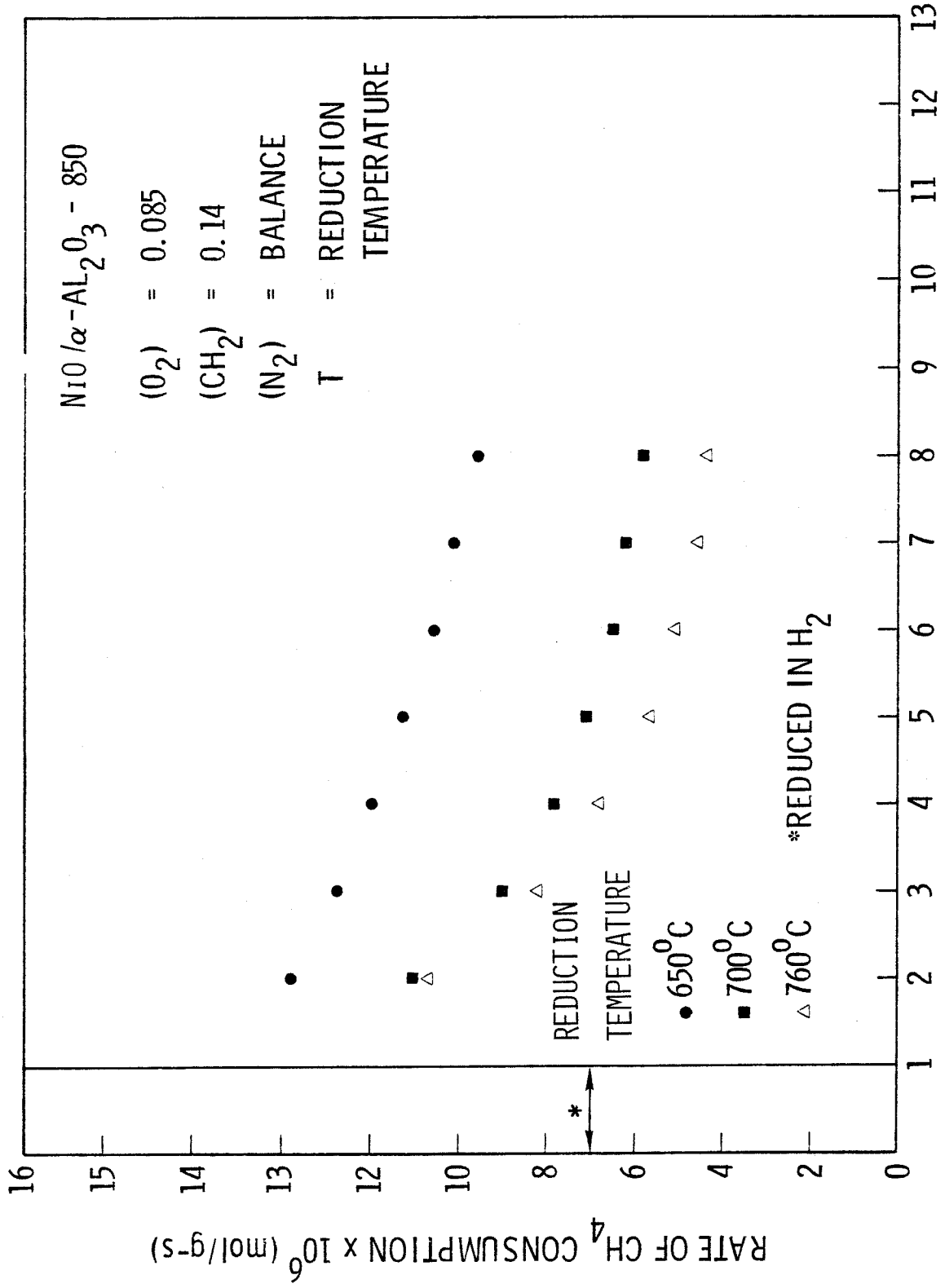

Fig. 12 Effect of Reduction Temperature on the Catalyst Activity

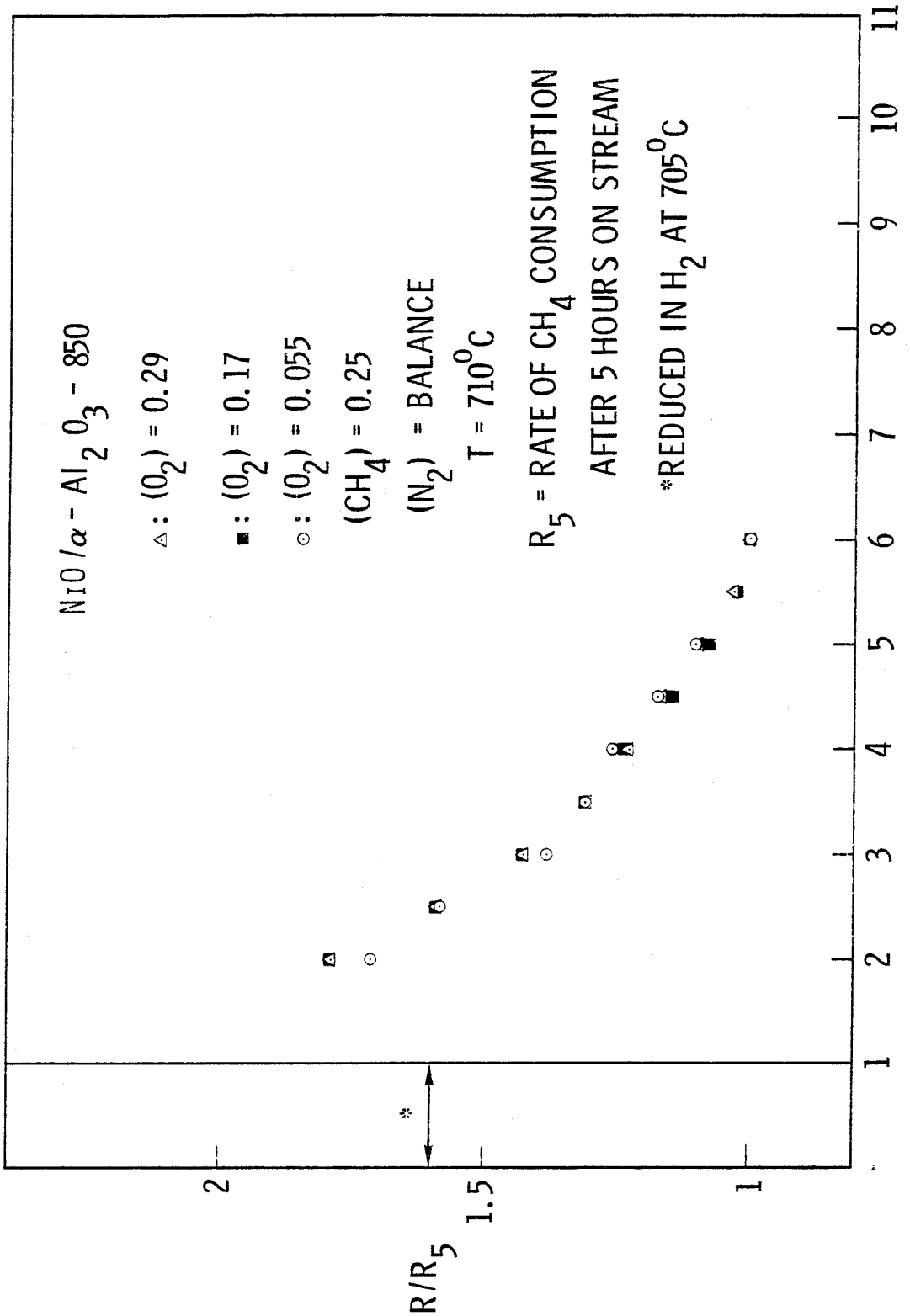

Fig. 13 Effect of Oxygen Partial Pressure on Deactivation

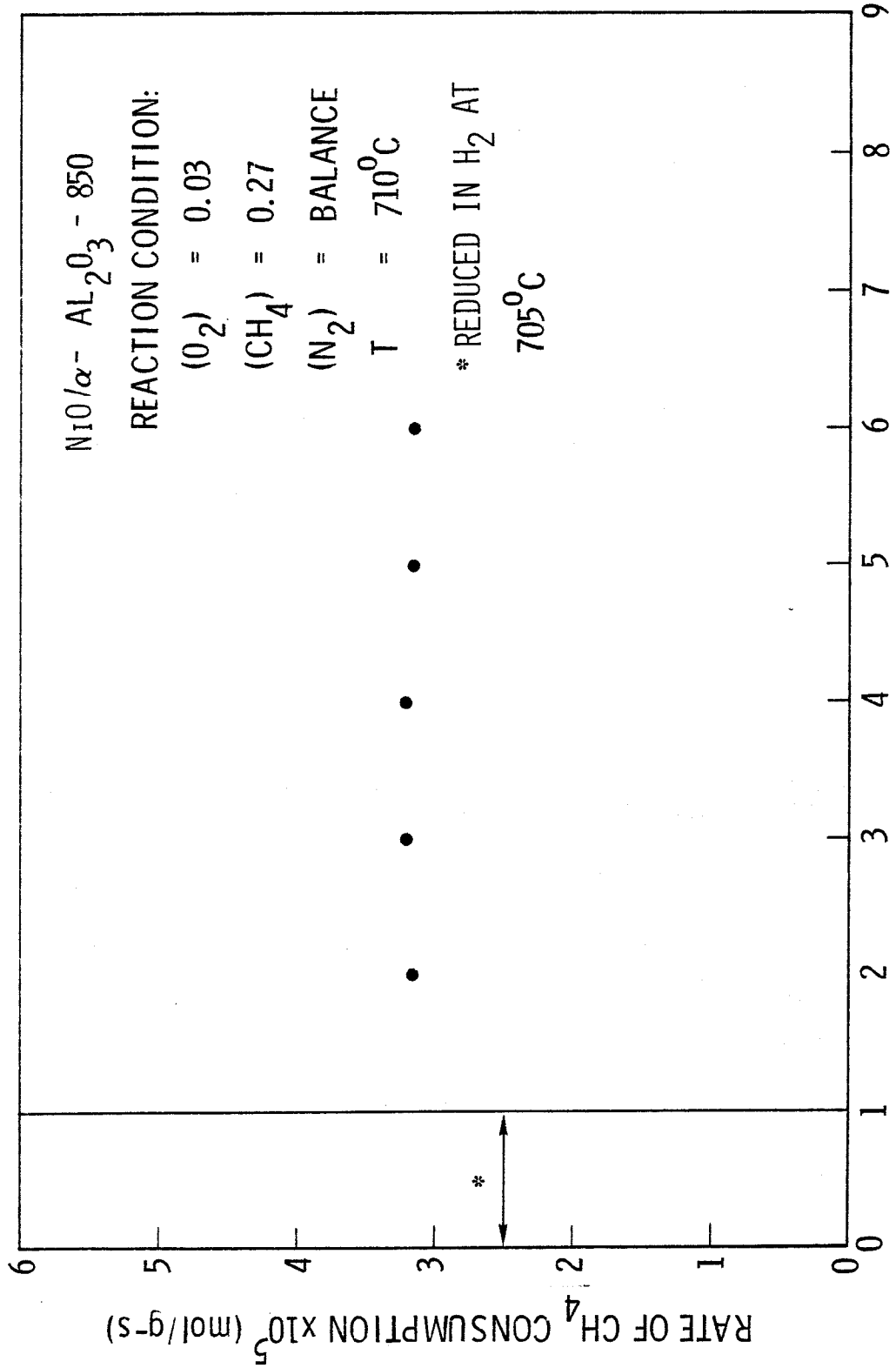

Fig. 14 Activity of NiO/α -Al_2O_3-850 After Reduction

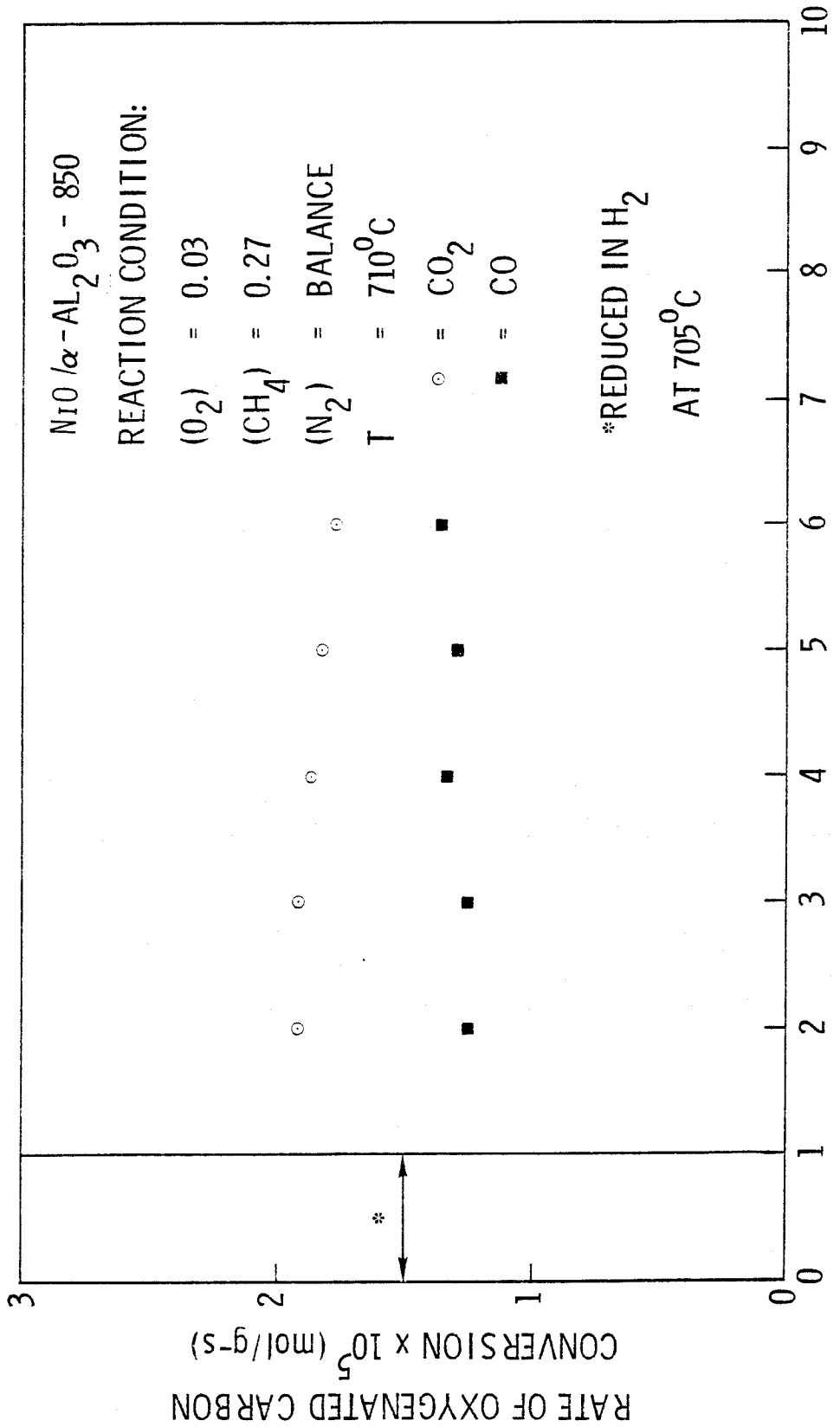

Fig. 15 Product Distribution at Low $O_{2/C}$ Ratio

was in the NiO form. However, when the O_2/CH_4 ratio at the inlet was lowered to 0.11, the activity (after reduction) did not decline (Fig. 14). Under these conditions, both CO and CO_2 were formed (Fig. 15) and the catalyst was in the metallic nickel form (1).

Finally, the reduced catalysts were found to have a grayish-black color irrespective of their original colors. Thus, it appears that the concentration of excess oxygen in calcined NiO is regained after reduction and reoxidation under reaction (2).

DISCUSSION

The results in this study have shown that the catalytic activity of supported NiO catalysts for CH_4 oxidation decreases dramatically with increasing calcination temperature. However, calcined catalysts can be reactivated by reduction in H_2 prior to reaction. This rather interesting change in activity has two explanations that are not mutually exclusive: 1) A change in the specific activity of NiO; 2) A change in the effective NiO surface area.

Catalytic Properties Of NiO

It has been shown that the change in the specific activity of NiO is the main cause of the change in catalyst activity. This dramatic dependence of the specific catalyst activity of NiO for CH_4 oxidation on the pretreatment atmosphere and temperature requires some discussion. In general, the catalytic properties of semiconductors are influenced by the following:

a) electronic interaction with the support

b) change in surface structure with crystallite size

c) collective electronic properties

d) localized surface properties

These apply to the system examined in the present study in the following ways;

a) Electronic interaction with the support

The electronic interaction between the catalysts and support has been discussed in the literature for many years. It is known (7,8) that the electronic interaction is significant only with the crystallite consisting of just a few atoms. Since the catalysts in this study have an average crystallite size of greater than 300 A^0, it is anticipated that the electronic interaction with the support is negligible.

b) Change in surface structure with crystallite size

An important factor that can affect the catalytic properties of supported catalysts is related to the change in structure with particle size. Van Hardeveld and Hartog (9,10) have shown that the surface structure of a crystallite becomes drastically different from that of a large particle only when the crystallite size is less than about $50A^{\circ}$. Although the average NiO crystallite size determined from X-ray line broadening is greater than $300A^{\circ}$ for all catalysts examined here, a small number of NiO crystallites of less than $50A^{\circ}$ size may have existed prior to calcination at high temperature. These crystallites may have possessed higher activities than large particles due to different coordinations or arrangements on the surface. During calcination at higher temperature, the crystallites would coalesce, and the catalyst activity would decrease drastically. However, the loss in

catalytic activity by this mechanism could not be reversed by reduction because small nickel crystallites coalesce extensively both under oxidizing and reducing atmosphere (11-13). Thus, the change in specific activity of NiO could not be explained by a change in crystallite size.

c and d) Collective electronic properties and localized properties.

The nonstoichiometric NiO is a p-type semiconductor in which the electrical conductivity increases with increasing concentration of excess oxygen (or Ni^{3+} ions). As indicated earlier, the concentration of excess oxygen in NiO decreases with increasing calcination temperature, appears to be stable under reaction and increases by reduction.

Several studies (14-18) have interpreted the catalytic properties of NiO in terms of its semiconductivity which can be modified by introducing altervalent cations or excess oxygen into the lattice. According to the electronic theory of catalysis (19-21), whenever change transfer is the rate determining step, the overall rate of reaction depends on the electronic properties of semiconductors. Krauss (14) has shown that the activity of NiO for the oxidation of NH_3 to N_2O is proportional to the amount of excess oxygen in lattice. Hauffe (15) and Winter (16) have shown that the activity of lithium-doped NiO for N_2O decomposition increases with the increasing conductivity. Parravano (17) and Schwab

and Black (18) demonstrated that the activation energies for CO oxidation on NiO doped with Li_2O or Cr_2O_3 were dependent on its semiconductivity.

Taking these prior facts into account, it appears that the changes in specific activity of NiO for CH_4 oxidation are related to the changes in concentration of excess oxygen. Similar to the studies mentioned above, we can phenomenologically explain the change in specific activity of NiO for CH_4 oxidation in terms of the change in its conductivity. However, the localized properties at the NiO surface must surely be affected in some manner by the change in conductivity. An obvious example is the concentration of Ni^{3+} ions in the surface layer. Moreover, it has been suggested (22) that the interaction of O_2 with the NiO surface takes place at surface defects such as ion vacancies, steps, etc. where the Ni^{2+} ions are more exposed. However, the relationship between the conductivity and the properties of the surface defects has not been established. Thus it is plausible to speculate that the specific activity of NiO for CH_4 oxidation may be related to the localized interaction at the surface.

Thus, we hypothesize that the specific activity of NiO for CH_4 oxidation is dependent on the concentration of excess oxygen. However, based on the limited data available, the significance of the collective electronic properties

versus the localized surface properties cannot be determined but requires further investigation.

Finally, it has been shown in chapter two that the concentration of excess oxygen in NiO is a function of calcination temperature. Based on the above interpretation, the specific activity of NiO after reduction is irrespective of the previous calcination temperature but dependent on the reoxidation temperature. It follows then that the difference in catalyst activity after reduction and reoxidation at the same temperature is due to the differences in NiO surface area. For example, the activity after reduction of the NiO/ZrO_2-1050 catalyst is higher than that of the NiO/ZrO_2-850 catalyst (Fig. 7), whereas the activity after reduction of the NiO/α-Al_2O_3-850 catalyst is higher than that of the NiO/α-Al_2O_3-1050 catalyst (Fig. 6), in agreement with their NiO surface areas after reduction and reoxidation (Table 1).

Increased NiO Surface Area

It has been shown in the last chapter that the NiO surface area increases sightly after reduction and reoxidation due to nickel redispersion. Although the increase in NiO surface area after reduction is not the main cause of the increase in catalyst activity, this phenomenon can explain the effect

of reduction time and temperature on the catlyst activity.

Since the nickel redispersion results from volume change during reduction (2), it must terminate when the reduction is completed. Preliminary calculations based on the results from a number of studies on NiO reduction (23-25), show that the reduction of all catalysts in the present study above 600°C is completed within an hour. Continued heat treatment in H_2 will not redisperse nickel crystallites any further but will instead cause the redispersed crystallites to coalesce. This phenomenon accounts for the decreases in activity gain after reduction at 705°C for >1 hour (Fig. 10) or for 1 hour at >650°C (Fig. 11 and 12).

It is now clear that a slow decline in activity gain after reduction in the alternating reduction and oxidation sequence (Fig. 8) is due to the decrease in NiO surface area. In order to explain this phenomenon, we must keep in mind that the nickel redispersion is more extensive after calcination in air at higher temperature prior to reduction (2). Thus, it can be seen that the nickel redispersion during the first reduction is more extensive than those during additional reductions. Following the first reduction, the redispersed NiO crystallites coalesce during reaction and the coalescence appears to offset the redispersion during additional reductions. As a result, the activity gains after additional reduction are less prominent.

LITERATURE CITED

1. Chapter 2
2. Chapter 3
3. Mears, D.E., Ind. Eng. Chem. Process. Develop. 10,4, 541 (1971)
4. Anderson, R.B., Stein, K.C., Feenan, J.J. and Hofer, L.J.E., Ind. Eng. Chem. 53,809 (1961)
5. Andrushkevich,T.V., Popovskii, V.V. and Boreskov, G.K., Kinet. Catal. 6,5,777 (1965)
6. Gulbransen, E.A. and Andrew,. K.F., J. Electrochem. Soc. 101,3,128 (1954)
7. Dalla Betta, R.A. and Boudart, M., Proc. 5th Int. Congr. Catal., Palm Beach, 1972, 2,1329 (1973)
8. Sinfelt, J.H., J. Catal. 29,308 (1973)
9. Van Hardeveld, R. and Hartog, F., J. Catal. 22,75 (1972)
10. Van Hardeveld, R. and Hartog, F., Surface Sci. 15, 189 (1969)
11. Shephard, F.E., J. Catal. 14,148 (1969)
12. Richardson, J.T. and Crump, J.G., J. Catal. 57, 417 (1979)
13. Kou, H.K., Ganesan, P. and De Angeles, R.J., J. Catal. 64,303 (1980)
14. Krauss, W., Z. Elektrochem. 53,320 (1948)
15. Hauffe, K., Glang, R. and Engell, H.J., Z. Physik Chem. (Leipzig) 201, 223 (1952)

16. Winter, E.R.S., Dis. Faraday Soc. 28, 183 (1959)

17. Parravano, G., J. Amer. Chem. Soc. 75,1452 (1952)

18. Schwab, G.M. and Block, J., Z. Physik. Chem. (Frankfurt) 1,42 (1954)

19. Wagner, C. and Hauffe, K., Z. Elektrochem. 44,1972 (1938)

20. Wolkenstein, F.F., VSP. Fiz. Nauk. 60, 249 (1956)

21. Hauffe, K., "Semiconductor Surface Physics", (Kingston, R.H. ed.), University of Pennsylvania Press, Philadelphia (1956) p.259

22. Charman, H.B., Dell, R.M. and Teale, S.S., Trans. Faraday Soc. 59,453 (1963)

23. Bandrowski, J., Bickling, R., Yang, K.H. and Hougen, O.A., Chem. Cng. Sci. 17,379 (1962)

24. Chiesa, F. and Rigand, M., Can. J. Chem. Eng. 49,617 (1971)

25. Szekely, J., Lin, C.I. and Sohn, H.Y., Chem. Eng. Sci. 28,1975 (1973)

Appendix I: O_2 Chemisorption by the Pulse Flow Method

Selective chemisorption is the most attractive method for determining the active nickel surface area and the dispersion of supported metal catalysts (1,2). Most of the previous studies have used H_2 (3-12), CO (3,5,13-20) and O_2 (21-26) as the adsorbates. The chemisorption is usually carried out in a static vacuum system. However, it has been found that the simpler and less time consuming continuous flow method (11,13) or pulse flow method (12,25,27) give essentially identical results with the static method.

In the pulse flow method, pulses of adsorbate are injected downstream of the reference thermal conductivity detector into the flow of He carrier gas (Fig. 1). After passing over the reduced nickel catalyst sample, the amount of adsorbate left in the carrier gas stream is detected by the thermal conductivity detector. During the first few pulses, no chromatographic peak is detectable. Eventually, a partial peak appears and when the nickel surface is completely covered, the area of subsequent peaks becomes constant (Fig. 2). The amount of adsorbed gas is the sum of completely adsorbed pulses plus partially adsorbed pulses. This method determines only the amount of irreversibly adsorbed gas because the reversibly adsorbed portion is swept from the nickel surface by the carrier gas. The amount of the reversibly adsorbed part can only be determined by a relatively lenghty analysis of the chromatographic peak using the theory of

equilibrium chromatography (11,28).

H_2 chemisorption has been the most extensively investigated method for the determination of nickel surface area. The stoichiometry of H_2 chemisorption on nickel is well established as one hydrogen atom per nickel surface atom (5,8,10), except at very low nickel loading and/or when the nickel-support interaction is prominent as in $NiTiO_2$ (3). However, H_2 is adsorbed on nickel both reversibly and irreversibly (3,12,25,29) and the amount of reversibly adsorbed part depends on pressure, temperature (25) and nickel crystallite size (29).

CO chemisorption has also been widely used to estimate the nickel surface area. However, CO is obviously not an ideal adsorbate because it can be adsorbed on nickel with the formation of linear and bridged forms depending on temperature, pressure, dispersion and preparation method (3,5,9,18,30,31). Recently (3,19,20), the presence of subcarbonyl

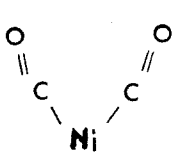

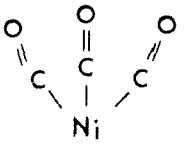

species and adsorption on unreduced NiO has been suggested. This stoichiometric uncertainty can cause a serious ambiguity in the reported area. In addition, at room temperature $Ni(CO)_4$ is formed (3,9,13,17,32) and, if not corrected can lead to overestimating the nickel surface area. Finally, similar to H_2, CO is adsorbed on nickel

both reversibly and irreversibly (3,27).

Published results on the chemisorption of O_2 on clean nickel single crystal (33), supported nickel catalyst (21,22,23,25,34), nickel powder (21,22) and evaporated nickel film (26,34,35) have demonstrated that the adsorption mechanism consists of two regions: first, a fast oxidation leading to two layers of epitaxial NiO and a slow oxygen incorporation into the nickel lattice. The rate of oxygen diffusion into the bulk nickel increases with increasing temperature. For all practical purpose, however, the amount of oxygen incorporation is negligible if the O_2 chemisorption experiment is conducted for less than an hour at room temperature (22,23,25). In addition to a known stoichiometry, the rapid chemisorption of oxygen on nickel is irreversible and independent of pressure between <1 torr and 100 torr (22,23,25). Thus, oxygen is apparently the most suitable adsorbate for the determination of nickel surface area by the pulse flow method.

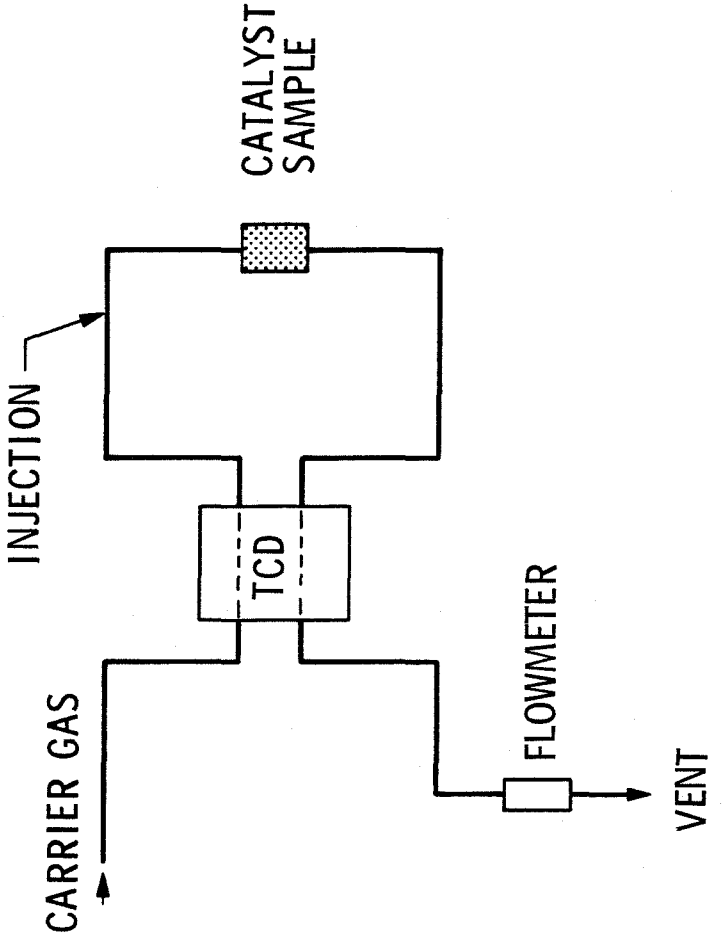

Fig. 1 Diagram of the Flow Apparatus

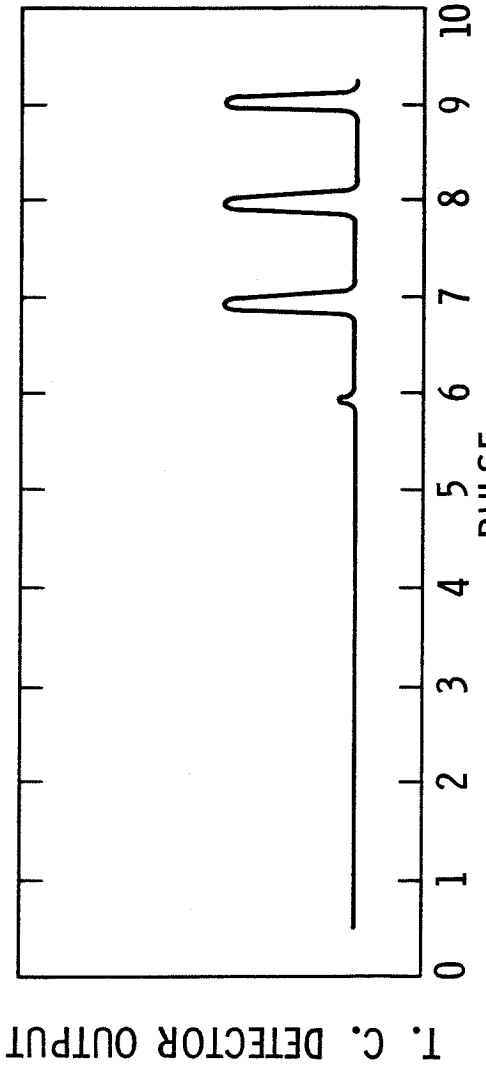

Fig. 2 Chromatogram for Oxygen Chemisorption

LITERATURE CITED

1. Muller, J., Rev. Pure & Appl. Chem. 19,151 (1969)
2. Farranto, R. J., AIChe Symp. Ser. 70 #143 PP 9-22 (1975)
3. Bartholomew, C.H. and Pannell, R.B., J. Catal. 65,390 (1980)
4. Bartholomew, C.H., J. Catal. 45, 41 (1976)
5. Brooks, C. S. and Christopher, G.L.M., Ibid 10,211 (1968)
6. Taylor, W.F., Sinfelt, J.H. and Yates, D.J.C., J. Phys. Chem. 69,3857 (1965)
7. Taylor, W.F., Sinfelt, J.H. and Yates, D.J.C., J. Phys. Chem. 68,2962 (1964)
8. Yates, D.J.C., Taylor, W.F., and Sinfelt, J.H., J. Amer. Chem. Soc. 86,2996 (1964)
9. Vlasneko, V.M. et al., Kinetika i Kataliz 2,337 (1964)
10. Selwood, P.W., J. Catal. 42,148 (1976)
11. Hansen, A. and Gruber, H.L., J. Catal. 20,97-105 (1971)
12. Roca, F.F. et al. Journal of Gas Chromotography 6,161 (1968)
13. Hughes, T.R., Houston, R.J. and Sieg, R.P., I & EC, Proc. Design & Devel. 1,2 96 (1962)
14. Emmet, P.H. and Skow, N., J. Amer. Chem. Soc. 65, 1029 (1943)
15. Germain, J.E., Ostyn, M. and Beaufils, J.P., J. Chim. Phys. 61, 686 (1964)
16. Schuit, G.C.A. and Van Reijen, L.L., Advan. Catal. 10, 242 (1958)
17. Yates, J.T. and Garland, C.W., J. Phys. Chem. 65, 617 (1961)
18. O'Neill, C.E. and Yates, D.J.C., J. Phys. Chem. 65, 901 (1961)

19. Rochester, C.H. and Terrel, R.J., J. Chem. Soc. Trans. Faraday I 73, 609 (1977)

20. Primet, M., Dalmon J.A. and Martin G.A., J. Catal 46, 25 (1977)

21. Ljubarskij, G.D., Avdeeva, L.B. and Kulkova, N.V., Kinetika i Kataliz 3, 123 (1962)

22. Muller, J., J. Catal. 6, 50 (1966)

23. Muller, J., Pour, V. and Regner, A., J. Catal. 11, 326 (1968)

24. Vlasenko, V.M., Rusov, M.T. and Juzefovic, G.E., Kinetika i Kataliz 2, 394 (1961)

25. Buyanova, N.E. et al. Kinetika i Kataliz 8, 868 (1967)

26. Brennan, D., Hayward, D. O. and Trapnell, B.M.W., Proc. Roy. Soc. (London) A256, 81 (1960)

27. Brooks, C.S. and Kehrer, Jr., V.J., Anal. Chem. 41, 1, 103 (1969)

28. Kiselev, V. and Yaskin, V.I., Gas-Adsorption Chromatography, Plenum Press (1969)

29. Slinken, A.A., Kucherov, A.V. and Rubinstein, A.M., Kinetika i Kataliz 19, (2), 415 (1978)

30. Eischens, R.P., Francis, S.A. and Pliskin, W.A., J. Phys. Chem. 60, 194 (1956)

31. Trapnell, B., "Chemisorption" (1958)

32. Goldberger, W.M. and Othmer, D.F., I & E.C., Process Design & Devel. 2, 3, 202 (1963)

33. Holloway, P.H. and Hudson, J.B., Surface Sci. 43, 123 (1974)

34. Roberts, M.W. and Wells, B.R., Dis. Faraday Soc. 41, 162 (1966)

35. Delchar, T. and Tompkins, F.C., Surface Sci. 8, 165 (1967)